TRACE ELEMENT GEOCHEMISTRY IN GROUNDWATER FLOW SYSTEMS

by

STEPHANIE SCHOLTEN WILLIS

Presented to the Faculty of the Graduate School of

The University of Texas at Arlington in Partial Fulfillment

of the Requirements

for the Degree of

DOCTOR OF PHILOSOPHY

THE UNIVERSITY OF TEXAS AT ARLINGTON

December 2010

ACKNOWLEDGEMENTS

This dissertation would not have been possible without the guidance and help of my advisor, Dr. Karen Johannesson. Through all the trips to New Orleans, long phone calls, and countless emails, you have given me the support and direction I needed to see this project to completion. Thanks to the faculty and staff in the Earth and Environmental Science Department at both the University of Texas at Arlington and Tulane University.

Finally, I would like to thank my family for their inspiration and support throughout my graduate experience. To my parents, Donald and Judith, thanks for your constant encouragement and reassurance. Above all, I give heartfelt thanks to my husband Joseph, for your endless loving support.

November 11, 2010

ABSTRACT

TRACE ELEMENT GEOCHEMISTRY IN

GROUNDWATER FLOW SYSTEMS

Stephanie Scholten Willis, PhD

The University of Texas at Arlington, 2010

Supervising Professor: Karen H. Johannesson, PhD

This research focuses on trace element geochemistry in three groundwater flow systems: the Carrizo Sand, the Upper Floridan, and the Aquia aquifers. The focus is threefold: (i) studying the geochemical behavior, concentrations, and fractionation patterns of rare earth elements (REEs) along two flow paths by examination of both groundwater and sediment samples, (ii) investigating the behavior of arsenic (As) and antimony (Sb) and comparing these data to reveal the biogeochemical processes affecting As and Sb concentrations and speciation as well as determining correlations between As and Sb concentrations, and (iii) formulating adsorption isotherms to demonstrate the adsorption capacity of As onto sediments from the Carrizo Sand and Aquia aquifers. The investigation of the Aquia aquifer groundwaters and sediments

indicated the chief source of REEs in the groundwater was due to the dissolution of carbonate minerals (i.e. shell fragments). A statistical relationship was found between As and Sb in the groundwaters of three well defined aquifers (the Carrizo Sand, the Upper Floridan, and the Aquia aquifers), with the best correlation occurring within the Aquia groundwaters. The adsorption isotherms indicate that As(V) strongly adsorbs to the Carrizo Sand aquifer sediments whereas As(III) more preferentially adsorbs to the Aquia aquifer sediments.

TABLE OF CONTENTS

LIST OF ILLUSTRATIONS

LIST OF TABLES

CHAPTER 1

INTRODUCTION

Rare earth elements (REEs), arsenic (As), and antimony (Sb) are all naturally occurring trace elements in groundwater. The study of these trace elements uncovers the mechanisms by which they are distributed throughout groundwater flow systems.

REEs unique and chemically coherent behavior, along with their sensitivity to changes in pH, redox conditions, and adsorption/desorption reactions, makes them useful as an efficient hydrological tool (Wood, 1990; Dia et al., 2000). Because the REEs typically behave coherently, changes in the expected patterns can lead to critical information on the types of processes occurring within a groundwater flow system (Guo et al., 2010). A number of studies have examined the biogeochemical processes that affect REE concentrations and their relative distribution across the lanthanide series (i.e., fractionation) along groundwater flow paths. In one study, Tang and Johannesson (2006) observed that changes in redox conditions, pH, and adsorption along the Carrizo Sand aquifer flow path in south Texas are also accompanied by changes in REE concentrations, shale-normalized patterns, and speciation. In another study, Guo et al. (2010) also observed changes in REE concentrations and shale-normalized patterns along with changes in redox conditions along a flow path in the shallow aquifer of the Hetao Basin, Inner Mongolia.

As and Sb are also of interest in the study of groundwater flow. Because of their identical s^2p^3 outer orbital electron configuration, As and Sb display the same range of oxidation states. Both most commonly occur as oxides, hydroxides, or oxoanions either

in the pentavalent state in relatively oxic environments (arsenates and antimonates) or in the trivalent state in anoxic environments (arsenites and antimonites) (Wilson et al., 2010). The toxicities of As and Sb strongly depends upon their speciation. The trivalent form of both As and Sb is more toxic than the pentavalent form (Bencze, 1994; Filella et al., 2002a, b; Ratnaike, 2003). As and Sb occur in more than 200 minerals on the earth and are derived from ore minerals or their alteration products that naturally contaminate the environment (Smedly and Kinniburgh, 2002; Filella et al., 2002a; Ghassemzadeh et al., 2006). Naturally, As and Sb occur in the form of organic and inorganic compounds. Exposure to inorganic compounds may occur in a variety of ways through certain industrial effluents, chemical alloys, pesticides, wood preservative agents, combustion of fossil fuels, fire retardants, and mining activities (Ghassemzadeh et al., 2006). The majority of Sb contamination in the environment originates from mining and industrial emission sources, often smelting, co-occurring frequently with As (Telford et al., 2009; Wilson et al., 2010). In the environment, As is considered to be one of the main problems with global groundwater quality. Cases of elevated levels of As in groundwater include aquifers in Australia (O'Shea et al., 2007), Argentina (Smedley and Kinniburgh, 2002; Bhattacharya et al., 2006), Bangladesh (Anawar et al., 2003; Shamsudduhu et al., 2008), Chile (Caceres et al., 1992), Mexico (Romero et al., 2004), and the United States of America (Haque and Johannesson, 2006a, b; Haque et al., 2008; Peters 2008; Welch et al., 2000).

Unlike As, the geochemistry of Sb in groundwater is poorly understood. Chen et al. (2003) discovered the importance of iron and manganese oxyhydroxides in controlling the behavior of Sb in the oxic interface of two lakes in Subury, Ontario. Under anoxic

conditions, they found dissolved Sb was released by the dissolution of manganese and iron oxyhydroxides. They also suggested that Sb solubility was controlled by iron sulfides in reducing sediments. Few studies have focused on the similarities between As and Sb. In one of these studies, Tighe et al. (2005) noted a strong relationship between As and Sb in their bioavalability in the Macleay catchment coastal floodplain in New South Wales, Australia. They also discerned there was no obvious relationship between the soil physical parameters and the As and Sb content of the soils. In a 17 month study of the Gironde Estuary in Western Europe, Masson et al. (2009) revealed that both As and Sb may be released into river water from particulate carrier phases in sediments and/or aquifers by microbially driven processes due to their similarities in seasonal variations.

Modeling the adsorption behavior of As is also crucial in understanding how trace elements evolve in groundwater flow systems. The bioavailability of As in aquifer sediments is largely governed by its adsorption-desorption reactions with aquifer sediment constituents (Naidu et al., 2009). Generally, As(V) adsorption to mineral oxides is favored at low pH, whereas As(III) adsorption occurs best at circumneutral pH (Raven et al., 1998; Arai et al., 2001; Dixit and Hering, 2003). The Fe oxide content, including the presence of Fe oxyhydroxide, in soils has been shown to enhance the capacity of soils to bind As (Manful et al, 1989; Manning and Goldberg 1997; Smith et al., 1999). Both As(III) and As(V) sorb strongly to Fe oxides/oxyhydroxides (Dixit and Hering, 2003). A number of studies have also focused on the adsorption of As onto clay minerals. Frost and Griffin (1977) discovered that montmorillonite sorbed both As(V) and As(III) more strongly than kaolinite and that As(III) was sorbed much less than

As(V) by both clay minerals. On the other hand, Goldberg and Glaubig (1988) found the As(V) adsorption capacity to be similar for both montmorillonite and kaolinite.

After an extensive review of the previously mentioned studies, a central hypothesis for this research was developed. Redox conditions, chemical weathering, and adsorption/desorption reactions affect the distribution and bioavalability of trace element in groundwater flow systems. In addition, trace elements should behave similarly with their close neighbors in the periodic table.

The following research objectives were examined to determine the validity of the central hypothesis:

(i) Examine the geochemical behavior, concentrations, and fractionation patterns of REEs along two flow paths by examining both groundwater and sediment samples,

(ii) Investigate the behavior of As and Sb in three well characterized aquifers and compare these data to gain insight into the biogeochemical processes affecting As and Sb concentrations and speciation along the flow path within these groundwater flow systems as well as determine if a correlation exists between As and Sb concentrations, and

(iii) Observe the adsorption behavior of As in two groundwater flow systems.

To fulfill the first objective (Chapter 2), both field and laboratory experiments were conducted on groundwater and sediment samples collected along two groundwater flow paths within the Aquia aquifer of coastal Maryland. A series of groundwater samples were collected along both the Eastern and Western shores of the Aquia aquifer. These samples were analyzed for REE concentrations as well as additional geochemical parameters (e.g., alkalinity, pH, temperature, specific conductance, dissolved oxygen, oxidation-reduction potential, iron speciation, silica, manganese, nitrate, ammonia, and

dissolved sulfide). The sediment samples were analyzed by sequential extraction and glauconite extraction. Results of this study demonstrate that the Aquia groundwaters evolve along the flow paths due to chemical weathering and changes in redox conditions. Groundwater REE concentrations are consistent with weathering of an upper continental crust source, such as Aquia aquifer sediments (i.e. carbonate minerals and glauconite), being the main source of REEs to the groundwaters. This also appears in the sequential extraction results for the Aquia aquifer sediments where the largest pool of REEs is associated with carbonate minerals (shell fragments).

To achieve the second objective (Chapter 3), field data from the Carrizo Sand aquifer (Texas), the Upper Floridan aquifer (Florida), and the Aquia aquifer (coastal Maryland) was analyzed. As and Sb concentrations from the three aquifers were compared with regard to specific geochemical parameters (e.g., Fe concentration/speciation, pH, and dissolved sulfide) along the flow paths. The results of the study indicate a statistical relationship between As and Sb concentrations, with the best correlation between As and Sb occurring in the Aquia aquifer.

To accomplish the third objective (Chapter 4), a series of As adorption experiments were conducted on bulk sediment samples from the Aquia and Carrizo Sand aquifers. Both As(III) and As(V) species were evaluated by varying initial As concentration and solution pH. The experimental data was then evaluated using the linearized Freunlich isotherm equation. The outcome of this study reveals that As(III) and As(V) adsorption are not strongly pH dependent to sediments of the Aquia and Carrizo Sand aquifers. The Freundlich isotherms showed that As(III) strongly adsorbs to

the sediments of the Carrizo Sand aquifer, while As(V) more preferentially adsorbs to the Aquia aquifer sediments.

In the following three chapters of this dissertation, I present three manuscripts in which trace element geochemistry along groundwater flow paths is discussed. Chapter 2 focuses on the evolution of REE concentrations along two flow paths in the Aquia aquifer. Chapter 2 presents geochemical data for each flow path and how this data affects the REE concentrations. Next, Chapter 3 presents a comparative study between As and Sb concentration in three groundwater flow systems (the Carrizo Sand aquifer, the Upper Floridan aquifer, and the Aquia aquifer) along with specific geochemical parameters. Additionally, Next, Chapter 4 analyses As adsorption for the Aquia and Carrizo Sand aquifers. Finally, Chapter 5 summarizes all previous chapters regarding trace elements in groundwater flow systems and concludes all the major findings presented in this dissertation.

CHAPTER 2

CONTROLS ON THE GEOCHEMISTRY OF RARE EARTH ELEMENTS IN SEDIMENTS AND GROUNDWATERS OF THE AQUIA AQUIFER, MARYLAND, USA

2.1 Introduction

Rare earth elements (REEs) are commonly used as geochemical tracers in groundwater flow systems due to the similarities between aquifer-rock REE patterns and the REE patterns found in some groundwaters (Banner et al., 1989; Smedley, 1991; Johannesson et al., 1999). The similar chemical behavior of the trivalent REEs makes these elements attractive in interpreting geochemical processes that fractionate the REEs from their nearest neighbors in the periodic table, Hf^{4+} and Ba^{2+}. Furthermore, the decrease in ionic radius of the REEs with increasing atomic number leads to predictable chemical differences across the lanthanide series, which can record subtle geochemical processes in natural systems that fractionate the REEs (De Baar et al., 1985a; Taylor and McLennan, 1988; Fee et al., 1992; Johannesson et al., 1997b). Although the REEs exist primarily in the trivalent oxidation state in low-temperature aqueous systems, Ce and Eu can also exist in +4 and +2 oxidation states, respectively. The differences in the oxidation states of these two lanthanides can lead to geologically significant input-normalized concentration anomalies for Ce and Eu that can be quantified and geochemically interpreted (De Baar et al., 1983, 1985b; Fee et al.,1992). The negative, shale-normalized Ce anomaly that characterizes seawater, for example, is interpreted to reflect the oxidation of Ce^{3+} to Ce^{4+}, and the subsequent removal of Ce^{4}+ from the water

column via scavenging onto settling particles (Moffett, 1990; DeCarlo et al., 1998). Positive Eu anomalies have been attributed to highly reducing conditions during sediment diagenesis or to hydrothermal inputs (Sverjensky, 1984; Michard and Albarède, 1986; Michard, 1989, MacRae et al., 1992; Klinkhammer et al., 1994; Leqis et al., 1997; van Middlesworth and Wood, 1998), whereas, negative Eu anomalies are common features of evolved felsic igneous rocks owing to preferential uptake of Eu^{2+} from such melts by plagioclase (Hanson, 1980; Saunders, 1984; Culler and Graf, 1984).

Chemical weathering reactions and microbial processes occurring in aquifers are revealed by changes in redox conditions, pH, and major solute concentrations along groundwater flow paths (e.g., Champ et al., 1979; Barcelona et al., 1989; Chapelle and Lovley, 1992; Edmunds et al., 2003; Park et al., 2006). Previous studies have shown that the REE can be sensitive traces of these geochemical processes as many of the important geochemical reactions that occur along groundwater flow paths fractionate the REEs (Johannesson et al., 1997, 2005; Dia et al., 2000, Leybourne et al., 2000; Tang and Johannesson, 2005a, 2006; Tweed et al., 2006). The sensitivity of REE concentrations and fractionation patterns to changes in redox conditions that affect Fe/Mn oxides/oxyhydroxides and/or organic matter in groundwater flow systems, processes that are known to be important in such environments, may thus be useful in interpreting groundwater chemistry (Dia et al., 2000; Tang and Johannesson, 2005a, 2006). By understanding the effects of chemical weathering reactions and microbial processes on REEs, we can better assess the application of REEs to tracing groundwater flow patterns (Tweed et al., 2006) as well as quantifying their global geochemical cycle (e.g., Johannesson and Burdige, 2007).

In this study, we investigate the geochemical behavior of REEs within the Aquia aquifer (Maryland, USA) along different flow paths on the Eastern and Western shores of the Chesapeake Bay. We also compare the REE concentrations and fractionation patterns to changes in groundwater composition (i.e. pH, major solute compositions) and redox conditions determined with a number of redox sensitive elements and field parameters. Aquifer sediments were also analyzed to evaluate the sediment source of REEs to Aquia aquifer groundwaters.

2.2 Study Area

The Aquia aquifer is located within the Atlantic Coastal Plain in eastern Maryland (Fig. 2.1). The Aquia aquifer is a Paleocene marine deposit that is confined above by the Paleocene and Eocene Marlboro clay, and below by the silt and clay of the Cretaceous Severn Formation (Chapelle, 1983). The Aquia aquifer outcrops between Washington D.C. and Annapolis, Maryland, and dips southeast beneath the Chesapeake Bay and towards the Atlantic ocean (Aeschbach-Hertig et al., 2002). Groundwater is recharged within the outcrop region and subsequently flows down the dip of the aquifer towards the southeast and beneath the Chesapeake Bay (Chapelle, 1983; Chapelle and Knobel, 1983, 1985; Aeschbach-Hertig et al., 2002). The composition of the Aquia aquifer is dominated by fine- to medium-grained quartz sand (50 to 75%), glauconite (20 to 40%), and carbonate shell debris (1 to 5%) ranging from 30 to 46 meters thick (Aeschbach-Hertig et al., 2002; Chapelle, 1983; Chapelle and Knobel, 1983). In addition, pelletal goethite, clay minerals, and minor hematite has been identified within the aquifer sands (Hansen, 1974; Haque et al., 2008).

In this study, we examine portions of the Aquia aquifer located on both Maryland's Eastern and Western shores (Fig. 2.1). A series of groundwater samples were collected in August 2006 along Maryland's Eastern shore and again in June 2007 along Maryland's Western shore. The groundwater flow paths sampled were identified and selected based on the predevelopment potentiometric surface levels for the Aquia aquifer (e.g., the Eastern shore flow path; Drummond, 2001; Haque et al., 2008) and because of the numerous previous studies conducted along the western shore flow path (see Chapelle, 1983; Chapelle and Knobel, 1983, 1985; Appelo, 1994; Purdy et al., 1996; Aeschbach-Hertig et al., 2002). For example, on Maryland's Eastern shore, the pre-development potentiometric surface indicates that groundwater recharged to the Aquia aquifer in its outcrop area, in northern Kent County, historically flowed south and then west, discharging to the Chesapeake Bay (Drummond, 2001). Moreover, potentiometric lows that are characteristic of lower elevations near the Chesapeake Bay and the Potomac River further suggests that the groundwater flows south and southwest on the Eastern shore and south and southeast on the Western shore (Chapelle 1983; Drummond, 2001; Curtin et al., 2002; Haque et al., 2008). In the case of each flow path, a portion of the Aquia groundwater is thought to discharge to the Chesapeake Bay in the vicinity of the shoreline (Chapelle 1983; Drummond, 2001; Curtin et al., 2002; Haque et al., 2008).

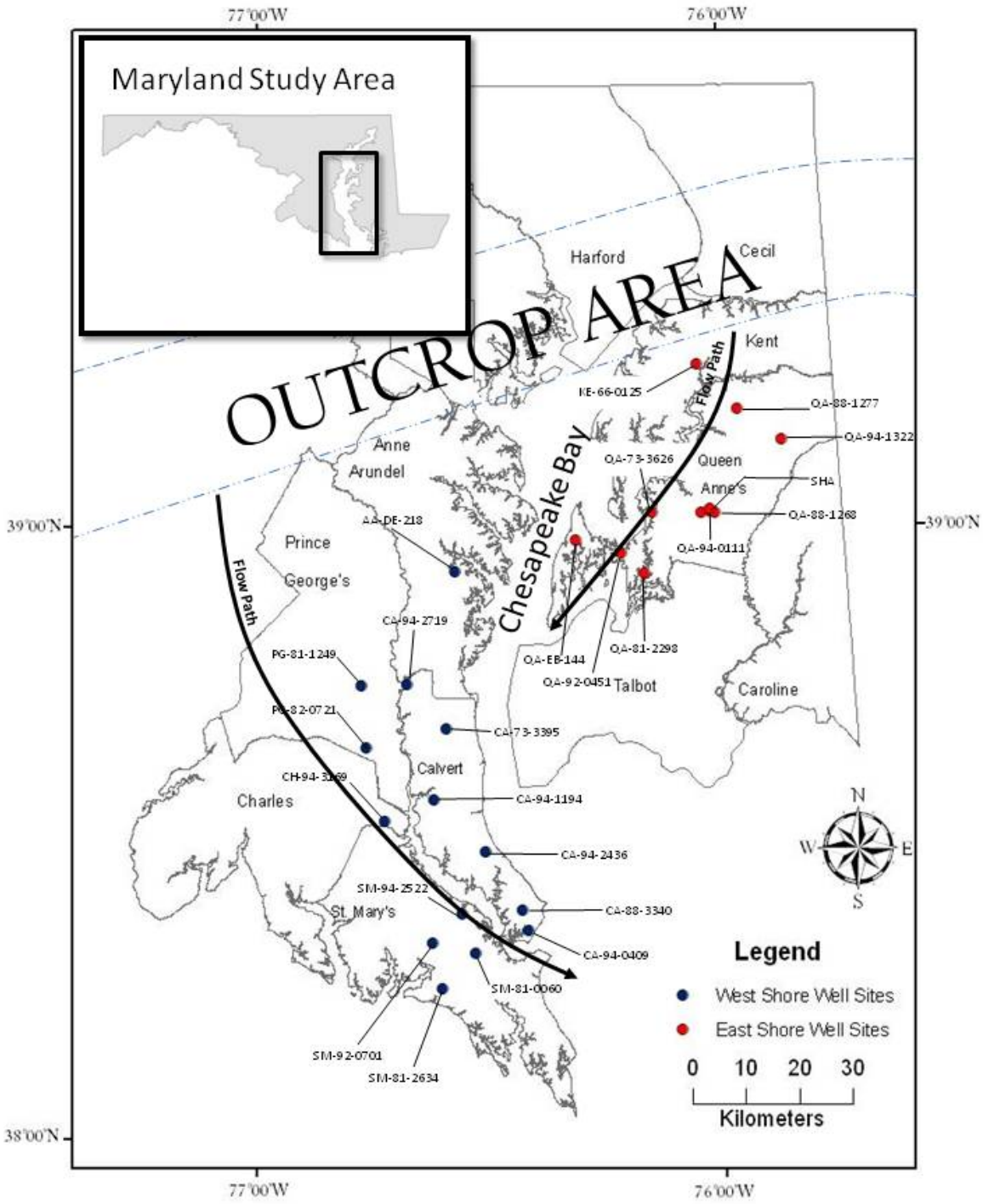

Figure 2.1. Map of the study area within central and east central Maryland showing location of outcrop area, investigated groundwater flow paths, and location of sampled wells. Groundwater flow directions are based on the predevelopment potentiometric surface (Drummond 2001).

2.3 Materials and Methods

2.3.1 Groundwater sampling and field analysis

All high density linear polyethylene (HDPE) sample bottles and Teflon® tubing used during sample collection and filtration were thoroughly cleaned using trace element cleaning procedures before being transported to the field (e.g., for details see Johannesson et al., 2004). Groundwater samples were collected from the Eastern Shore flow path of the Aquia aquifer in August 2006 and from the Western Shore flow path in June 2007. In order to ensure the groundwaters sampled were true representations of water from the aquifer and not water from the boreholes, the wells sampled were purged by pumping for at least 30 minutes, and until the pH, specific conductance, and water temperature stabilized before collecting the samples.

During each of these field sampling campaigns, measurements of alkalinity, pH, temperature, specific conductance, dissolved oxygen (DO), oxidation-reduction potential (Eh), iron speciation, dissolved silica, manganese, nitrate, ammonia, and sulfide concentrations were conducted on site (e.g., Haque et al., 2008). A Hydrolab MiniSonde 5 with a flow-through cell was used to quantify the Eh, pH, specific conductance, and temperature. The flow-through cell was connected to each well by a polyethylene tube, which allowed the Eh of the groundwaters to be measured without exposure to the atmosphere.

Alkalinity was titrated in the field using a standard colorimetric indicator approach and either 1.6 N or 0.16 N H_2SO_4. Results obtained during the June 2007 sampling of groundwater from the Western shore flow suggested that either the acid or colorimetric indicator powders had degraded. Consequently, alkalinity was also

estimated for these groundwaters by charge balance considerations, such that the alkalinity ≈ ∑cations (in equivalents) - ∑anions (in equivilants) (e.g., Lyons et al., 1992; Goldsmith et al., 2010).

A portable UV/VIS spectrophotometer (Hach DR/2400) was used to determine iron speciation and dissolved oxygen, silica, manganese, nitrate, ammonia, and sulfide concentrations using separate sample aliquots and standard spectrophotometric techniques. For example, Fe(II) was determined using the 1,10 phenanthroline method, total Fe (Fe_T) was quantified by the FerroVer method, (Eaton et al., 1995), and Fe(III) was subsequently calculated by difference. The method detection limits for Fe(II) and Fe_T are 0.36 μmol kg^{-1} and 0.16 μmol kg^{-1}, respectively (Hach, 2004). High range dissolved oxygen concentrations were determined using the High Range spetrophotometric method with a detection limit of 18.8 μmol kg^{-1} (Hach, 2004), whereas low range dissolved oxygen concentrations were determined using the Indigo Carmine method, for which the detection limit is 0.38 μmol kg^{-1} (Gilbert et al., 1982). Mn concentrations were determined using the 1-(2-Pyridylazo)-2-Napthol method (method detection limit 0.13 μmol kg^{-1}; Manzoori et al., 1999). Dissolved NO_3^-, NH_4^+, and Si concentrations were determined using the Cadmium 16 reduction method (Gal et al., 2004), the Salicylate method (Krom, 1980), and the Heteropoly Blue method (Schelske et al., 1984), respectively. The method detection limits for NO_3^-, NH_4^+, and Si were 0.16 μmol kg^{-1}, 0.55 μmol kg^{-1}, and 0.36 μmol kg^{-1}, respectively (Hach, 2004). Dissolved S(-II) was determined using the Methylene Blue method, for which the detection limit is 0.16 μmol kg^{-1} (Eaton et al., 1995).

Groundwater samples for determination of major solutes and REEs were first collected in collapsible "trace clean" low density polyethylene cubitainers® (Hedwin Corporation, Baltimore, MD, USA) from each of the wells and then immediately filtered through 0.45 μm Gelman Sciences in-line groundwater filter capsules (polyether sulfone membrane) using a peristaltic pump and Teflon® tubing. The groundwater sample was pumped directly through the in-line filter capsule and into "trace clean" 1 L HDPE bottles, which were rinsed three times with the filtered groundwater sample to "condition" the bottle before filling the bottle with the filtered groundwater sample. The filtered groundwater sample was then immediately acidified to pH < 2 using ultra-pure HNO_3 (Seastar Chemical, Baseline) for the cation samples (Ca^{2+}, Mg^{2+}, Na^{+}, K^{+}) and the REE samples. The anion samples (Cl^{-}, SO_4^{2-}) were not acidified. After collection, all samples were stored ~ 4˚C prior to analysis.

2.3.2 Sediment sampling

Sediment samples were collected from five depth intervals (i.e., 61 mbgs, 65 mbgs, 72 mbgs, 86.5 mbgs, and 104 mbgs, where mbgs is meters below ground surface) from an archived drill core stored at the Maryland Geological Survey (see Haque et al., 2008, for details). The sediment core is from the vicinity of well KE 66-0125 in Kent County, Maryland on the Eastern shore of the Chesapeake Bay (see Fig. 1 in Haque et al., 2008). The sediment samples were stored in clean plastic Ziploc©-style sample bags at 4ºC prior to the sequential extractions analysis.

2.3.3 Groundwater major solute and REE analysis

Samples were analyzed for major anions and cations by ion chromatography with a Dionex DX-120 (Sunnyvale, CA) ion chromatograph following the approach of Welch

et al. (1996). The instrument has a single piston, isocratic pump that produces a constant flow rate set at 1.2 mL per minute, and eluted ions are quantified via an electrical conductivity detector. For the cation analyses, a Dionex IonPac CS12A analytical column (4x250mm) and a CG12A guard column (4x50mm) was used. The eluent is 0.13% methanesulfonic acid solution. A CSRS Ultra Cation Self-Regenerating Suppressor was used. For the anions, a Dionex IonPac AS14 analytical column (4x250m) and an AG14 guard column (4x50mm) was used. The eluent is a 1.0mM $NaHCO_3$ and 3.5mM Na_2CO_3 solution. An ASRS Ultra Anion Self-Regenerating Suppressor was used. In addition, dissolved organic carbon (DOC) was analyzed in five of the groundwater samples by high temperature catalytic oxidation (HTCO) using a Shimazdu TOC-5000 total carbon analyzer (Burdige and Gardner, 1998).

All groundwater samples collected for REE analysis were first loaded onto Poly-Prep columns (Bio-Rad Laboratories) packed with AG 50W-X8 (100 – 200 mesh, hydrogen form, Bio-Rad Laboratories) cation-exchange resin at approximately 1 mL $minute^{-1}$ in order to separate the REEs from the major salts and to concentrate the REEs into a smaller solution volume (Johannesson et al., 2005). Iron and Ba were subsequently eluted from the columns using 1.75 M ultra-pure HCl (Seastar Chemicals, Baseline, sub-boiling, distilled in quartz) and 2 M ultra-pure HNO_3 (Seastar Chemicals, Baseline), respectively (Elderfield and Greaves, 1983; Greaves et al., 1989; Klinkhammer et al., 1994; Stetzenhach et al., 1994). The REEs were then eluted from the columns using 8 M ultra-pure HNO_3 (Seastar Chemicals, Baseline) and collected in Teflon® beakers. The eluant was subsequently taken to dryness by heating the Teflon® beakers on a hot plate, and the residue then redissolved in 10 mL of a 1% v/v ultra-pure HNO_3 solution. Each

10 mL sample was then spiked with 10 ppb of ^{115}In as an internal standard to monitor instrument drift, which varied less than ± 10%, and analyzed for the REEs by high resolution (magnetic sector) inductively coupled plasma mass spectrometry (HR-ICP-MS, Finnigan MAT Element II) at Tulane University.

We monitored ^{139}La, ^{140}Ce, ^{141}Pr, ^{143}Nd, ^{145}Nd, ^{146}Nd, ^{147}Sm, ^{149}Sm, ^{151}Eu, ^{153}Eu, ^{155}Gd, ^{157}Gd, ^{158}Gd, ^{159}Tb, ^{161}Dy, ^{163}Dy, ^{165}Ho, ^{166}Er, ^{167}Er, ^{169}Tm, ^{172}Yb, ^{173}Yb, and ^{175}Lu (low- and medium-resolution mode) as many of these isotopes are free of isobaric interferences, and because monitoring more than one isotope provides an additional check for potential interferences (Stetzenbach et al., 1994; Shannon and Wood, 2005). In addition, the Eu isotopes and the HREEs were also monitored in high resolution mode, which allowed us to resolve interferences on ^{151}Eu and ^{153}Eu from BaO^+ species formed in the plasma stream, and $LREEO^+$ and middle $REEO^+$ ($MREEO^+$) species on the HREEs. The HR-ICP-MS was calibrated and the concentrations of REEs in the samples confirmed with a series of REE calibration standards of known concentrations (1 ng kg^{-1}, 2 ng kg^{-1}, 5 ng kg^{-1}, 10 ng kg^{-1}, 100 ng kg^{-1}, 500 ng kg^{-1}, and 1000 ng kg^{-1}). The calibration standards were prepared from NIST traceable High Purity Standards (Charleston, SC). In addition, check standards were prepared using Perkin Elmer multi-element solutions and the NIST Standard Reference Material (SRM) "Trace Elements in Water No. 1643b and the National Research Council Canada (Ottawa, Ontario, Canada) SMR for river waters (SRLS-3) were analyzed for each sample run to check for accuracy (Tang and Johannesson, 2006). Analytical precision of the REE analyses was always better than 4% relative standard deviation (RSD), and generally better than 2% RSD.

2.3.4 Sequential extraction analysis

The methods used for sequential extraction of REEs from Aquia aquifer sediments are based on the methods of Tessier et al. (1979). The sequential extraction procedure provides a semi-quantitative tool to evaluate the solid-phase speciation of metals, such as the REEs, with operationally defined sediment/mineral phases. These phases include an exchangeable phase, an acidic phase, a reducible phase, an oxidizable phase, and the residual phase. It is important to note that sequential extraction techniques are subject to possible artifacts in the results that arise from incomplete dissolution and/or readsorption of trace elements, and thus should be viewed with caution (e.g., Tipping et al., 1985; Sholkovitz, 1989). Nonetheless, sequential extraction procedures can provide useful semi-quantitative information regarding the speciation of trace elements within aquifer sediments.

With regards to the sequential extraction procedure used here, the exchangeable phase refers to trace elements weakly associated with clays, hydrated oxides of iron and manganese, and humic substances that are readily mobilized by changes in ionic strength. The acidic phase represents the trace elements bound to sediment carbonates, which are susceptible to carbonate dissolution as sediments are leached with a weak acid. The trace elements bound to iron and manganese oxides are considered to be within the reducible phase. These trace elements will be released as Fe/Mn oxides are reduced and solubilized under anoxic conditions. The oxidizable phases represent trace elements that are released to solution when the sediment is subjected to a strong oxidizer. Such trace elements are likely to be either in the sediments in the form of metal sulfides, or bound to sedimentary organic matter. Finally, the residual phase refers to the trace elements held

within the crystal structure of primary and secondary silicate minerals within the sediments. Trace elements within the crystalline structure of these silicate minerals are not expected to be released into the solution over a reasonable time span under natural conditions. Below, we outline the procedure for each extraction, which was performed on Aquia sediment samples from 61, 72, and 86.5 mbgs.

Before sequential extraction, the sediment samples were ground in an aluminum oxide mortar and pestle and then further reduced in size by passing the ground sediment sample through a 1 mm sieve, to achieve a particle size less than 1 mm.

Fraction 1: A 0.5 gm (dry weight) aliquot of each sediment sample was placed into an acid-washed 50 mL centrifugation tube (Fisher Scientific), along with 8 mL of 1 M CH_3COONa reagent (pH 8.2) at room temperature (23±1ºC). The mixture was subsequently agitated for 1 hour on a shaker (VWR Mini Shaker), and then centrifuged (Labofuge 400, Heraeus Instruments) for 10 minutes at 2000 rpm. The resultant supernatant was filtered (0.4 μm membrane Nuclepore® filters), acidified with ultrapure HNO_3 (Seastar Chemical, Baseline), and stored at 4˚C prior to analysis. The residue was then washed with 8 mL of ultrapure Milli-Q water (18.2 Ω-cm) and centrifuged for 10 minutes at 2000 rpm. This supernatant was discarded and the residual sediment was used for the subsequent extraction steps.

Fraction 2: The sediment residue from fraction 1, contained in a 50 mL centrifugation tube, was leached at room temperature with 8 mL of 1M CH_3COONa. The pH was adjusted to 5.0 with CH_3COOH. The mixture was subsequently agitated for 5 hours on the Mini Shaker.

Fraction 3: The sediment residue from fraction 2, contained in a 50 mL centrifugation tube, was extracted with 20 mL of 0.04 M $NH_2OH{\cdot}HCl$ in 25% (v/v) CH_3COOH for 6 hours at 96 ± 1˚C. The mixture was agitated every 30 minutes.

Fraction 4: The sediment residue from fraction 3, contained in a 50 mL centrifugation tube, was extracted with 3 mL of 0.02 M HNO_3 and 5mL of 30% H_2O_2. The pH was adjusted to 2.0 with ultrapure HNO_3. The mixture was heated to 85 ± 1˚C for 2 hours with occasional agitation. Next, 3 mL of 30% H_2O_2, adjusted to pH 2.0 with ultrapure HNO_3, was added to the mixture and heated to 85 ± 1˚C for 3 hours with occasional agitation. After cooling the mixture to room temperature, 5 mL of 3.2 M CH_3COONH_4 in 20% (v/v) HNO_3 was added and the mixture was diluted to 20 mL. The mixture was subsequently agitated for 30 minutes on the Mini Shaker.

Fraction 5: The sediment residue from fraction 4 was subsequently digested in a 50 mL Teflon® beaker with 10 mL of ultrapure HF (Seastar, Baseline) and the mixture was evaporated to near dryness. Next, 10 mL of HNO_3 was added to the remaining residue and the mixture was evaporated to near dryness. Finally, another 10 mL of ultrapure HF was added to the remaining residue and the mixture was evaporated to near dryness. The resulting residue was then redissolved in 1% (v/v) ultrapure HNO_3 and diluted with ultrapure Milli-Q water up to 25 mL. The resulting solution was subsequently acidified as described above.

Between each of the above fractions, the resulting sediment-reagent slurries were centrifuged, filtered, and acidified. The residues were washed with minimal amounts (8 mL) of ultrapure Milli-Q water to avoid excessive solubilization of solid material, particularly organic matter.

Initial Sediment Digestion: A 0.2 gm (dry weight) aliquot of each sediment sample was digested according to the same procedure as fraction 5. The resulting residue was then dissolved and diluted with ultrapure Milli-Q water up to 25 mL. The resulting solution was subsequently acidified as described above.

Concentrations of REEs from the sequential extraction procedure were analyzed by ICP-MS (Perkin Elmer/ Sciex Elan DRC II) at The University of Texas at Arlington (UTA)by monitoring ^{139}La, ^{140}Ce, ^{141}Pr, ^{143}Nd, ^{145}Nd, ^{146}Nd, ^{147}Sm, ^{149}Sm, ^{151}Eu, ^{153}Eu, ^{155}Gd, ^{157}Gd, ^{158}Gd, ^{159}Tb, ^{161}Dy, ^{163}Dy, ^{165}Ho, ^{166}Er, ^{167}Er, ^{169}Tm, ^{172}Yb, ^{173}Yb, and ^{175}Lu as described above. The instrument was calibrated using a series of calibration standards of known concentration ranging from 99.57 ppb to 0.009893 ppb.

2.3.5 Glauconite extraction analysis

The Aquia aquifer sediments contain a substantial amount of glauconite (Hansen, 1974; Chapelle, 1983; Haque et al., 2008). Consequently, two 0.5 (dry weight) aliquots of glauconite grains/pellets from 65 mbgs and another from 104 mbgs were hand-picked and separated from the bulk sediments using stainless steel forceps for REE analysis. The glauconite grains/pellets were next placed in a 50 mL Teflon® beaker and rinsed three times with ultrapure Milli-Q water. The grains/pellets were then air dried in a Class 100 Laminar flow bench. The dried grains/pellets were then digested with 10 mL of ultrapure HF and the mixture was evaporated to near dryness. Next, 10 mL of ultrapure HNO_3 was added to the remaining residue and the mixture was evaporated to near dryness. Finally, another 10 mL of ultrapure HF was added to the remaining residue and the mixture was evaporated to near dryness. The resulting residue was then redissolved and diluted with ultrapure Milli-Q water up to 25 mL. The resulting solution was

subsequently centrifuged, filtered, and acidified as described above and analyzed for REE as described above by ICP-MS at Tulane University.

2.3.6 Speciation Modeling

Speciation of the REEs in Aquia aquifer groundwaters was modeled using a version of Humic Ion-Binding Model V, originally developed by Tipping and co-workers (Tipping and Hurley, 1992; Tipping, 1993, 1994), and subsequently modified to allow for predictions of REE complexation with both inorganic and organic ligands (Tang and Johannesson, 2003). Model V was employed because the majority of the important model parameters (n_A, pK_A, pK_B, ΔpK_A, ΔpK_B, P, f_{pr}, pK_{MHB}) have been established and separately fixed for humic and fulvic acids, and because Model V has been widely validated for many trace elements including some of the 14 naturally occurring REEs (Tipping, 1993; Lead et al., 1998). Consequently, only one parameter, pK_{MHA}, is required to fit the model predictions to metal binding data (Tipping, 1993). The pK_{MHA} parameter is the intrinsic equilibrium constant for metal-proton exchange reactions involving type A sites on the model humic substances (see Tipping, 2002; Tang and Johannesson, 2003). The pK_{MHA} parameters were previously estimated using linear free-energy relationships between the pK_{MHA} values for other trace elements in the Model V database, and first hydrolysis constants and stability constants for these metals with lactic and acetic acid (Martell and Smith, 1977; Tang and Johanneson, 2003). We further modified the Model V data base by inclusion of stability constants describing REE complexation with inorganic ligands (Lee and Byrne, 1992; Schijf and Byrne, 1999, 2004; Klungness and Byrne, 2000; Luo and Byrne, 2000, 2001, 2004). We note that although Model V has

been updated (Model VI, Tipping, 1998), the new code does not result in significantly different speciation results compared to Model V (Lead et al., 1998).

2.4 Results

2.4.1 Groundwater chemistry

Field measurements (i.e. pH, temperature, conductivity, Eh, DOC, alkalinity, iron speciation, and sulfide concentrations) are presented in Tables 2.1 and 2.2 and major solute data is presented in Table 2.3 for Aquia aquifer groundwaters collected from the two flow paths on the Eastern and Western shores of the Chesapeake Bay (Fig. 2.1). Concentrations of REEs in Aquia aquifer groundwaters from the Eastern and Western shores flow paths are presented in Table 2.4. Our data indicates that the Aquia groundwaters are neutral to slightly alkaline, with the pH values ranging between 7.6 and 8.4 for the groundwaters collected from the Eastern Shore flow path, and between 7.8 and 9.7 for groundwaters from the Western Shore. On the Eastern Shore, alkalinity, expressed as HCO_3, displays an overall increasing trend with flow down-gradient along the flow path, whereas the calculated alkalinity (i.e., based on charge balance; Lyons et al., 1992; Goldsmith et al., 2010) of the Western Shore groundwaters show less variation and exhibit an overall decreasing trend along the flow path (Fig. 2.2).

For groundwaters from the Eastern Shore, total iron (Fe_T) concentrations range from below detection to 18 μmol kg^{-1}, Fe(II) concentrations range from below detection to 9.9 μmol kg^{-1}, and Fe(III) concentrations range from below detection to 14.5 μmol kg^{-1}. On the Western Shore, total iron (Fe_T) concentrations in groundwaters range from 0.25 to 5.3 μmol kg^{-1}, Fe(II) concentrations range from below detection to 5.3 μmol kg^{-1}, and Fe(III) concentrations range from below detection to 8.7 μmol kg^{-1}. Iron

concentrations are much greater in groundwaters from the Eastern Shore flow path (mean ± SD Fe_T = 10.6 ± 4.7 μmol kg^{-1}) than groundwaters from the Western Shore flow path (mean ± SD Fe_T = 1.9 ± 1.4 μmol kg^{-1}). The iron speciation data for groundwaters from the Eastern Shore of the Aquia shows a sharp transition from Fe(III) to Fe(II) around 52 km down-gradient along the flow path (Fig. 2.2; Haque et al., 2008).

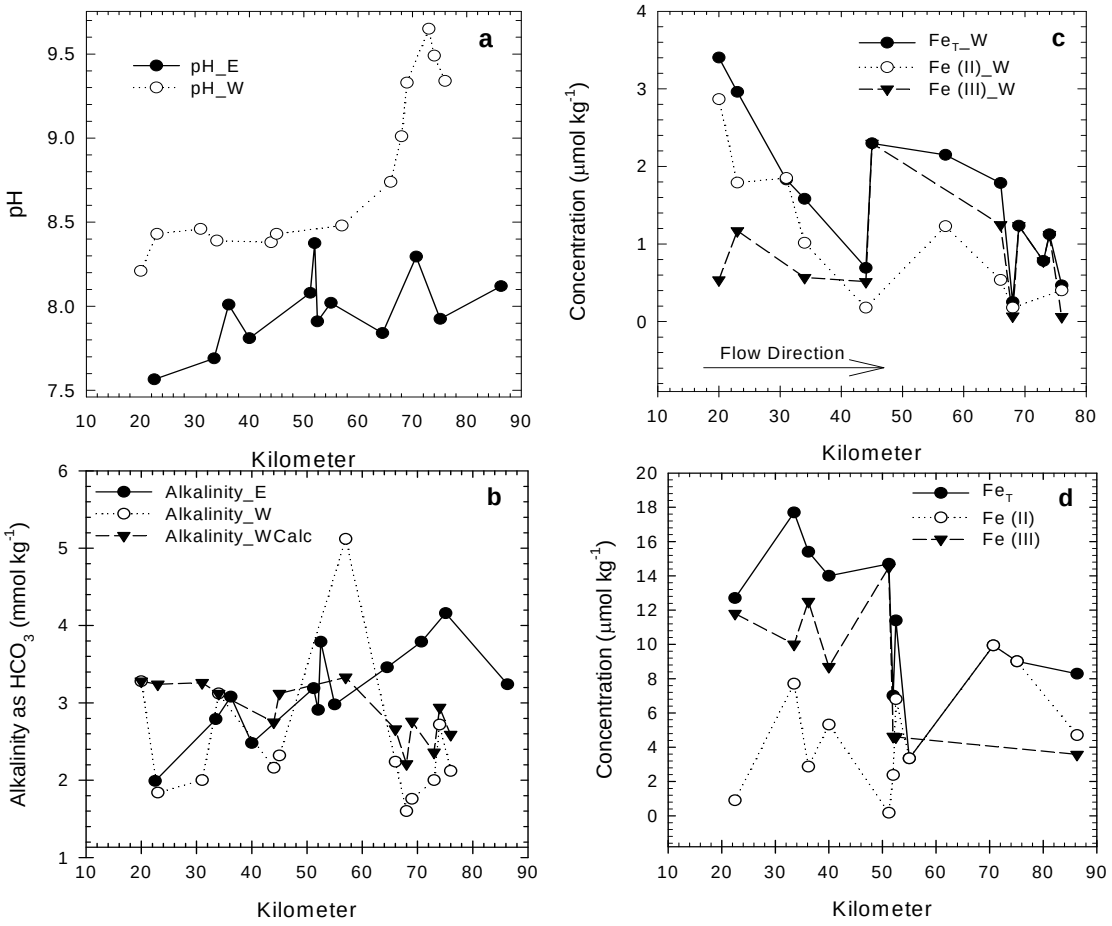

Figure 2.2. Aquia aquifer data: (a) pH; (b) alkalinity; (c) Fe speciation on the Western shore; (d) Fe speciation on the Eastern shore as a function of distance from the recharge zone.

Dissolved oxygen (DO) concentrations range between 9.4 and 51 μmol kg^{-1} on the Eastern shore and between 32.3 and 464 μmol kg^{-1} on the Western shore. Dissolved oxygen concentrations are slightly higher on the Western shore than the Eastern shore, except at well CA 88-3340 on the Western shore, were the DO concentration is 464 μmol

kg^{-1} (Fig. 2.3). Dissolved S(-II) concentrations range from below detection to 0.40 μmol kg^{-1} on the Eastern shore concentrations range from below detection to 1.8 μmol kg^{-1} on the Western shore. In general, S(-II) concentrations remain low along both shores of the flow path, such that 16 out of the 25 wells sampled were below the detection limit (Fig. 2.3).

Table 2.1. Hydrogeochemical data for groundwaters from the Aquia aquifer.

Sample	Distance km	pH	Temp °C	Cond mScm	Eh mV	TDS mg kg^{-1}	DO μmol kg^{-1}	Alkalinity (HCO_3) mmol kg^{-1}
Eastern Shore Wells								
KE 66-0125	22.5	7.57	16.6	222	25.5	143	51.0 ± 1.80	1.99
QA 88-1277	33.5	7.69	15.6	296	44.0	189	13.5 ± 0.21	2.79
QA 94-1322	36.2	8.01	18.6	330	-11.0	211	19.6 ± 0.10	3.08
QA 88-1268	51.2	8.08	16.7	303	-10.5	194	16.8 ± 0.07	3.19
SHA	52	8.38	19.7	305	-46.0	196	21.4 ± 0.11	2.91
QA 94-0111	52.5	7.91	16.2	366	-3.00	234	11.1 ± 0.05	3.79
QA 95-0611	55	8.02	16.1	302	-18.0	194	50.0 ± 0.00	2.98
QA 73-3626	64.5	7.84	16.9	351	27.5	213	23.3 ± 0.12	3.46
QA 81-2298	70.7	8.30	17.5	296	-11.0	189	20.3 ± 0.05	3.79
QA 92-0451	75.1	7.93	17.8	422	11.5	267	12.0 ± 0.10	4.16
QA EB 144	86.3	8.12	15.9	366	-53.0	271	9.38 ± 0.08	3.24
Western Shore Wells								
PG-81-1249	20	8.21	16.2	293	-1.0	187	82.3 ± 1.80	3.28
CA-94-2719	23	8.43	15.6	300	-25.0	192	53.1 ± 0.00	1.84
PG-81-0721	31	8.46	16.5	282	43.0	181	85.4 ± 1.80	2.00
CA-73-3395	34	8.39	17.7	282	-15.0	181	139 ± 1.80	3.12
AA DE 218[a]	40	7.81	14.5	300	60.5	192	124 ± 1.80	2.48
CH-94-3169	44	8.38	17.2	257	3.0	165	32.3 ± 1.80	2.16
CH-94-1194	45	8.43	16.9	293	23.0	188	95.8 ± 3.61	2.32
CH-94-2436	57	8.48	18.5	290	-11.0	185	107 ± 1.80	5.12
SM-94-2523	66	8.74	15.8	239	-58.0	153	78.1 ± 0.00	2.24
SM-92-0701	68	9.01	17.3	214	-84.0	137	63.5 ± 1.80	1.60
CA-88-3340	69	9.33	18.9	239	88.0	152	464 ± 1.80	1.76
SM-81-0060	73	9.65	18.4	228	-159.0	146	69.8 ± 1.80	2.00
CA-94-0409	74	9.49	18.9	271	-120.0	174	72.9 ± 1.80	2.72
SM-81-2634	76	9.34	19.3	284	115.0	182	72.9 ± 1.80	2.12

*Alkalinity values in parenthesis were calculated based on charge balance (Lyons et al., 1992; Goldsmith et al., 2010).

[a] This well was sampled during the 2006 field sampling campaign.

Dissolved NO_3^- concentrations range from below detection to 3.2 μmol kg^{-1} on the Eastern shore and from below detection to 2.4 μmol kg^{-1} on the Western shore. Dissolved NO_3^- concentrations remain relatively low along the flow path for both shores, with the highest concentration on the Eastern shore at 52 km (State Hwy Admin well) and on the Western shore at 57 km (CH 94-2436 well) (Fig. 2.3). Dissolved NH_4^+

concentrations range from 0.42 to 15 μmol kg^{-1} on the Eastern shore and from below detection to 17 μmol kg^{-1} on the Western shore. As groundwater flows along the Eastern Shore flow path, the dissolved NH_4^+ concentrations exhibit higher concentrations beyond 36 km (Fig. 2.3). Measured Eh values range between -53 to 44 mV on the Eastern shore and between -159 to 115 mV on the Western shore (Fig. 2.3).

2.4.2 REE Concentrations

Rare earth element concentrations in the Aquia are low but relatively similar to other circumneutral pH groundwaters (e.g.; Johannesson et al., 1997a, 1999; Tang and Johannesson, 2006) (Table 2.4). On the Eastern shore of the Aquia, neodymium concentrations range from 56.3 pmol kg^{-1} to 71.4 pmol kg^{-1}, and exhibit a mean concentration of 65.0 ± 4.8 pmol kg^{-1}. Neodymium concentrations on the Western shore are fairly similar with a range of 41.5 pmol kg^{-1} to 77.9 pmol kg^{-1} and a mean concentration of 56.7 ± 11.1 pmol kg^{-1}. Groundwaters that exhibit high Fe(II) concentrations (e.g., QA 92-0451 on the Eastern shore and CA 94-2719 on the Western shore) have high neodymium concentrations (71.4 and 77.9 pmol kg^{-1}, respectively); whereas, groundwaters that exhibit low Fe(II) concentrations (e.g., KE 66-0125 on the Eastern shore and SM 81-2634 on the Western shore) have low neodymium concentrations (56.3 and 43.2 pmol kg^{-1}, respectively).

Shale-normalized REE patterns are shown in Fig. 2.4 for groundwaters from both studied flow paths within the Aquia aquifer. Again, the Aquia aquifer groundwater REE concentrations are normalized to the North American Shale Composite (Haskin et al., 1968; Taylor and McLennan, 1985). All of the Aquia aquifer groundwaters from both flow paths studied have strikingly similar NASC-normalized REEs patterns (Fig. 2.4).

The average Eastern Shore groundwater pattern for Yb/Nd_{NASC} was 0.76 ± 0.12 and the groundwater pattern for the Western Shore Yb/Nd_{NASC} was 0.72 ± 0.11. Furthermore, all but one sample exhibits a slight enrichment in the LREEs relative to the HREEs when compared to NASC (Figs. 2.4, 2.5).

2.4.3 Speciation model results

The results of the speciation modeling for groundwaters from the Eastern Shore flow path of the Aquia aquifer are presented in Fig. 2.6, whereas those for the Western Shore flow path are plotted in Fig. 2.7. The model predicts that the REEs are predominantly complexed with carbonate ions in Aquia aquifer groundwater, i.e., $LnCO_3^+$ and $Ln(CO_3)_2^-$, where Ln indicates any of the 14 naturally occurring lanthanides (i.e., rare earth elements). For the majority of the Aquia aquifer groundwaters, the model predicts that the dicarbonato complex is the chief form of dissolved REE in solution, and further that this species, $Ln(CO_3)_2^-$ increases in importance with increasing atomic number across the REE series and with increasing pH. The only exceptions include the lower pH waters from wells KE 66-0125 (pH 7.57) and to a lesser extent AA De-218 (pH 7.81) where carbonato complexes account for significant fractions of the LREEs in solution (Figs. 2.6, 2.7). Free metal ions, Ln^{3+}, account for ~4% of the La in groundwater from KE 66-0125, and slightly more than 1% of La in groundwater from the AA De-218 well. In all other groundwater samples modeled, the free metal ion and all other potential aqueous complexes including REE complexed with dissolved organic ligands are predicted to account for much less than 1% of each REE in solution (Figs. 2.6, 2.7).

Table 2.2 Concentrations and speciation data for dissolved Fe, S(-II), Mn, N, and Si of groundwaters from the Aquia aquifer.

Sample	Distance (km)	Fe Total μmol kg-1	Fe (II) μmol kg-1	Fe (III) μmol kg^{-1}	S(-II) μmol kg^{-1}	Si mmol kg^{-1}	Mn μmol kg^{-1}	NO_3^- μmol kg^{-1}	NH_4^+ μmol kg^{-1}	DOC mg kg^{-1}
Eastern Shore Wells										
KE 66-0125	22.5	12.7 ± 0.21	0.90 ± 0.03	11.8 ± 2.58	BDL	1.26 ± 0.05	1.02 ± 0.00	BDL	0.42 ± 0.19	0.24
QA 88-1277	33.5	17.7 ± 0.01	7.70 ± 0.00	10.0 ± 0.27	0.23 ± 0.18	0.41 ± 0.00	0.15 ± 0.01	0.48 ± 0.00	2.03 ± 0.19	0.33
QA 94-1322	36.2	15.4 ± 0.05	2.87 ± 0.10	12.5 ± 0.34	BDL	0.32 ± 0.00	BDL	1.13 ± 0.00	14.8 ± 0.00	--
QA 88-1268	51.2	14.7 ± 0.08	0.18 ± 0.00	14.5 ± 0.39	0.10 ± 0.18	0.44 ± 0.00	0.42 ± 0.01	0.32 ± 0.00	9.12 ± 0.93	--
SHA	52	7.01 ± 0.06	2.38 ± 0.10	4.63 ± 0.12	0.40 ± 0.02	0.24 ± 0.00	0.00 ± 0.00	3.23 ± 0.00	6.77 ± 0.00	0.50
QA 94-0111	52.5	11.4 ± 0.10	6.80 ± 0.10	4.60 ± 0.12	BDL	0.23 ± 0.00	BDL	0.00 ± 0.00	3.22 ± 0.00	--
QA 95-0611	55	3.35 ± 0.02	3.35 ± 0.09	BDL	BDL	0.57 ± 0.00	BDL	0.76 ± 0.09	4.83 ± 0.00	--
QA 73-3626	64.5	BDL	BDL	BDL	BDL	0.44 ± 0.00	0.44 ± 0.01	1.13 ± 0.00	7.73 ± 0.00	--
QA 81-2298	70.7	9.94 ± 0.27	9.94 ± 0.27	BDL	0.34 ± 0.03	0.20 ± 0.00	0.04 ± 0.01	0.65 ± 0.00	15.1 ± 0.00	--
QA 92-0451	75.1	9.01 ± 0.24	9.01 ± 0.24	BDL	BDL	0.38 ± 0.00	BDL	0.48 ± 0.00	9.02 ± 0.00	--
QA EB 144	86.3	4.71 ± 0.13	4.71 ± 0.13	3.58 ± 0.00	0.16 ± 0.00	0.22 ± 0.00	0.11 ± 0.01	0.48 ± 0.00	1.39 ± 0.19	1.32
Western Shore Wells										
PG-81-1249	20	3.40 ± 0.02	2.87 ± 0.18	0.54 ± 0.20	BDL	0.18 ± 0.00	0.02 ± 0.00	0.22 ± 0.00	11.35 ± 0.34	--
CA-94-2719	23	2.96 ± 0.01	1.79 ± 0.00	1.17 ± 0.01	BDL	0.16 ± 0.00	1.22 ± 0.03	1.83 ± 0.09	5.28 ± 0.00	--
PG-81-0721	31	1.83 ± 0.03	1.85 ± 0.10	BDL	BDL	0.21 ± 0.00	0.59 ± 0.01	1.56 ± 0.09	6.46 ± 0.00	--
CA-73-3395	34	1.58 ± 0.01	1.01 ± 0.10	0.57 ± 0.10	BDL	0.25 ± 0.00	BDL	0.48 ± 0.00	9.39 ± 0.00	--
AA DE 218[a]	40	5.32 ± 0.10	5.32 ± 0.10	8.70 ± 0.23	0.52 ± 0.18	0.37 ± 0.00	0.76 ± 0.02	0.32 ± 0.00	BDL	0.42
CH-94-3169	44	0.69 ± 0.01	0.18 ± 0.00	0.51 ± 0.01	BDL	0.18 ± 0.00	0.61 ± 0.01	0.43 ± 0.09	9.20 ± 0.34	--
CH-94-1194	45	2.30 ± 0.04	BDL	2.30 ± 0.04	BDL	0.21 ± 0.00	0.60 ± 0.00	BDL	14.09 ± 0.00	--
CH-94-2436	57	2.15 ± 0.01	1.23 ± 0.00	BDL	BDL	0.01 ± 0.00	BDL	2.42 ± 0.00	10.76 ± 0.34	--
SM-94-2522	66	1.77 ± 0.11	0.54 ± 0.00	1.25 ± 0.11	BDL	0.15 ± 0.00	0.41 ± 0.01	0.48 ± 0.00	12.33 ± 0.00	--
SM-92-0701	68	0.25 ± 0.02	0.18 ± 0.00	0.07 ± 0.02	0.28 ± 0.00	0.18 ± 0.00	0.40 ± 0.00	0.48 ± 0.00	9.98 ± 0.00	--
CA-88-3340	69	1.24 ± 0.06	BDL	1.24 ± 0.06	1.81 ± 0.00	0.18 ± 0.00	0.31 ± 0.00	0.81 ± 0.00	9.39 ± 0.00	--
SM-81-0060	73	0.78 ± 0.01	BDL	0.78 ± 0.01	BDL	0.16 ± 0.00	1.41 ± 0.01	0.48 ± 0.00	7.24 ± 0.34	--
CA-94-0409	74	1.12 ± 0.01	BDL	1.12 ± 0.01	BDL	0.23 ± 0.00	0.32 ± 0.01	0.97 ± 0.00	17.22 ± 0.68	--
SM-81-2634	76	0.47 ± 0.00	0.40 ± 0.00	0.06 ± 0.00	0.07 ± 0.02	0.12 ± 0.00	0.54 ± 0.01	2.15 ± 0.09	6.65 ± 0.34	--

[a]This well was sampled during the 2006 field sampling campaign.
BDL denotes below detection limit.

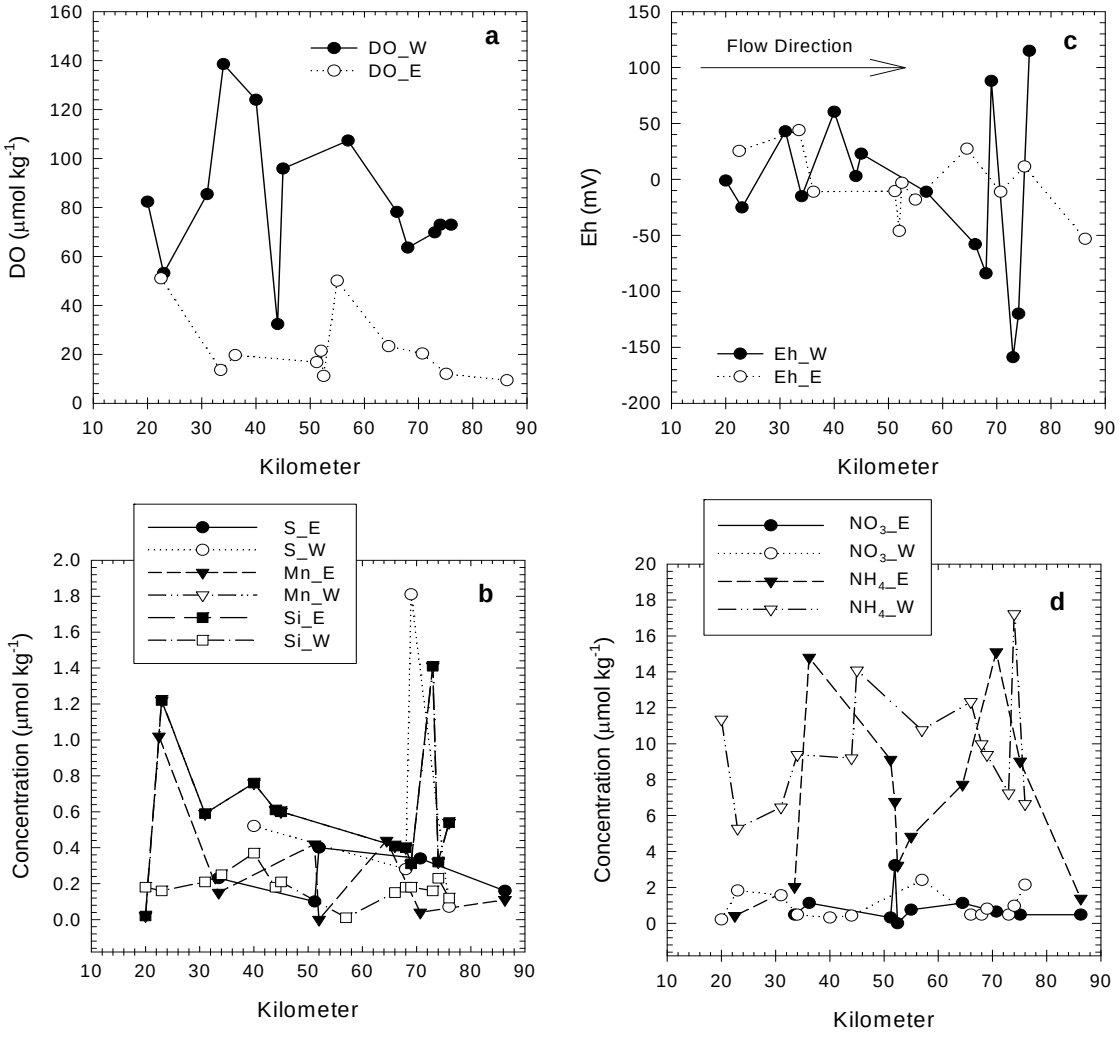

Figure 2.3 Aquia aquifer data: (a) dissolved oxygen; (b) S(-II), Mn, and Si; (c) Eh; (d) N speciation as a function of distance from the recharge zone.

Table 2.3 Concentrations of major solutes (in mmol kg^{-1}) of groundwaters from the Aquia aquifer, Maryland.

	Distance (km)	Ca	Mg	Na	K	Cl	SO_4
Eastern Shore Wells							
KE 66-0125	22.5	0.925	0.083	0.085	0.056	0.105	0.127
QA 88-1277	33.5	1.42	0.137	0.179	0.072	0.062	0.077
QA 94-1322	36.2	0.943	0.647	0.382	0.313	0.026	0.028
QA 88-1268	51.2	0.715	0.601	0.484	0.362	0.022	0.039
SHA	52	0.317	0.230	2.39	0.152	0.043	0.042
QA 94-0111	52.5	0.985	0.752	0.347	0.393	0.053	0.058
QA 95-0611	55	0.810	0.532	0.355	0.323	0.039	0.071
QA 73-3626	64.5	1.25	0.525	0.358	0.239	0.057	0.041
QA 81-2298	70.7	0.669	0.548	0.607	0.363	0.038	0.054
QA 92-0451	75.1	0.733	0.583	2.13	0.306	0.041	0.050
QA EB 144	86.3	1.23	0.313	1.83	0.060	0.000	0.077
Western Shore Wells							
PG-81-1249	20	1.18	0.375	0.175	0.148	0.036	0.065
CA-94-2719	23	0.993	0.520	0.216	0.206	0.017	0.090
PG-81-0721	31	0.865	0.621	0.216	0.294	0.031	0.088
CA-73-3395	34	0.806	0.544	0.181	0.300	0.018	0.118
AA DE 218[a]	40	1.60	0.054	0.037	0.087	0.070	0.052
CH-94-3169	44	0.582	0.593	0.303	0.374	0.018	0.120
CH-94-1194	45	0.638	0.667	0.325	0.414	0.020	0.106
CH-94-2436	57	0.528	0.565	0.862	0.429	0.046	0.042
SM-94-2522	66	0.270	0.226	1.49	0.378	0.042	0.075
SM-92-0701	68	0.213	0.123	1.59	0.215	0.031	0.111
CA-88-3340	69	0.084	0.024	2.50	0.162	0.055	0.061
SM-81-0060	73	0.101	0.038	2.11	0.191	0.064	0.075
CA-94-0409	74	0.082	0.027	2.78	0.142	0.058	0.063
SM-81-2634	76	0.055	0.020	2.55	0.134	0.060	0.084

[a] This well was sampled during the 2006 field sampling campaign.

Table 2.4 Concentrations of REEs in (pmol kg^{-1}) of groundwaters from the Aquia aquifer.

Eastern Shore Wells

	KE 66-0125	AA De-218	AA De-218 Dup	QA 88-1268	QA 95-0611	QA 81-2298	QA 81-2298 Dup	QA 92-0451	QA Eb-144
La	76.9	151.7	54.5	69.4	116.8	52.2	52.8	106.6	89.3
Ce	93.1	106.3	91.8	92.9	103.6	97.8	99.5	158.7	100.0
Pr	8.5	7.9	6.2	6.7	7.7	7.1	7.3	10.7	6.6
Nd	56.3	68.4	62.0	65.9	71.0	62.8	63.2	71.4	64.0
Sm	8.3	9.2	8.1	6.1	9.7	6.0	6.1	7.6	9.8
Eu	2.3	2.4	1.4	4.1	2.4	0.9	0.8	1.3	7.4
Gd	8.1	8.8	7.5	8.5	8.2	6.8	7.0	8.2	7.9
Tb	2.3	2.1	2.0	2.0	2.2	2.2	2.0	2.5	1.8
Dy	6.1	11.9	10.7	11.1	12.8	12.0	11.7	13.4	10.1
Ho	1.3	1.2	0.96	1.1	1.3	1.1	1.1	1.5	1.00
Er	3.5	4.5	3.87	3.89	4.60	4.26	4.43	5.81	3.84
Tm	0.72	0.63	0.51	0.53	0.63	0.56	0.49	0.77	0.50
Yb	3.1	3.6	3.2	3.5	4.0	3.9	3.9	5.6	3.5
Lu	0.75	0.61	0.54	0.65	0.67	0.65	0.64	0.98	0.62
$(Yb/Nd)_{NASC}$	0.7	0.67	0.65	0.67	0.72	0.8	0.78	1.0	0.69

Western Shore Wells

	PG 81-1249	CA 94-2719	PG 81-0721	CA 73-3395	CH 94-3169	CA 94-1194	SM 94-2523	SM 92-0701	SM 81-0060	SM 81-2634
La	78.7	50.9	58.4	41.4	53.9	43.7	125.8	41.2	39.5	58.6
Ce	108.8	99.4	104.6	63.4	90.0	85.3	105.4	76.9	73.0	65.0
Pr	7.1	6.9	7.2	4.3	6.1	6.0	8.1	5.6	5.7	4.8
Nd	65.4	77.9	62.6	41.5	54.5	59.2	62.1	52.3	48.6	43.2
Sm	8.9	10.0	6.0	4.1	5.2	5.1	7.2	4.8	4.7	4.2
Eu	7.5	0.96	1.9	1.0	0.71	0.72	1.9	0.63	0.82	0.54
Gd	7.8	5.5	5.9	3.9	5.0	6.2	7.9	5.6	7.9	4.9
Tb	1.7	2.0	1.8	1.2	1.7	2.0	2.1	2.0	2.5	1.6
Dy	10.7	11.0	11.0	7.3	9.9	11.5	11.9	10.6	11.9	8.5
Ho	1.0	1.0	1.0	0.69	0.96	1.1	1.2	0.96	1.0	0.78
Er	3.9	3.9	3.8	2.6	3.7	4.1	4.6	3.8	4.1	3.1
Tm	0.50	0.47	0.48	0.32	0.45	0.51	0.58	0.44	0.47	0.37
Yb	3.8	3.2	3.0	2.1	3.3	3.6	3.7	2.8	3.4	2.4
Lu	0.67	0.52	0.53	0.33	0.57	0.63	0.57	0.53	0.54	0.40
$(Yb/Nd)_{NASC}$	0.75	0.52	0.61	0.63	0.77	0.77	0.76	0.69	0.9	0.72

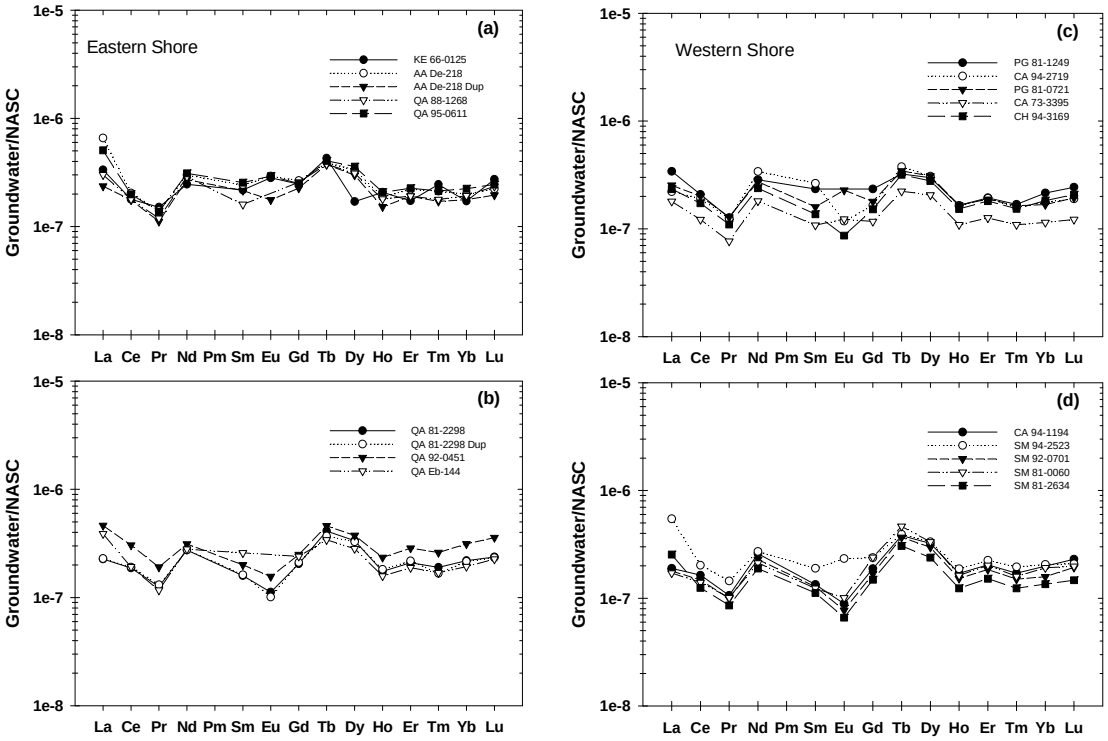

Figure 2.4 Shale-normalized REE patterns for groundwaters from the Aquia aquifer, Maryland; (a) and (b) eastern shore wells, August 2006; (c) and (d) western shore wells, June 2007. The shale composite used for normalization is the North American Shale Composite, for which the values of the REEs (in ppm) are: La (32); Ce (73); Pr (7.9); Nd (33); Sm (5.7); Eu (1.24); Gd (5.2); Tb (0.85); Dy (5.8); Ho (1.04); Er (3.4); Tm (0.5); Yb (2.8); and Lu (0.48) (Haskin et al., 1968; Taylor and McLennan, 1985).

2.4.4 Sequential extraction and glauconite extraction of Aquia sediments

The results of the sequential extraction analysis of the three samples of Aquia aquifer sediments are presented in Tables 2.5 and 2.6. In addition, Fig. 2.8 shows the shale-normalized REE patterns for each of the extraction phases and the residual phase for the three Aquia aquifer sediment samples. Figure 2.9 presents the percent-weighted amount that each fraction contributes to the overall REE inventory in the sediment samples. An outstanding feature of the sequential extraction data is that for each sediment depth sampled of Aquia aquifer, the majority of the total REE content of Aquia aquifer sediments occurs in the acidic phase (i.e., Fraction 2). As discussed above, the acidic

phase generally consists of carbonate minerals that are readily dissolved by leaching with a weak acid (i.e., acetic acid). These results suggest that the ubiquitous shell fragments that characterize large portions of the Aquia aquifer are the largest reservoir of REEs in the aquifer sediments.

Substantial amounts of La, Ce (86.5 mbgs), and the other REEs are also associated with the oxidizable phase, Fraction 4, which presumably reflects metal sulfides or sedimentary organic matter. Up to 30% of the LREEs in the Aquia aquifer sediments are associated with the exchangeable phase, Fraction 1, and this fraction generally decreases with increasing atomic number across the REE series (Fig. 2.9). Again, the exchangeable phase likely reflects REEs that are weakly adsorbed to surface sites on clays and/or metal oxide/oxyhydroxides within the sediments. The greater association of LREEs compared to the HREEs with the exchangeable phase of the Aquia aquifer sediments is consistent with the larger degree of adsorption reported for LREEs than HREEs for aqueous solutions like Aquia aquifer groundwaters with strong REE-complexing ligands such as carbonate ions (Koeppenkastrop and DeCarlo, 1992, 1993; Tang and Johannesson, 2005b; Quinn et al., 2006). Finally, REEs associated with the residual fraction, Fraction 5 (i.e., silicates), of Aquia aquifer sediments represents a relatively small percentage of the REEs within these sediments that is similar to the reducible fraction, Fraction 3 (Table 2.6). The relatively low amounts of REEs in the residual phases likely reflects the fact the quartz, which is the predominant silicate mineral in the aquifer sediments, generally exhibits low REE contents (e.g., Götze et al., 2004).

The results of the REE analyses of the glauconite samples from Aquia aquifer sediments (65 and 104 mbgs) are presented in Table 2.7, and plotted as shale-normalized ratios in Fig. 2.10. The REE content of glauconite separates from the two depths from the Aquia aquifer are remarkably similar, and exhibit an overall enrichment in the HREEs relative to LREEs such as Pr and Nd. The glauconite separates also possess substantial positive Ce anomalies, somewhat smaller, positive Eu anomalies, and relatively low Pr contents compared to La and Nd.

Table 2.5 Concentrations of extractable REEs (in μmol kg^{-1}) in sediment samples collected from the Aquia aquifer.

Sample Depth (m)	Element	F1	F2	F3	F4	F5
61	La	4.31	12.58	0.95	2.87	2.89
	Ce	7.14	34.67	3.85	6.92	14.32
	Pr	0.68	3.41	0.36	0.66	0.66
	Nd	3.06	15.07	1.67	2.72	2.91
	Sm	0.50	2.85	0.40	0.60	0.86
	Eu	0.14	0.56	0.07	0.11	0.34
	Gd	0.93	6.07	0.62	1.10	0.86
	Tb	0.09	0.50	0.06	0.10	0.08
	Dy	0.19	2.29	0.34	0.56	0.48
	Ho	0.06	0.38	0.06	0.10	0.08
	Er	0.12	1.32	0.20	0.32	0.27
	Tm	0.04	0.15	0.03	0.04	0.04
	Yb	0.07	1.09	0.24	0.33	0.31
	Lu	0.05	0.16	0.03	0.05	0.05
	$(Yb/Nd)_{NASC}$	0.29	0.92	1.84	1.55	1.36
72	La	17.31	25.05	1.00	32.37	1.45
	Ce	28.92	75.47	4.47	14.60	7.52
	Pr	2.81	7.42	0.37	1.29	0.27
	Nd	12.87	29.40	1.68	5.63	1.04
	Sm	1.84	5.92	0.39	1.18	0.45
	Eu	0.38	1.19	0.07	0.22	0.23
	Gd	3.02	9.96	0.56	1.89	0.39
	Tb	0.20	0.98	0.06	0.17	0.04
	Dy	0.66	4.98	0.32	0.98	0.31
	Ho	0.09	0.86	0.05	0.17	0.06
	Er	0.31	2.93	0.18	0.52	0.18
	Tm	0.02	0.36	0.03	0.07	0.03
	Yb	0.12	2.61	0.21	0.49	0.23
	Lu	0.02	0.38	0.03	0.07	0.03
	$(Yb/Nd)_{NASC}$	0.12	1.13	1.60	1.11	2.82
86.5	La	27.79	24.72	0.82	28.68	2.72
	Ce	38.92	55.65	15.47	40.95	22.97
	Pr	5.04	7.70	0.34	1.10	0.63
	Nd	24.80	34.93	1.69	5.49	3.06
	Sm	3.60	6.80	0.41	1.05	0.73
	Eu	0.73	1.49	0.08	0.18	0.32
	Gd	6.04	11.47	1.25	3.62	1.17
	Tb	0.40	1.16	0.06	0.15	0.08
	Dy	1.32	6.08	0.31	0.81	0.45
	Ho	0.16	1.02	0.05	0.13	0.07
	Er	0.58	3.35	0.17	0.42	0.25
	Tm	0.02	0.37	0.02	0.05	0.03
	Yb	0.18	2.67	0.18	0.39	0.28
	Lu	0.02	0.37	0.02	0.05	0.04
	$(Yb/Nd)_{NASC}$	0.09	0.98	1.36	0.91	1.17

Table 2.6 Fraction of REEs in Aquia sediments.

Sample Depth (m)	% Element	F1	F2	F3	F4	F5
	% La	18.26	53.29	4.04	12.15	12.25
	% Ce	10.68	51.82	5.75	10.35	21.40
	% Pr	11.82	59.17	6.18	11.39	11.44
	% Nd	12.05	59.26	6.57	10.69	11.43
	% Sm	9.50	54.68	7.73	11.51	16.58
	% Eu	11.46	46.07	6.06	8.67	27.74
61	% Gd	9.69	63.42	6.43	11.49	8.97
	% Tb	10.63	60.14	7.37	11.71	10.14
	% Dy	4.88	59.44	8.90	14.39	12.40
	% Ho	8.26	56.19	8.70	14.45	12.39
	% Er	5.23	59.36	8.84	14.39	12.18
	% Tm	14.24	48.68	9.60	14.57	12.91
	% Yb	3.34	53.59	11.59	16.21	15.28
	% Lu	13.98	48.63	10.03	13.68	13.68
	% La	22.42	32.46	1.30	41.94	1.88
	% Ce	22.08	57.62	3.41	11.14	5.74
	% Pr	23.10	61.07	3.04	10.61	2.18
	% Nd	25.42	58.08	3.32	11.12	2.05
	% Sm	18.81	60.52	4.01	12.03	4.62
	% Eu	17.97	56.97	3.35	10.54	11.16
72	% Gd	19.08	63.00	3.52	11.95	2.45
	% Tb	13.61	67.49	3.92	11.96	3.02
	% Dy	9.13	68.72	4.37	13.45	4.32
	% Ho	7.24	70.00	4.39	13.90	4.47
	% Er	7.41	71.08	4.33	12.73	4.45
	% Tm	3.23	72.18	5.24	13.91	5.44
	% Yb	3.23	71.35	5.80	13.44	6.19
	% Lu	3.23	72.49	5.69	12.52	6.07
	% La	32.80	29.18	0.96	33.85	3.20
	% Ce	22.37	31.99	8.89	23.54	13.20
	% Pr	34.04	51.99	2.30	7.45	4.22
	% Nd	35.44	49.93	2.42	7.84	4.38
	% Sm	28.62	54.01	3.23	8.33	5.81
	% Eu	26.20	53.22	2.68	6.47	11.44
86.5	% Gd	25.65	48.73	5.29	15.38	4.96
	% Tb	21.70	62.91	3.10	7.99	4.30
	% Dy	14.70	67.76	3.50	9.08	4.96
	% Ho	11.20	71.12	3.34	9.19	5.15
	% Er	12.20	70.25	3.48	8.85	5.22
	% Tm	4.05	75.30	3.85	10.53	6.28
	% Yb	4.96	72.13	4.96	10.47	7.47
	% Lu	4.27	74.39	4.47	9.35	7.52

Table 2.7 REE contents (in nmol kg-1) in glauconite separates from sediments from the Aquia aquifer.

	65 m	104 m
La	0.78	2.18
Ce	8878.92	3081.50
Pr	0.38	0.84
Nd	11.67	12.29
Sm	14.17	13.71
Eu	15.04	12.87
Gd	3.71	4.23
Tb	1.24	1.24
Dy	6.65	7.95
Ho	4.04	3.75
Er	13.32	11.50
Tm	8.65	7.16
Yb	16.37	13.41
Lu	11.01	9.01

2.5 Discussion

2.5.1 Groundwater geochemistry and redox conditions along flow the paths

Our geochemical analysis of Aquia aquifer groundwaters indicates that chemical composition, and to a lesser extent redox conditions, change along the flow path in agreement with earlier investigations (Chapelle, 1983; Chapelle and Knobel, 1983, 1985; Appelo, 1994; Haque et al., 2008). Chapelle (1983) demonstrated, for example, that groundwater chemistry along a flow path that is broadly consistent with our Western Shore flow path exhibited systematic changes with flow down-gradient, such that the flow path could be divided into three distinct regions. With groundwater flow from the recharge/outcrop area to approximately 42 km down-gradient along the flow path (i.e., region I of Chapelle, 1983), groundwater in the Aquia aquifer is characterized as a Ca-Mg-HCO_3 type water. With flow down-gradient beyond region I to roughly 80 km from the recharge zone (region II), Na concentrations increase as the concentrations of both Ca and Mg decrease, whereas the HCO_3 concentrations remain relatively constant (Chapelle,

1983). With continued flow down-gradient beyond ~80 km from the recharge zone (i.e., region III of Chapelle, 1983), Aquia aquifer groundwaters exhibit low concentrations of Ca and Mg but increasing concentrations of both Na and HCO_3. The major solute groundwater chemistry in region I predominantly reflects dissolution reactions involving carbonate shell fragments within the aquifer sediments. In region II, Chapelle (1983) argued that Ca and Mg produced by carbonate shell material dissolution in region I reacts with Na-rich glauconite in the sediments, leading to cation-exchange of this Na with Ca and Mg in the groundwater. In region III, the cation exchange reactions involving glauconite continue and dissolution of carbonate shell fragments again becomes important (Chapelle, 1983; Chapelle and Knobel, 1983; Purdy et al., 1996). In addition to these general geochemical reactions, the evolution of the major ion chemistry with flow down-gradient along the flow path within in the Aquia aquifer is consistent with the freshening of the aquifer as recharge waters of meteoric origin replace the original seawater that occupied the pore space when these marine sediments were deposited (Appelo, 1994). Indeed, freshening of the aquifer groundwater and sediments explains why cation-exchange is not significant in Region I as rapid dissolution of shell materials in the recharge area has stripped Na from glauconite by cation-exchange with Ca^{2+} and Mg^{2+} over the course of the Aquia aquifer's geologic history (Chapelle, 1983; Appelo, 1994).

Aquia aquifer groundwaters also exhibit increasing pH with flow down gradient along flow paths (Fig. 2.2). The increasing pH along the flow paths has previously been attributed to chemical weathering of glauconite and the dissolution of shell materials

within the aquifer sediments (Wolff 1967; Chapelle and Knobel, 1983; Chapelle, 1983; Haque et al., 2008). Alkalinity and specific conductance exhibit overall increasing trends with flow down gradient along the Eastern Shore flow path but remain relatively constant along the Western Shore flow path (Fig. 2.2, Table 2.1). These trends are generally consistent with chemical weathering of aluminosilicate (i.e., glauconite) and carbonate minerals within the aquifer sediments as well as microbial respiration (Chapelle, 1983; Chapelle and Knobel, 1983, 1985; Chapelle et al., 1987; Penny et al., 2003; Lee et al., 2007).

The measured Eh values are high in the region of the aquifer proximal to the recharge zone and generally decrease with flow down gradient beyond 34 km along both flow paths (Fig. 2.3). These measured Eh values are consistent with suboxic conditions along the majority of both studied flow paths. We note, however, that the Eh values exhibit large variations towards the end of the studied flow path on the Western Shore, which is also reflected in the alkalinity and Fe concentration measurements. The large variations in Eh along the lower reaches of the Western Shore flow path may indicate percolation of oxygenated meteoric water into this region of the aquifer via, for example, municipal wells as the population in this region exceeds that of the Eastern Shore. Alternatively, variations in Eh, alkalinity, and Fe concentrations along the lower reaches of the Western Shore flow path probably reflect multiple flow paths/flow lines within the aquifer (e.g., Basu et al., 2007). This hypothesis is supported by the fact that wells sampled along the lower reaches of the flow path are from St. Mary's County (wells identified by "SM") to the south of the Patuxet River and Calvert County (wells

identified with "CA") north of the river (Fig. 2.1). The distance between these wells transverse to the flow direction is as much as 30 km.

The Fe and dissolved S(-II) concentrations measured along the Aquia groundwater flow paths provide important insight into the redox reactions occurring within the aquifer. Specifically, the data suggests that Fe(III) reduction is the chief reaction that buffers the redox conditions along the flow path within the aquifer on the Eastern Shore (Haque et al., 2008). For example, around 52 km down gradient along the Eastern Shore flow path, a distinct transition in Fe speciation occurs from predominately Fe(III), presumably colloidal, to soluble Fe(II) (Fig. 2.2), which is consistent with redox conditions being buffered by Fe(III) reduction (Haque et al., 2008). The opposite appears to be the case for the Western Shore flow path where a shift from predominantly Fe(II) to Fe(III) in groundwater at 44 km along the flow path occurs. However, comparison of Fe concentrations and speciation for Western Shore groundwaters to those from the Eastern Shore reveals the Fe concentrations are substantially lower in groundwaters from the Western Shore flow path (Table 2.2; Fig. 2.2). Because the method detection limit for Fe_T and Fe(II) are 0.16 μmol kg^{-1} and 0.32 μmol kg^{-1}, respectively, we suggest that the Fe speciation data for the Eastern Shore groundwaters are more reliable than those of the Western Shore because of the substantially higher Fe values detected in Eastern shore groundwater. Nevertheless, assuming that the Fe_T concentrations measured in groundwaters from the Western Shore flow path are the most accurate representation of Fe concentrations along this flow path, these data indicate that Fe concentrations are highest nearest to the recharge zone and subsequently decrease with flow down gradient

along the flow path until ~ 44 km from the recharge zone. The decrease in Fe concentrations may reflect adsorptive processes (Haque et al., 2008) or precipitation of Fe(III) oxides/oxyhydroxides as these groundwaters are all oversaturated with respect to ferrihydrite, goethite, and hematite (mean ± SD $SI^{ferrihydrite}$ = 1.05 ±0.46, $SI^{goethite}$ = 6.67 ± 0.46, $SI^{hematite}$ = 15.3 ± 0.93). It should be noted that Aquia aquifer groundwater from the Eastern Shore are also oversaturated with respect to these Fe(III) oxides/oxyhydroxides (mean ± SD $SI^{ferrihydrite}$ = 2.11 ±0.24, $SI^{goethite}$ = 6.59 ± 0.25, $SI^{hematite}$ = 14.1 ± 0.5). With flow beyond 44 km, the Fe_T concentration roughly doubles, which may indicate Fe(III) reduction even though our measured Fe(II) are at or below detection. Iron concentration then generally decrease with flow down gradient along the flow path, reflecting either sorption, precipitation of Fe oxides, or possible siderite formation (see below).

Because dissolved S(-II) concentrations are at or below the detection limit in the majority of the Aquia groundwaters sampled (Table 2.2), sulfate reduction does not appear to occur along either of the studied flow paths (e.g., Haque et al., 2008). Owing to the low dissolved sulfide concentrations, Aquia groundwaters can be classified as suboxic based on the classification scheme proposed by Berner (1981; i.e., 1 μm $kg^{-1} \leq O_2 \leq 30$ μmol kg^{-1}; see also Anderson et al., 1994; Fig. 2.3b). The concentrations of dissolved oxygen in the Aquia groundwaters also indicate suboxic conditions, although several wells sampled on the Western shore generally exhibit oxic conditions ($O_2 \geq 30$ μmol kg^{-1}; Fig. 2.3a). Another indication of the suboxic groundwaters of the Aquia are the relatively high concentrations of NH_4^+ compared to the low concentrations of NO_3^- (Fig. 2.3d).

The accumulation of NH_4^+ along the flow path indicates dissimilatory nitrate reduction to ammonia (Fryar et al., 2000).

2.5.2 Controls on REE concentrations and shale-normalized REE patterns

All Aquia aquifer groundwaters exhibit relatively flat shale-normalized REE patterns (Fig. 2.4), albeit, with slight enrichments in the LREEs compared to HREEs. The slight overall enrichments in the LREEs are exemplified by the shale-normalized Yd/Nd ratios, [i.e.,$(Yb/Nd)_{NASC}$, Fig. 2.5] all of which are less than 1.0, except for groundwater from the QA 92-0451 well on the Eastern shore. The relatively flat shale-normalized REE patterns of Aquia aquifer groundwaters are broadly similar to shale composites such as NASC, as well as other upper continental crustal rocks (e.g., Taylor and McLennan, 1985), although the absolute concentrations of the REEs in these groundwaters are between 10^6 and 10^7 times lower than the corresponding rock/sediment contents (Fig. 2.4). The REE data for Aquia aquifer groundwaters are consistent with weathering of an upper continental crustal source, such as Aquia aquifer sediments, being the chief source of REEs to the groundwaters. This conclusion is further supported by the sequential extraction results for Aquia aquifer sediments, the majority of which also exhibit relatively flat NASC-normalized REE patterns (Table 2.5; Fig. 2.8).

The relatively flat, NASC-normalized REE patterns of Aquia aquifer groundwaters are generally consistent with preferential release of REEs to solution via chemical weathering reactions. Once released to Aquia groundwaters, the speciation model results indicate the REEs form strong and stable aqueous complexes with carbonate ions (Figs. 2.6, 2.7). Although chemical weathering of Aquia aquifer sediment

is likely the chief mechanism of REE release to Aquia groundwaters, desorption and/or reductive dissolution of Fe(III) oxides/oxyhydroxides may also be important. Others have demonstrated that LREE and MREEs are preferentially adsorbed onto Fe(III) oxides/oxyhydroxides compared to HREEs in the presence of strong complexing ligands such as CO_3^{2-} and dissolved organic matter, which typically form stronger solution complexes with HREEs (Luo and Byrne, 2004; Quinn et al., 2006; Sonke and Salters, 2006; Tang and Johannesson, in review). Consequently, changes in groundwater compositions related to chemical weathering reactions that lead to increases in dissolved solute concentrations and pH could conceivably promote desorption of weakly surface-sorbed REEs (e.g., Hall et al., 1996). We note, however, that the relatively constant specific conductance and total dissolved solids concentrations along both flow paths studied in the Aquia aquifer (Table 2.1) suggests that ionic strength related REE desorption is probably relatively minor in Aquia aquifer groundwaters. Another likely mechanism of REE release involves microbial reduction of Fe(III) oxides/oxyhydroxides within Aquia aquifer sediments (e.g,. Haque et al., 2008) and subsequent release of adsorbed and/or co-precipitated REEs to Aquia groundwaters. Because Fe(III) oxides/oxyhydroxides preferentially scavenge LREEs and MREEs relative to HREE from solution during precipitation (e.g., Koeppenkastrop and DeCarlo, 1993; Sholkovitz et al., 1994; Quinn et al., 2004), the subsequent dissolution of these metal oxides/oxhydroxides by reductive processes is expected to release relatively more LREEs and MREEs to solution than HREEs. However, shale-normalized REE patterns of the reducible fraction of Aquia aquifer sediments (i.e., Fraction 3), which likely reflects Fe(III)

oxides/oxyhydroxides, are flat to slightly enriched in the HREEs compared to the LREEs (Fig. 2.8). The NASC-normalized Yb/Nd ratios, for example, of the Fraction 3 sequential extracts of the 61 m, 72 m, and 86.5 m depth samples of the Aquia aquifer sediments are 1.84, 1.60, and 1.36, respectively (Table 2.5). Thus, although reductive dissolution of Fe(III) oxides/oxyhydroxides appears to play an important role in As mobilization in Aquia aquifer groundwaters (Haque et al., 2008), our sequential extraction data suggest that chemical weathering reactions of other minerals, and possibly oxidation of organic matter or reduced minerals (see below), contribute relatively more REEs to Aquia aquifer groundwaters than release via reductive dissolution of Fe(III) oxides/oxyhydroxides.

The sequential extraction data indicate that the readily exchangeable fraction of REEs in Aquia aquifer sediments (Fraction 1), which includes REEs weakly associated (e.g., physisorbed) with surfaces on Fe(III) oxides/oxyhydroxides and/or clay minerals such as glauconite, can release comparatively large amounts of the LREEs and MREEs to Aquia aquifer groundwater relative to the reducible phase in these sediments (Figs. 2.8, 2.9). Moreover, the oxidizable fraction (Fraction 4) has high, NASC-normalized LREE (especially for La and Ce) and HREE concentrations compared to the all other sequential extraction fractions, except Fraction 2, suggesting that oxidation of organic matter, or possibly sulfide minerals like pyrite, may contribute REEs to Aquia aquifer groundwaters. It is well known that REEs are strongly complexed by organic ligands (Tang and Johannesson, 2006, in review; Yamamoto et al., 2005; Sonke and Salters, 2006; Pourret et al., 2007), and microbial conversion of organic matter into small organic molecules (fermentation) or CO_2 (respiration) could conceivably lead to the release of

associated REEs to the groundwaters. Alternatively, other researchers have suggested that REEs may be associated with metal sulfides in some marine settings, including sediments, either as co-precipitates or via surface (sorptive) reactions (Schijf et al., 1995; DeCarlo et al., 1998; Chaillou et al., 2006), whereas others have demonstrated adsorption of the REE, Eu, onto oxidized pyrite surfaces (Naveau et al., 2006). Hence, the possibility that metal sulfide minerals could be important in REE cycling in aquifers and other saturated sediments warrants further examination.

Despite the relative importance of readily exchangeable, physisorbed REEs and those associated with oxidizable phases (i.e., organic and/or metal sulfides) within Aquia aquifer sediments, the sequential extraction data indicate that REEs associated with mineral phases that are mobilized by treatment with a weak acid (i.e., acetic acid) represents the largest pool of REEs in Aquia aquifer sediments (Figs. 2.8, 2.9). As mentioned above, this fraction (Fraction 2) chiefly represents REEs associated with carbonate minerals (shell fragments) within the Aquia aquifer sediments (e.g., Tang et al., 2004; Tessier et al., 1979). Shell fragments composed of both calcite and aragonite are common within these sediments, accounting for between 1 and 8% of Aquia aquifer sediments by volume (Chapelle, 1983; Chapelle and Knobel, 1983; Aeschbach-Hertig et al., 2002). Both calcite and aragonite are commonly enriched in REEs, reflecting the relative ease with which REEs substitute for Ca within the calcium carbonate mineral lattice (Carroll, 1993; Meinrath and Takeishi, 1993; Sholkovitz and Shen, 1995; Zhong and Mucci, 1995; Elzinga et al., 2002). The ionic radii of trivalent REEs in six-fold and seven-fold coordination ranges from 1.032 to 0.861 Å (mean ± SD = 0.94 ± 0.05 Å) and

1.11 to 0.925 Å (mean ± SD = 1.01 ± 0.06 Å), respectively, which are similar to divalent Ca in six-fold and seven-fold coordination (1.0 and 1.06 Å, respectively; Shannon, 1976). The similarity in ionic radii between REEs and Ca in six- and seven-fold coordination is one reason for the general compatibility of trivalent REEs within $CaCO_3$ minerals, despite difference in charge (Elzinga et al., 2002). Nonetheless, we note that all of the Aquia aquifer groundwaters sampled as part of our study are saturated to slightly oversaturated with respect to calcite and aragonite. For example, the mean ± SD for the saturation index (*SI*) for calcite and aragonite in Aquia aquifer groundwaters are $SI^{calcite}$ = 0.43 ± 0.17 and $SI^{aragonite}$ = 0.28 ± 0.17, as determined by PHREEQC and The Geochemist's Workbench® (Parkhurst and Appelo, 1999; Bethke, 2008).

Because the computed saturation indices indicate that Aquia aquifer groundwaters are either at equilibrium or oversaturated with respect to calcite and aragonite, precipitation and not dissolution of these minerals is energetically favored. This suggests that shell fragment dissolution is not occurring along the portions of the aquifer sampled in this study. In some of the groundwaters siderite dissolution is favored (e.g., $SI^{siderite}$ for groundwaters from wells KE 66-0125, CA 88-3340, and SM 81-2634 are -1.14, -2.81, and -3.67, respectively), although the majority of Aquia aquifer groundwaters are also at equilibrium with respect to siderite (mean ± SD $SI^{siderite}$ excluding these three well waters is -0.005 ± 0.41). Consequently, if carbonate mineral phases within the aquifer sediments (i.e., shell fragments) are the chief source of dissolved REEs to Aquia aquifer groundwaters, then dissolution of these mineral must be occurring in the recharge zone prior to attainment of equilibrium with respect to these carbonate phases. This would

require that REEs are added to Aquia aquifer groundwaters near the aquifer's outcrop region, and within the first 20 - 30 km of each flow path because by well QA 88-1277 along the Eastern Shore flow path (33.5 km), and well PG 81-1249 (20 km) on the Western Shore, Aquia aquifer groundwaters are already saturated to oversaturated with respect to both calcite and aragonite (QA 88-1277, $SI^{calcite}$ = 0.24, $SI^{aragonite}$ = 0.07; PG 81-1249, $SI^{calcite}$ = 0.62, $SI^{aragonite}$ = 0.47). This hypothesis is supported by the major solute data (i.e., Ca^{2+}, Mg^{2+}, HCO_3^-) for Aquia aquifer groundwater, which indicates that dissolution of shell fragments within the aquifer sediments is the chief control on groundwater compositions along the first ~40 km of the flow path (Region I; Chapelle, 1983). Indeed, the majority of the shell fragment dissolution occurs within the first 10 km of the flow path studied by Chapelle (1983). Therefore, we suggest that the bulk of the REEs in Aquia groundwater are added in and near the recharge zone (e.g., first 20 – 30 km of the flow paths) as relatively low pH meteoric and soil zone water interact with the abundant shell fragments in the aquifer (e.g., Johannesson et al., 1999, 2005; Tweed et al., 2006). The REEs released by shell fragment dissolution are subsequently transported, relatively conservatively (see below) with advecting groundwater along the remaining ~ 60 km of each studied flow path (also see McCarthy et al., 1998). We note that pH as low as 6.0 has been reported for groundwaters from near the recharge zone (Chapelle, 1983). The fact that REE concentrations and NASC-normalized fractionation patterns are relatively constant along the lengths of both studied flow paths suggests steady-state conditions and thus relatively conservative transport of REEs (Bigot et al.,

1984; Johannesson et al., 1997a, b; Dia et al., 2000; Olías et al., 2005; Tweed et al., 2006).

Finally, we note that all of the Aquia aquifer groundwaters exhibit negative Pr anomalies relative to La, Ce, and Nd (Fig. 2.4). We suggest that the negative Pr anomalies may reflect a weathering signature inherited from glauconite as our glauconite analyses indicate anomalously low Pr contents relative to La, Ce, and Nd (Fig. 2.10). However, because the NASC-normalized REE patterns of the two Aquia aquifer glauconite separates different dramatically from a glauconite separate from an shallow aquifer on Cape Cod, Massachusetts (Bau et al., 2004), more investigation of REEs associated with glauconite is required before sound conclusions can be drawn regarding the importance of glauconite weathering on Aquia groundwater REE signatures.

2.5.3 REEs along the flow paths

Although all of the Aquia aquifer groundwater samples analyzed exhibit similar, relatively flat shale-normalized REE patterns, close examination reveals that the fractionation patterns change slightly along the flow path such that the degree of LREE enrichment decreases with flow down gradient along the flow path. However, the small changes in REE fractionation patterns along the studied flow paths in the Aquia aquifer are negligible when compared to those reported for the Carrizo Sand aquifer in Texas and a shallow, alluvial-fill aquifer in southern Nevada (Johannesson et al., 1999; Tang and Johannesson, 2005a, 2006). Furthermore, other than pH and alkalinity, the slight decrease in LREE enrichment along the flow paths within the Aquia aquifer does not appear to correspond to any other changes in solution composition or redox conditions

(compare Fig. 2.5 with Figs. 2.2 and 2.3). Compared to the Carrizo Sand aquifer where pH ranges between 6 and 9 and distinct Fe- and sulfate-reducing zones occur along the flow path (Tang and Johannesson, 2006; Haque and Johannesson, 2006a; Basu et al., 2007), the groundwater pH along each studied flow path in the Aquia aquifer varies by at most one pH unit. Furthermore, Fe-reduction appears to be the chief redox-buffering reaction within Aquia aquifer groundwaters (Haque et al., 2008; Fig. 2.2).

Previous studies indicate that in some groundwater flow systems, groundwaters obtain REE signatures in or near the aquifer recharge zones where acidic meteoric water and soil zone waters, charged with CO_2 from plant and microbial respiration, mobilize REEs from aquifer minerals via congruent and incongruent chemical weathering reactions (Johannesson et al., 1997a, b, 1999, 2005; Tang and Johannesson, 2005a, 2006; Tweed et al., 2006). Equilibrium thermodynamics indicates that meteoric water in equilibrium with atmospheric CO_2 at 25°C will have a pH of ~5.67 (e.g., Drever, 1997), whereas soil zone waters can have pH values as low as 4 or 5 (Nesbitt, 1979). Once mobilized, REEs concentrations and fractionation patterns are subsequently modified with flow down gradient along flow paths by solution and surface complexation reactions, mineral precipitation/dissolution reactions, changing redox conditions, and mixing/dilution processes (Johannesson et al., 1997a, b, 1999; 2005; Tang and Johannesson, 2005a, 2006; Tweed et al., 2006).

As discussed above, our data suggest that REEs are mobilized near the recharge zone of the Aquia aquifer by dissolution of shell fragments within the aquifer sediments. Once REEs are released into solution in the Aquia aquifer they form strong aqueous

complexes with carbonate ions, including both carbonato complexes, $LnCO_3^+$, and especially dicarbonato complexes, $Ln(CO_3)_2^-$ (Figs. 2.6, 2.7). More specifically, the speciation modeling predicts that relatively more of each HREE occurs in Aquia aquifer groundwaters as dicarbonato complexes compared to each LREE (Figs. 2.6, 2.7). For example, the percentage of Yb predicted to occur in solution as $Yb(CO_3)_2^-$ ranges from 68.23 to 99.64 (mean ± SD = 90.18 ± 9.03), whereas $La(CO_3)_2^-$ accounts for between 15.72 to 96.18 (mean ± SD = 53.34 ± 22.25). The rest of the La in solution occurs as positively charged $LaCO_3^+$ and La^{3+} species or complexed with organic ligands (Figs. 2.6, 2.7). Because the point of zero (ZPC) charge for goethite and other Fe(III) oxides/oxyhydroxides, which forms coatings on quartz grains in Aquia aquifer sediments (Haque et al., 2008) ranges between pH 6 and 8 (Dzombak and Morel, 1990; Drever, 1997), and the ZPC for glauconite ranges between pH 4.8 and 6.3 (Hao et a., 1987; Smith et al., 1996), adsorption of negatively charged dicarbonato complexes is expected to be relatively minor in the circumneutral to alkaline pH Aquia aquifer groundwaters (e.g., Johannesson et al., 1999, 2005; Tang and Johannesson, 2005b). Consequently, the relatively constant REE concentrations and NASC-normalized fractionation patterns that characterize Aquia aquifer groundwaters reflects rapid dissolution of shell fragments within the aquifer sediments near the recharge zone, which releases REEs to the groundwaters, followed by relatively conservative transport of REEs in the form of $Ln(CO_3)_2^-$ aqueous complexes down gradient along the flow path as these negatively charged complexes will exhibit a low affinity to sorb to negatively charged mineral surface sites that are expected to predominate in the Aquia aquifer groundwater flow

system. Tweed et al. (2006) similarly argued that relatively constant REE concentrations and fractionation patterns in a shallow, fractured rock aquifer from southern Australia reflected REE mobilization within the aquifer recharge area followed by conservative transport of REE carbonate complexes along the length of the studied flow path.

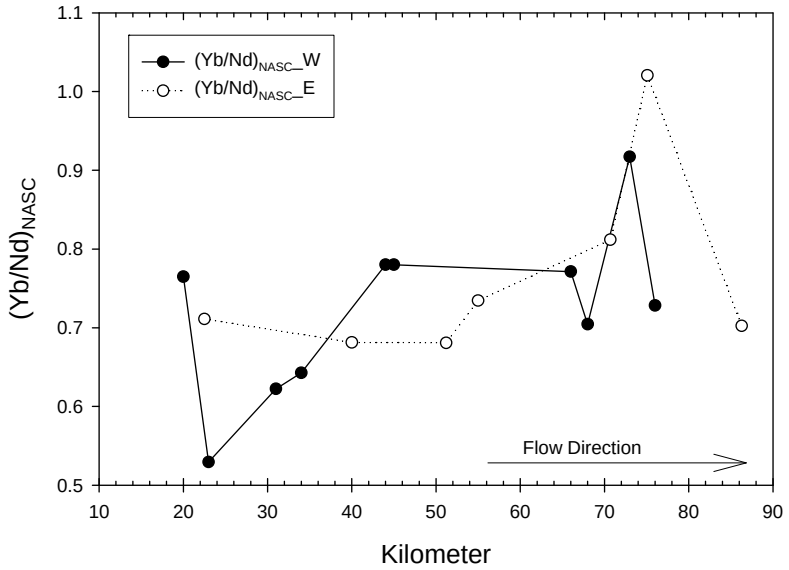

Figure 2.5 Shale-normalized Yb/Nd ratios for groundwaters from the Aquia aquifer as a function of distance from the recharge zone.

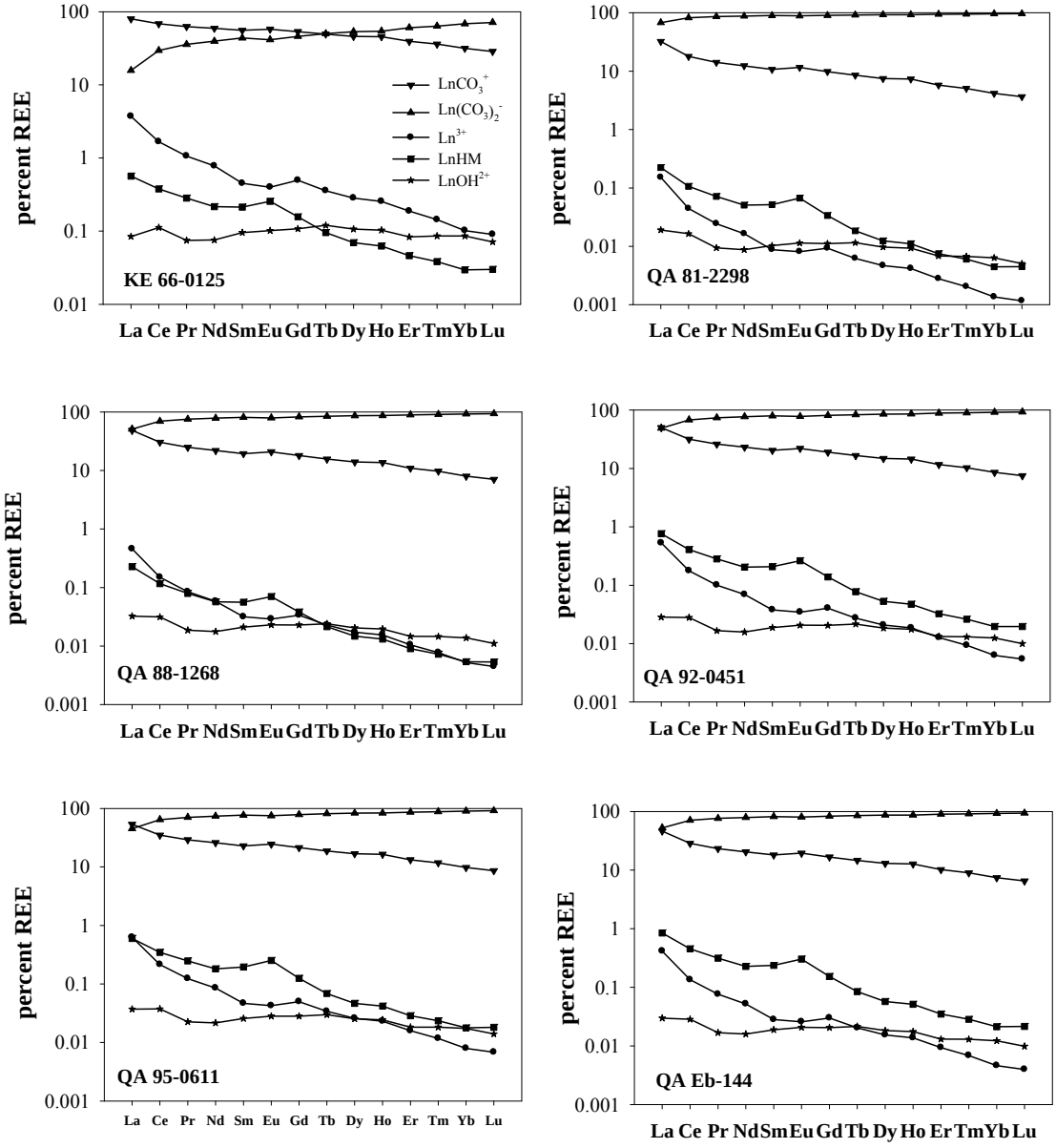

Figure 2.6 Results of speciation modeling of REEs in some Aquia aquifer groundwaters from the Eastern Shore flow path. Ln refers to any of the lanthanide series elements (i.e., the REEs), and HM indicates dissolved humic matter (i.e., humic acid and/or fulvic acid).

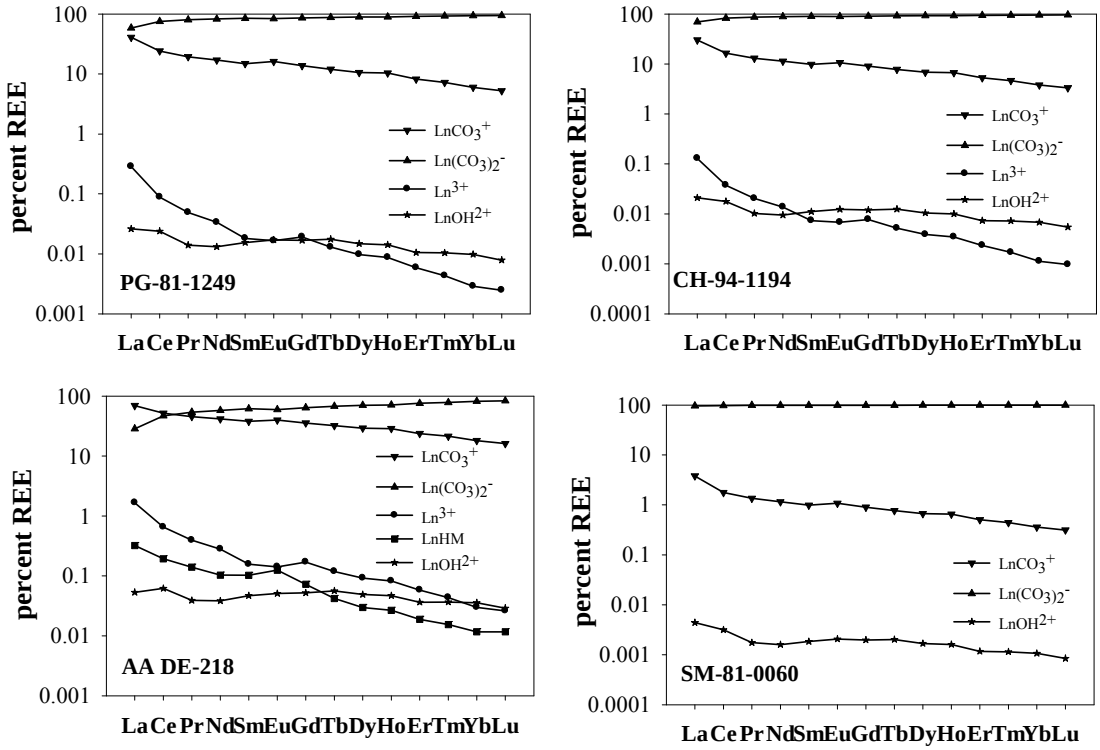

Figure 2.7 Results of speciation modeling of REEs in some Aquia aquifer groundwaters from the Western Shore flow path.

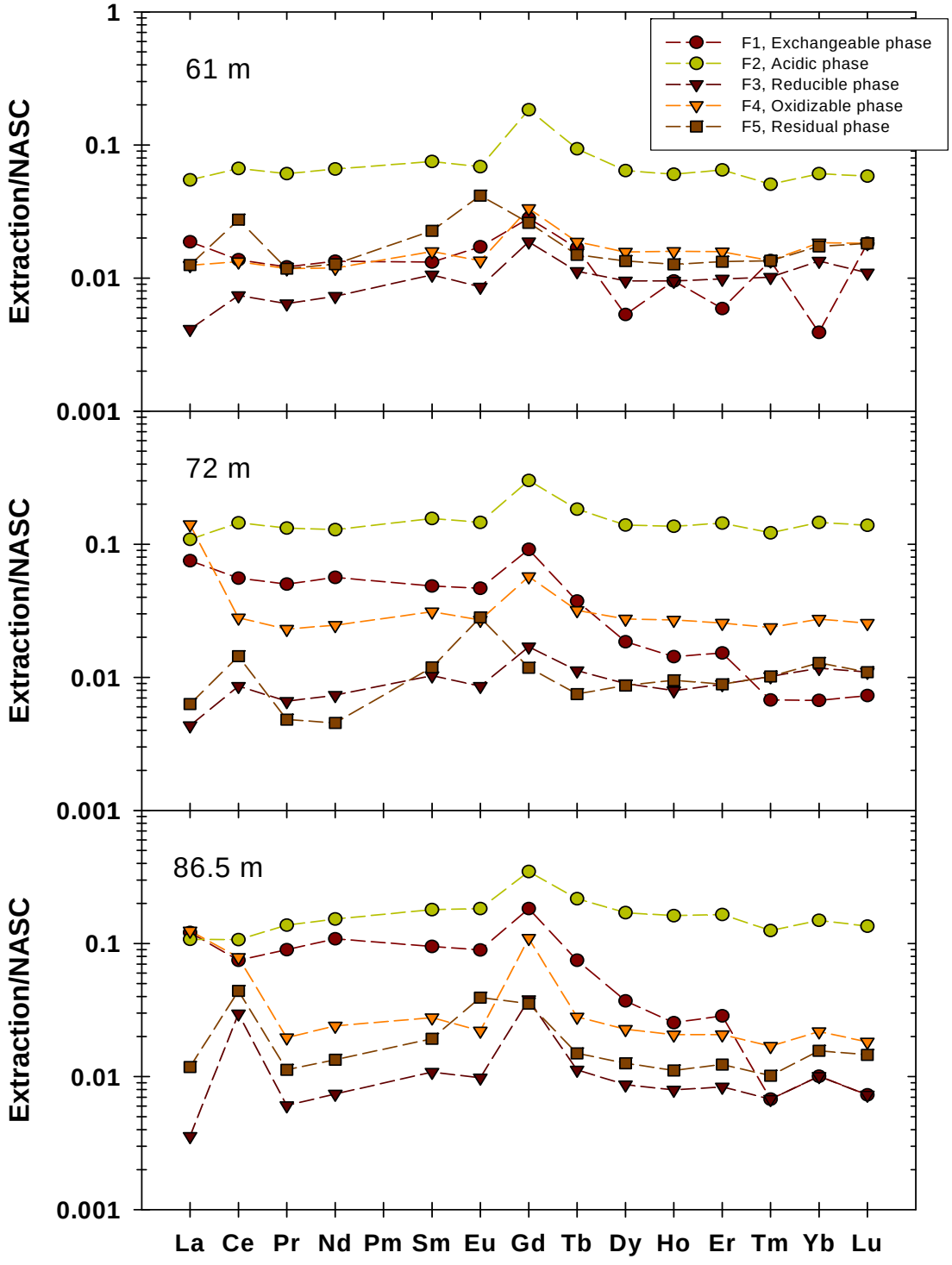

Figure 2.8 Shale-normalized REE patterns in the Aquia sediments at (a) 61 m; (b) 72 m; (c) 86.5 m.

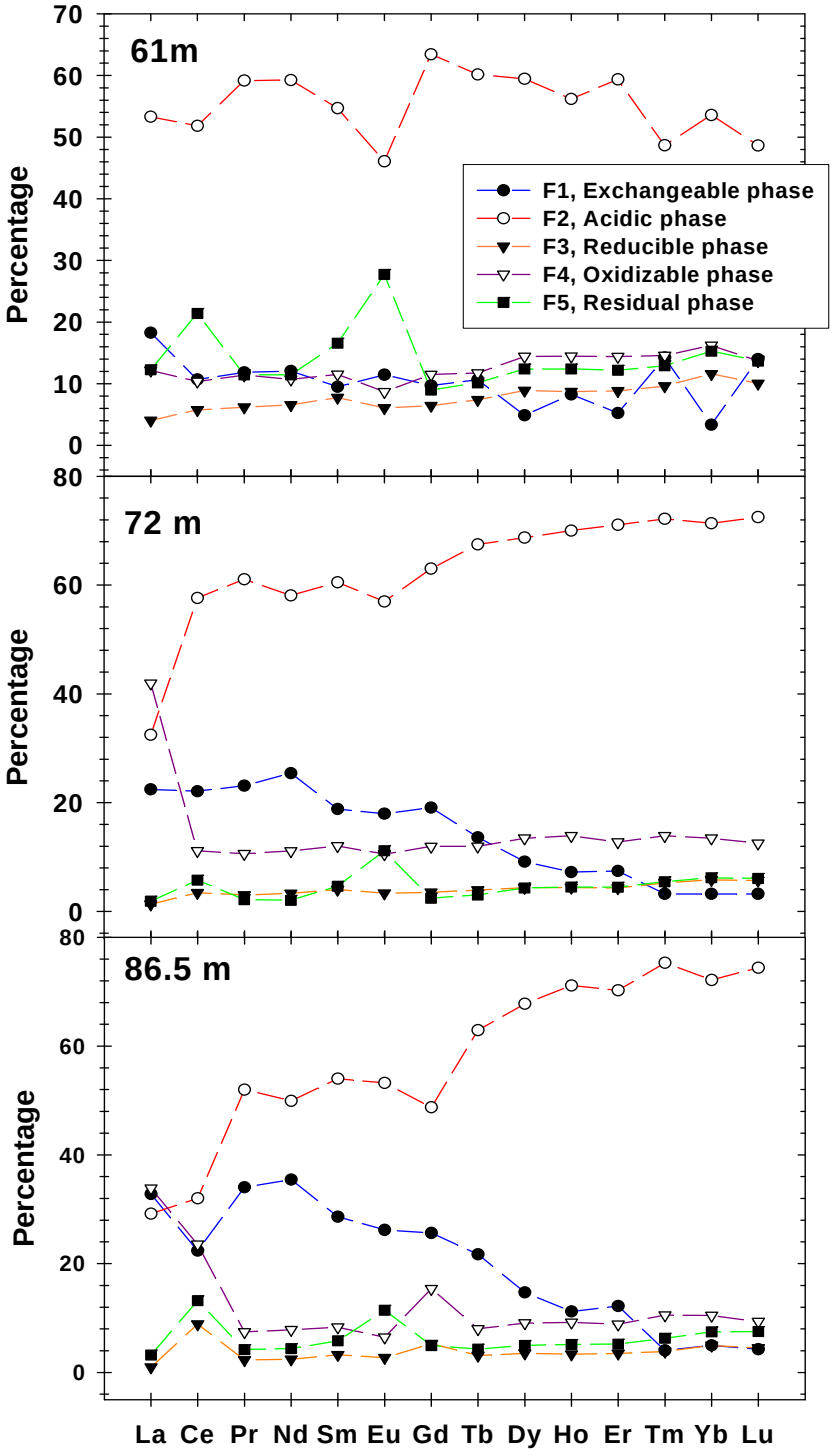

Figure 2.9 Percent-weighted amount that each fraction contributes to the content of each REE in Aquia aquifer sediment samples from (a) 61 m; (b) 72 m; and (c) 86.5 m below ground surface.

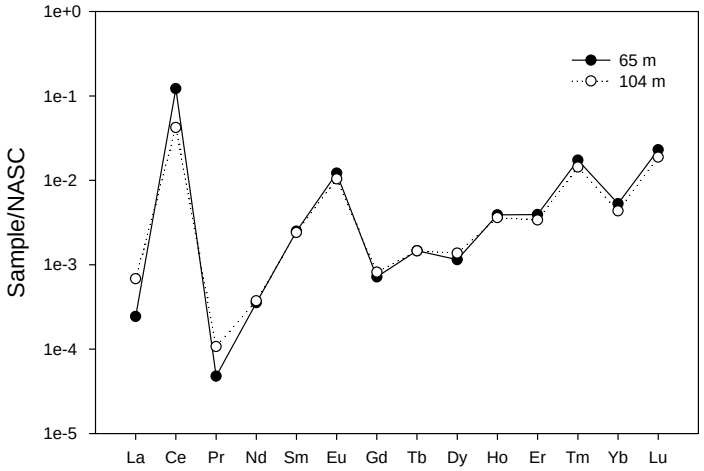

Figure 2.10 Shale-normalized REE patterns for glauconite extraction from the Aquia aquifer sediments.

2.6 Conclusion

The data in this study demonstrate that the groundwaters samples collected from the Aquia aquifer evolve along the flow paths due to chemical weathering and changes in redox conditions. Redox indicators, such as Eh, dissolved oxygen, Fe concentrations and speciation, dissolved S(-II), indicate that the Aquia groundwaters are suboxic and non-sulfidic. The suboxic groundwater conditions are also reflected by the high concentrations of NH_4^+ compared to the low concentrations of NO_3^- for the Aquia groundwaters.

Dissolved REE behavior exhibits relatively flat shale-normalized REE patterns, with slight LREE anomaly, along the entire lengths of groundwater flow paths in the Aquia aquifer. In general, the Aquia groundwaters exhibit a slight enrichment in LREEs over HREEs. The similarity between the NASC-normalized REE patterns and the REE concentrations of Aquia aquifer groundwaters implies the comparatively homogeneous

groundwater compositions and redox conditions in the Aquia aquifer. Groundwater REE concentrations are consistent with weathering of an upper continental crust source, such as Aquia aquifer sediments, being the main source of REEs to the groundwaters. This also appears in the sequential extraction results for the Aquia aquifer sediments where the majority of the NASC-normalized REE patterns are relatively flat. Sequential extraction analyses of Aquia aquifer sediments further indicate the largest pool of REEs in Aquia aquifer sediments is associated with carbonate minerals (shell fragments). Computed saturation indices calculations indicate that groundwaters are saturated to oversaturated with respect to both calcite and aragonite. Therefore, dissolution of carbonate minerals (shell fragments) must be occurring in or near the recharge zone prior to attainment of equilibrium with respect to these carbonate phases. Major solute (i.e. Ca^{2+}, Mg^{2+}, HCO_3^-) for Aquia aquifer groundwater also denotes that dissolution of shell fragments within the aquifer sediments is the primary control on groundwater compositions along the first 20 km of the flow paths. In addition, speciation modeling indicates that REEs form strong aqueous complexes with carbonate ions, including carbonato complexes, $LnCO_3^+$, and especially dicarbonato complexes, $Ln(CO_3)_2^-$, which exhibit a low affinity to sorb to negatively charged mineral surface sites in the aquifer sediments.

CHAPTER 3

ARSENIC AND ANTIMONY IN GROUNDWATER FLOW SYSTEMS: A COMPARATIVE STUDY

3.1 Introduction

Arsenic (As) and antimony (Sb) are considered priority pollutants by the U. S. Environmental Protection Agency (USEPA, 1979) and the European Union (Council of the European Communities, 1976). Consequently, the US EPA and the World Health Organization recommend a maximum contaminant level (MCL) of 133 nmol kg^{-1} (i.e., 10 ppb) for As in drinking waters, and the US EPA has set an MCL of 49 nmol kg^{-1} (6 ppb) for Sb in drinking waters. The European Union also set maximum admissible concentrations for As of 133 nmol kg^{-1} and 41 nmol kg^{-1} (i.e., 5 ppb) for Sb in drinking waters (Council of the European Union, 1998).

The toxicity of As to humans is well known and most people are exposed to As via consumption of drinking water sources with elevated As concentrations (Smith et al., 1992; NRC, 1999, 2001; Gebel, 2000; Ratnaike, 2003). Indeed, the relatively recent recognition of the mass poisoning of tens of millions of people in the Ganges – Brahmaputra river delta plain of Bangladesh and West Bengal, India, via consumption of high As groundwaters, has focused much research towards understanding the biogeochemical reactions responsible for As mobilization in groundwater flow systems (Das et al., 1995; Bhattacharya et al., 1997, 2002; Nickson et al., 1998; Chowdhury et

al., 2000; McArthur et al., 2001, 2004, 2008, 2010; Smedley and Kinniburgh, 2002; Islam et al., 2004; van Geen et al., 2004; Zheng et al., 2004, 2005; Mailloux et al., 2009; Neumann et al., 2010). Chronic exposure to As via drinking water has been linked to numerous poor health outcomes including skin keratosis, skin and bladder cancer, type 2 diabetes, heart disease, and respiratory diseases among others, and As is commonly recognized as the most serious naturally occurring carcinogen (Smith et al., 1992; NRC, 1999, 2001; Hughes, 2002; Nriagu, 2002; Ratnaike, 2003; Yoshida et al., 2004; Meliker and Nriagu, 2007; Navas-Acien et al., 2008; Hughes et al., 2009; Ravenscroft et al., 2009). Moreover, As(III) is estimated to be ~10 to 60 times more toxic than As(V) (Ratnaike, 2003). Although much less is currently known about the toxicity of Sb, especially regarding the processes responsible for its genotoxicity, like As, it is also clastogenic (Gebel, 1997, 1998). Moreover, as with As, the trivalent form of Sb is reported to be more toxic than the pentavalent form (Bencze, 1994; Fiella et al., 2002a, b). Despite its toxicity and identification as a priority pollutant, much less is known about the biogeochemistry of Sb in the environment compared that of As (e.g., see Wilson et al., 2010 for a recent review).

Because As and Sb belong to Group VA (i.e., subgroup 15) of the periodic table of elements, they exhibit broadly similar chemical properties and, hence, comparable geochemical behavior in the environment (Crecelius et al., 1975). Moreover, due to decreased electronegativity, both exhibit the properties of metals and non-metals, and are thus generally referred to as metalloids (Pauling, 1988). Arsenic and Sb can exist in four oxidation states (-III, 0, III, V), but most commonly occur as (III) and (V) in the

environment (Filella et al., 2002a, b; Smedley and Kinniburgh, 2002). Nevertheless, few studies have focused on the correlation between these two elements in the environment. Mitsunobu et al. (2006) compared the behavior of As and Sb in soil and water samples from the Ichinokawa mine pit in Ehime, Japan. The results from their study suggest that the behaviors of As and Sb are closely related to the biogeochemical cycling of Fe and Mn in the soil profile. However, they suggested, based on the predominance of Sb(V) and the co-occurrence of As(V) and As(III) that there was no relationship between As and Sb abundances in soil water due to differences in their redox properties (Mitsunobu et al., 2006).

In this study we examine the relationship between As and Sb geochemistry in three groundwater flow systems; the Carrizo Sand aquifer in Texas, the Upper Floridan aquifer in Florida, and the Aquia aquifer of coastal Maryland. Previously, we measured As and selenium (Se) concentrations and speciation along the groundwater flow paths in these aquifers (e.g., Haque and Johannesson, 2006a, b; Basu et al., 2007; Haque et al., 2008). Here, we present new Sb and As data (Aquia aquifer only) and compare these data to gain insight into the biogeochemical processes affecting As and Sb concentrations and speciation along the flow path within these groundwater flow systems.

3.2 Study Areas

3.2.1 Carrizo Sand aquifer

The Carrizo Sand aquifer is an unconsolidated, chiefly confined aquifer located within the Gulf Coastal Plain of southeastern Texas (Fig. 3.1). The aquifer outcrops

along a sand ridge that roughly parallels the Texas coast, and dips towards the southeast and the Gulf of Mexico. Groundwater is recharged along the sand ridge and subsequently flows southeast towards the Gulf of Mexico at an average rate of approximately 2 m a^{-1} (Pearson and White, 1967; Stute et al., 1992; Castro et al., 2000; Castro and Goblet, 2003). The aquifer is composed of mostly fine- to medium-grained, Eocene quartz sand with minor amounts of clay, lignite, calcite, and pyrite (Pearson and White, 1967). Within the recharge area the sands are coated with Fe(III) oxides/oxyhydoxides, including goethite and hematite, and clay minerals (chiefly kaolinite and illite; Basu et al., 2007). From the outcrop in Atascosa County towards the south in southern McMullen County the thickness of the Carrizo Sand varies from 100 to 360 m, showing an increase along the flow path (Castro et al., 2000). The porosity of the aquifer is estimated to range from ~30 to 40% (Pearson and White, 1967). Using ^{14}C measurements, Pearson and White (1967) suggested the age of Carrizo groundwater increases from ~5,000 years near the outcrop area in northern Atascosa County to ~30,000 years in southern McMullen County. In this contribution, groundwater samples were collected along a well studied flow path beginning in the recharge zone in northern Atascosa County, Texas, and continuing to the southeast into northern McMullen County (Pearson and White, 1967; Stute et al., 1992; Castro et al., 2000; Castro and Goblet, 2003; Haque and Johannesson, 2006a; Tang and Johannesson, 2006; Basu et al., 2007).

3.2.2 Upper Floridan aquifer

The Upper Floridan aquifer consists of a highly permeable carbonate rock succession that includes the Suwannee Limestone (Oligocene), the Ocala Limestone (upper Eocene), and the Avon Park (middle Eocene) Formation (Stringfield, 1966; Miller, 1986). The Upper Floridan aquifer is chiefly composed of calcite (~66%) and dolomite (~33%), along with minor amounts of gypsum, anhydrite, chert, quartz, apatite, metal oxides, sulfides, lignite, and clay minerals (Hanshaw et al., 1965a, b; Rye et al., 1981; Plummer et al., 1983; Sacks et al., 1995). The thickness of the Upper Floridan aquifer ranges from 60 to 640 m (Miller, 1986). In this study, groundwater samples were collected along a well characterized flow path located within west-central Florida (Fig. 3.1, see Haque and Johannesson, 2006b; Basu et al., 2007). The chosen flow path closely follows "path II" defined by Plummer and Sprinkle (2001) as well as the flow path investigated by Hanshaw et al. (1965a, b) and Back and Hanshaw (1970). Groundwater is recharged to the Upper Floridan aquifer in the vicinity of Polk City, where the aquifer is largely unconfined (Back and Hanshaw, 1970; Miller, 1986; Plummer and Sprinkle, 2001). Here, the overlying Hawthorn Formation, which typically acts as a confining layer, is absent allowing for direct recharge to the Upper Floridan aquifer as evidenced by the predevelopment potentiometric high centered on Polk City (e.g., Stringfield 1966; Hanshaw et al., 1965a, b; Johnston et al., 1980). From the Polk City region, groundwater historically flowed radially outward towards the coast, discharging in the case of our studied flow path, to the Gulf of Mexico in the vicinity of Venice, Florida (Fig. 3.1; Bush and Johnston, 1988; Wicks and Herman,

1994; Sacks et al., 1995; Plummer and Sprinkle, 2001). Again, the reader is referred to the above cited studies as well as Haque and Johannesson (2006b) and Basu et al. (2007) for more details.

3.2.3 Aquia aquifer

The Aquia aquifer is an unconsolidated, principally confined Coastal Plain aquifer that outcrops along a southwest to northeast trend from proximal to Washington, DC, through Annapolis, Maryland, and across the Chesapeake Bay to Kent County, Maryland (Fig. 3.3; Chapelle, 1983; Aeschbach-Hertig et al., 2002; Haque et al., 2008). The Aquia aquifers dips to the southeast, beneath Chesapeake Bay, ending in a facies change to progressively more clay-rich, and hence, less permeable sediments approximately 90 km from the outcrop area (Chapelle, 1983; Aeschbach-Hertig et al., 2002; Haque et al., 2008). The Aquia is overlain by the confining Marlboro clay and is underlain by the silts and clays of the Cretaceous Severn Formation (Chapelle, 1983). The Aquia aquifer is a Paleocene and Eocene marine deposit consisting of quartz sand (~55%), glauconite (~30%), and shell fragments (~8%), in addition to clay minerals, iron oxides/oxyhydroxides, including magnetite, hematite, and goethite, as well as minor garnet, hornblende, pyrite, and lignite (Page, 1957; Wolff, 1967; Hansen, 1974; Chapelle, 1983; Haque et al., 2008). The aquifer ranges in thickness from 23 to 30 m near the Chesapeake Bay (Harsh and Laczniak, 1980). The groundwater flow patterns within the Aquia are dominated by flow from the recharge areas towards the south and east, although the predevelopment potentiometric surface indicates that flow within portions of the aquifer on the eastern shore of the Chesapeake Bay historically flowed

south and west towards the Bay (Chapelle, 1983; Aeschbach-Hertig et al., 2002; Drummond, 2001, 2007; Haque et al., 2008). In this study, groundwaters were collected from a flow path located on the Eastern Shore that was previously investigated by Haque et al. (2008). Earlier investigations chiefly focused on flow paths on the Western Shore of Chesapeake Bay (e.g, Chapelle, 1983; Chapelle and Knobel, 1983, 1985; Purdy et al., 1996; Aeschbach-Hertig et al., 2002).

Figure 3.1 Location of the three studies areas (Carrizo Sand aquifer, Texas; Upper Floridan aquifer, Florida; Aquia aquifer, Maryland) within the United States of America. See Tang and Johannesson (2006), Haque and Johannesson (2006a, b), and Haque et al. (2008) for details concerning each field site.

3.3 Materials and Methods

3.3.1 Sample collection and field analysis

Before groundwater sample collection all sample bottles (HDPE), field containers (LDPE), Teflon® tubing, and lab-ware were rigorously cleaned using trace element clean procedures (Johannesson et al., 2004). Furthermore, during sample bottle cleaning and field sampling, laboratory and field personnel wore similarly cleaned poly gloves. After sample bottles were cleaned and bagged, they were placed within clean plastic ice chests for transport to and from the field collection sites.

Groundwater samples were collected from 10 wells in the Carrizo Sand aquifer (June 2004), 10 wells in the Upper Floridan aquifer (July 2004), and 11 wells in the Aquia aquifer (July 2006) for analysis of As, Sb, dissolved Fe species [i.e., Fe(II), Fe(III)], sulfide [S(-II)], and a number of ancillary geochemical parameters including pH, temperature, alkalinity, major solutes, dissolved oxygen, and Eh (e.g., Haque and Johannesson, 2006a, b; Basu et al., 2007; Haque et al., 2008). In order to ensure that groundwater samples collected from each of the aquifers were actually representative of groundwaters from the aquifer and not the individual well bores, all of the wells were purged for at least 30 minutes or until pH, temperature, and conductivity stabilized.

A Hydrolab MiniSonde 5 with a flow-through cell was used to quantify the Eh, pH, specific conductance, and temperature of the groundwater samples. The flow-through cell was directly connected to each well by a polyethylene tube, which allowed the Eh of the groundwaters to be measured by minimizing exposure of the sample to the atmosphere. A portable UV/VIS spectrophotometer (Hach DR/2400) was used to

determine iron speciation and dissolved S(-II) concentrations using separate sample aliquots. Specifically, Fe(II) was determined using the 1,10 phenanthroline method (Eaton et al., 1995), whereas total Fe (Fe_T) was determined using the Ferrozine method (Stookey, 1970; Hach, 2004). The Fe(III) concentration in each groundwater sample was then determined by difference. The method detection limits for Fe(II) and Fe_T are 0.36 μmol kg^{-1} and 0.16 μmol kg^{-1}, respectively (Haque et al., 2008). Dissolved S(-II) concentrations were determined using the Methylene Blue method, for which the method detection limit is estimated to be 0.16 μmol kg^{-1} (Eaton et al., 1995). Dissolved oxygen concentrations were also estimated using the portable spectrophotometer on separate aliquots of each groundwater sample via both the High Range dissolved oxygen (method detection limit: 18.8 μmol kg^{-1}; Hach, 2004) and Indigo Carmine methods (method detection limit: 0.38 μmol kg^{-1}; Gilbert et al., 1982) for a range of dissolved oxygen values.

Groundwater samples for determination of As and Sb were first collected into collapsible "trace cleaned" low density polyethylene cubitainers® from each of the wells and then immediately filtered through 0.45 μm Gelman Sciences in-line groundwater filter capsules, by pumping the groundwater sample from the cubitainers® through pre-cleaned Teflon® tubing connected to the in-line filter capsule, and subsequently into in 500 mL opaque, amber HDPE sample bottles. The amber sample bottles, which were used in order to prevent photocatalyzed oxidation of As(III) and Sb(III) (e.g., McCleskey et al., 2004), were first rinsed three times with the filtered groundwater sample in order to "condition" the bottle before filling the bottle with the groundwater

sample (Haque et al., 2008). The sample was then acidified to pH < 2 with ultrapure HNO_3 (Seastar Chemical, Baseline) to preserve the total dissolved metalloid concentrations (i.e., As_T, Sb_T) and prevent precipitation of Fe/Mn oxides/oxyhydroxides within the collected samples. A separate ~ 60 mL aliquot of the filtered groundwater was subsequently acidified to pH ~3.5 with ultra-pure HNO_3 (Seastar Chemical, Baseline), and passed through an anion exchange column (i.e., Bio-Rad Poly-Prep 0.8x4 cm chromatography columns) packed with Bio-Rad AG® 1x8, 50-100 mesh, anion exchange resin converted to the acetate form (see Wilkie and Hering, 1998). At a pH of ~3.5, As(V) is retained on the anion-exchange resin owing to the negative charge of the predominant anionic species, $H_2AsO_4^-$, whereas As(III), which occurs as the neutral species, $H_3AsO_3^0$ at this pH, passes through the column. The eluted fractions containing As(III) were collected in pre-cleaned, amber HDPE bottles, and then acidified to pH < 2 with ultrapure HNO_3. Sample aliquots for total As and Sb and As(III) and Sb(III) [i.e., Aquia aquifer only, see below] were subsequently placed within pre-cleaned poly bags, and then into a clean plastic ice chest for cold (i.e., ~ 4˚C) storage and transport back to the laboratory for analysis.

3.3.2 Analytical techniques

All groundwater samples collected were analyzed for As and Sb using inductively coupled plasma mass spectrometry (ICP-MS). The Carrizo Sand aquifer and Upper Floridan aquifer samples were quantified using a Perkin Elmer/Sciex Elan 6100 DRC ICP-MS at The University of Texas at Arlington. This instrument contains a reaction cell, which allows for precise measurement at very low concentrations (low

nanomolal to high picomolal levels) in groundwaters where $ArCl^+$ formed in the plasma stream can interfere with ^{75}As detection using standard quadrupole instruments (Haque and Johannesson, 2006a). The Aquia aquifer samples were quantified using a high resolution Finnigan MAT ELEMENT 2 (magnetic sector) ICP-MS at Tulane University. The high resolution (HR) mode of the HR-ICP-MS allows ^{75}As to be distinguished from possible $ArCl^+$ interferences and the low resolution mode allows Sb to be detected. Both ICP-MS instruments were calibrated using aqueous standard solutions, of the same acid concentrations as in the samples, prepared from stock solutions by subsequent dilution in the range of 0.01 – 100 ppb for each element (for details see Haque and Johannesson, 2006a, b; Haque et al., 2008). The stock As and Sb solutions were prepared from both Perkin Elmer Pure Plus As standards and NIST traceable High Purity Standards (As and Sb: Charleston, SC). In addition, all standards and sample solutions were spiked with indium as an internal standard to correct for instrument drift. The NIST Standard Reference Material (SRM) "Trace Elements in Water" No. 1643b and the National Research Council Canada (Ottawa, Ontario, Canada) SRM for trace elements in river water (SRLS-3) were included in our analyses as additional quality control checks.

3.3.3 Geochemical modeling

Geochemical modeling for groundwaters from the Carrizo Sand, Upper Floridan, and Aquia aquifers was conducted using the React program of the Geochemist's Workbench® (release 7.0; Bethke, 2008) and the Lawrence Livermore National Laboratory thermodynamic database "thermo.com.v8.r6+" (Delany and

Lundeen, 1990). The database was modified by addition of dissolved antimony species and minerals using additional thermochemical data from Wagman et al. (1982), Brookins (1986), and Pitman et al. (1957). The Eh-pH diagrams were calculated using the Act2 program of the Geochemist's Workbench® (release 7.0; Bethke, 2008).

3.4 Results

Arsenic concentrations and speciation for groundwaters from the Carrizo Sand aquifer, Upper Floridan aquifer, and Aquia aquifer were previously published (Haque and Johannesson, 2006a, b; Haque et al., 2008), and are thus reproduced here in Appendices A – C. The new Sb concentration and speciation (Aquia aquifer only) data are presented here in 3.1. These Sb data are plotted along with the previously published As, Fe, and dissolved sulfide concentrations for the Carrizo Sand aquifer, Upper Floridan aquifer, and the Aquia aquifer as a function of distance along the studied flow paths in Figs. 2 – 4. The reader is again referred to our previously published reports on these three aquifers (i.e., Tang and Johannesson, 2005a, 2006; Haque and Johannesson, 2006a, b; Basu et al., 2007; Haque et al., 2008) for more details of the studied flow paths.

Within the Carrizo Sand aquifer, As_T concentrations range from 0.37 to 2.47 nmol kg^{-1}, and Sb_T concentrations range from 16 to 198 pmol kg^{-1}, or roughly 2 to 154 times lower than the measured As_T concentrations. In addition, Sb_T concentrations show a general increase with flow down-gradient along the flow path as the groundwater becomes more sulfidic (Fig. 3.2). Arsenic predominantly occurs as As(V) in Carrizo Sand groundwaters (Haque and Johannesson, 2006a; Fig. 3.2). In the Upper

Floridan aquifer, As_T ranges from 0.72 to 18.6 nmol kg^{-1}, whereas Sb_T concentrations range from 8.1 to 1462 pmol kg^{-1} (Table 3.1, Fig. 3.3). The As_T concentrations in the Upper Floridan aquifer are between a factor of 2 lower than the Sb_T concentrations, to as much as ~2300 times higher than Sb_T. In the Upper Floridan aquifer, As(V) predominates in groundwaters from near the recharge zone and with flow down-gradient beyond 45 km, As(V) and As(III) exhibit similar, low concentrations (Fig. 3.3). For the Aquia aquifer, As_T concentrations range from 0.75 to 1072 nmol kg^{-1}, and Sb_T concentrations range between 23 and 512 pmol kg^{-1} (Fig. 3.4). Hence, As_T concentrations are between a factor of ~1.5 to ~47,000 times higher than Sb_T in Aquia aquifer groundwaters. Both metalloids occur predominantly in the reduced form as As(III) and Sb(III) in Aquia aquifer groundwaters (Fig. 3.4).

Table 3.1 Antimony concentrations (in pmol kg^{-1}) in groundwater samples collected from the Carrizo Sand aquifer (Texas), Upper Floridan aquifer (Florida), and Aquia aquifer (Maryland).

	Distance (km)	pH	Temp (°C)	Eh (mV)	Eh* (mV)	SbT (pmol kg-1)	Sb(III) (pmol kg-1)	Sb(V) (pmol kg-1)
Carrizo								
F-1	0.5	6.56	24.6	-40	268.7	16.1		
N-1	4.29	6.58	25.4	78	375.7	20.3		
KS-1	7.4	6.3	24.6	282	261.6	27		
N-3	9.37	6.07	30.4	166	271.2	25.8		
G-1	12.8	6.21	26.5	137	254.1	42.9		
Poteet	14.5	6.13	28.2	170	309.3	24.4		
PCW-1	25.1	7.22	34.5	48	171.9	22.9		
Peeler-1	41.1	8.46	27.9	-114	-318.6	166		
AC74R-2	59	8.5	55	-137	-352.1	198		
SMA74R-2	65.8	8.24	41.6	-122	-318.8	52		
Upper Floridan								
ROMP 76A	0	7.93	23.5	265	159.1	1462		
ROMP 59	32.2	7.82	22.8	73	122	125		
ROMP 45	46.3	7.83	27	-30	-255.7	25.1		
ROMP 31	78.8	7.7	29.4	-68	-245.9	18.5		
ROMP25	90.8	7.42	27.7	-34	-223.9	47		
ROMP 18	112	7.38	27.1	-83	-233	16.3		
ROMP 19E	123	7.3	25.9	-43	-214.7	8.08		
ROMP 19W	133	7.26	26.8	-84	-215.9	9.06		
ROMP 5-2	138	7.07	27.6	-53	-201.7	6.38		
ROMP 5-1	144	7.12	26.1	-71	-204.2	14.5		
Aquia								
KE 66 0125	22.5	7.57	16.6	25.5	242.2	23.2 ± 6.53	21.2 ± 6.53	2 ± 0.00
QA 88 1277	33.5	7.69	25.6	44	323.5	23.2 ± 5.52	21.2 ± 5.52	2 ± 0.00
QA 94 1322	36.2	8.01	28.8	-11	291.4	324 ± 8.17	289 ± 6.57	34.8 ± 4.86
QA 88 1268	51.2	8.08	26.7	-10.5	287.8	512 ± 27.1	510 ± 27.1	2 ± 0.00
SHA*	52	8.38	29.7	-46	268.9	435 ± 12.7	435 ± 12.7	2 ± 0.00
QA 94 0111	52.5	7.91	26.2	-3	114.8	294 ± 9.82	247 ± 8.35	47.2 ± 5.16
QA 95 0611	55	8.02	16.1	-18	298.7	280 ± 22.8	196 ± 11.2	83.8 ± 19.9
QA 73 3626	64.5	7.84	16.9	27.5	309.1	43.7 ± 11.2	31.7 ± 7.25	12 ± 8.52
QA 81 2298	60.7	8.3	17.5	-11	247.5	91.2 ± 5.26	48.2 ± 1.75	43 ± 4.96
QA 92 0451	75.1	7.93	17.8	11.5	297.9	144 ± 12.8	127 ± 11.2	16.7 ± 6.15
QA EB 144	86.3	8.12	15.9	-53	293.4	27.2 ± 8.44	25.2 ± 8.44	2 ± 0.00

pH, temperature, and Eh values are from Haque and Johannesson (2006a), Haque and Johannesson (2006b), and Haque et al. (2008).

*Eh values calculated using the SpecE8 program of Geochemist's Workbench®

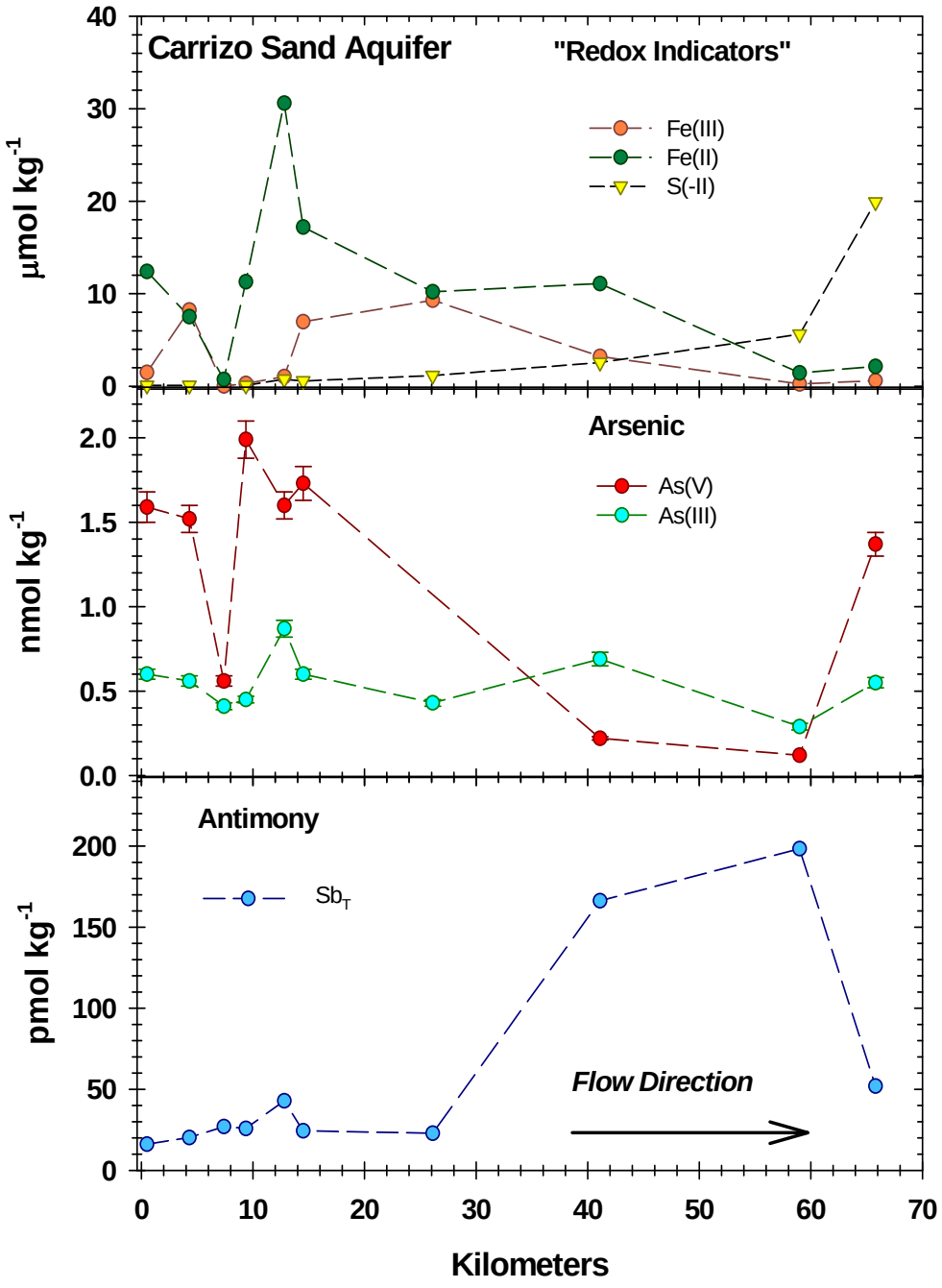

Figure 3.2 Redox sensitive parameters [i.e., Fe(II), Fe(III), S(-II); µmol kg^{-1}], arsenic species [As(V), As(III); nmol kg^{-1}], and total dissolved antimony (pmol kg^{-1}) concentrations in groundwaters collected along the flow path within the Carrizo Sand aquifer. See Haque and Johannesson (2006a) for details.

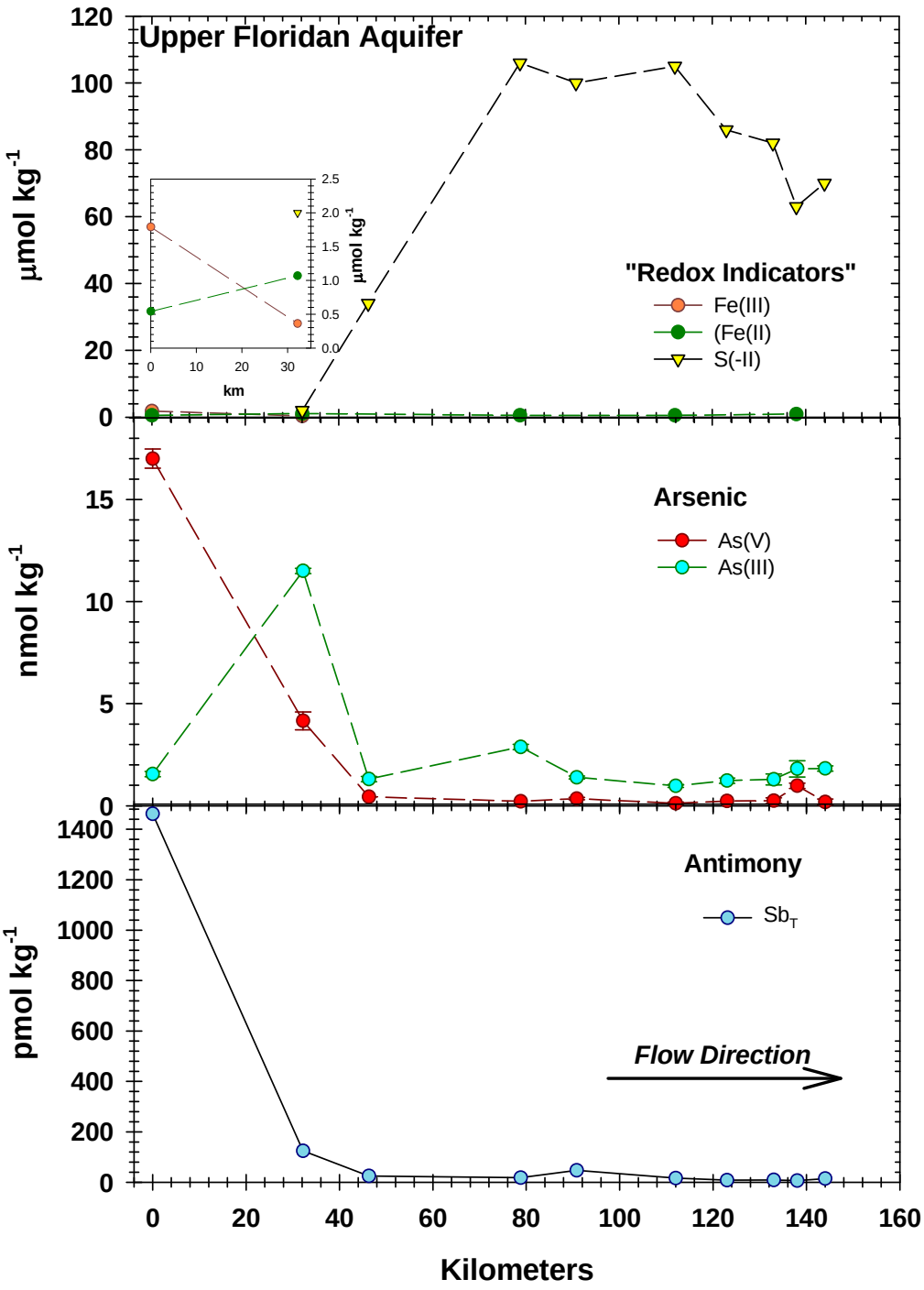

Figure 3.3 Redox sensitive parameters [i.e., Fe(II), Fe(III), S(-II); µmol kg^{-1}], arsenic species [As(V), As(III); nmol kg^{-1}], and total dissolved antimony (pmol kg^{-1}) concentrations in groundwaters collected along the flow path within the Upper Floridan aquifer. See Haque and Johannesson (2006b) for details.

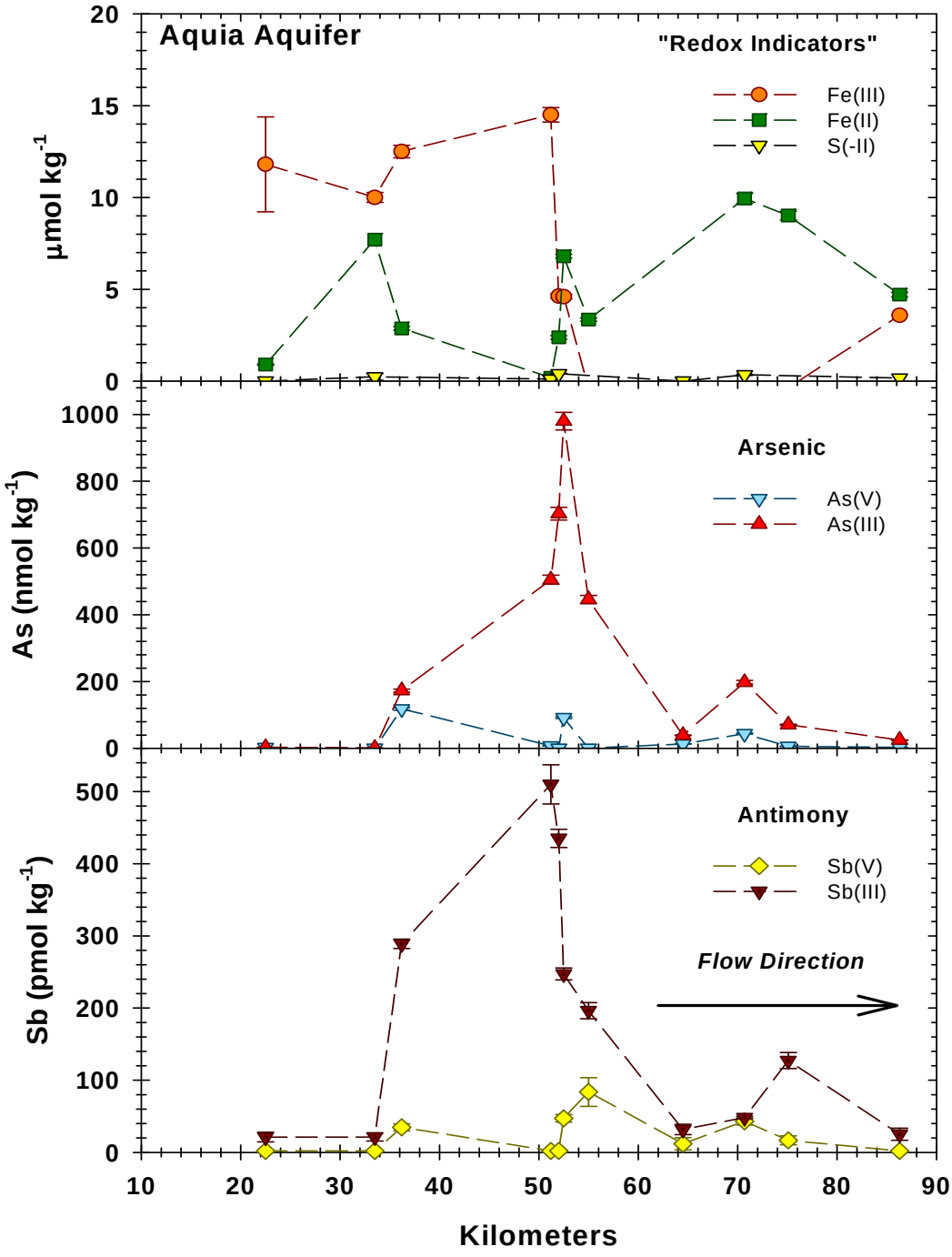

Figure 3.4 Redox sensitive parameters [i.e., Fe(II), Fe(III), S(-II); µmol kg^{-1}], arsenic species [As(V), As(III); nmol kg^{-1}], and antimony species [Sb(V), Sb(III); pmol kg^{-1}] concentrations in groundwaters collected along the flow path within the Aquia aquifer. See Haque et al. (2008) for details.

3.5 Discussion

3.5.1 Correlation between As and Sb

Because As and Sb are members of Group VA within the periodic table, and exhibit the same valence states (i.e., trivalent and pentavalent), they are commonly expected to exhibit broadly similar geochemical behavior in the environment, including within groundwater flow systems. Nevertheless, many investigators have reported differences in their geochemical behavior that appear to reflect their coordination with oxygen (e.g., As(V) tetrahedrally coordinated, whereas Sb(V) is octahedrally coordinated), redox potential, and solution pH (Crecelius et al., 1975; Brookins, 1986; Byrd, 1990; Filella et al., 2002a, b; Mitsunobu et al., 2006; Wilson et al., 2010). The general trends in As_T and Sb_T concentrations in groundwaters collected along the flow paths in the Upper Floridan and Aquia aquifers are indeed broadly similar, although close examination reveals subtle differences in how As and Sb concentrations vary along the flow paths in both aquifer (Figs. 3.3, 3.4). However, within the Carrizo Sand aquifer the trends in the As_T and Sb_T concentrations along the flow path are decoupled in that regions of the aquifer where As_T concentrations are high generally exhibit the lowest Sb_T concentrations, and vice versa (Fig. 3.2).

The Sb_T concentrations for groundwater sampled from all three aquifers exhibit a weak ($r = 0.32$) correlation with the corresponding As_T concentrations (Fig. 3.5). The correlation between Sb_T and As_T in groundwaters from all three aquifers is stronger for the log transformed concentrations (i.e., log As_T vs. log Sb_T, $r = 0.67$; Fig. 3.6; Haque and Johannesson, 2007). The positive relation between Sb_T and As_T in these

groundwaters chiefly reflects the correspondence between the concentrations of these metalloids in the Aquia and Upper Floridan aquifer groundwaters ($r = 0.76$ and $r = 0.78$, respectively, both significant at > 99% confidence level; Haque and Johannesson, 2007). As suggested by the concentration trends along the flow path, Sb_T and As_T exhibit a moderate, inverse correlation within the Carrizo Sand aquifer groundwaters ($r = -0.57$; significant at > 90% confidence level). Closer examination of the Sb and As data from Aquia aquifer groundwaters, for which we have speciation data for both metalloids, reveals that the positive correlation between the Sb_T and As_T is driven by the correlation between Sb(III) and As(III) in these groundwaters ($r = 0.72$, significant at > 95% confidence level; Fig. 3.7). The correlation coefficient for the oxidized species of these metalloids in Aquia aquifer groundwaters suggests a weak, positive relationship between Sb(V) and As(V) ($r = 0.4$), however, this relationship is not statistically significant.

Although the Sb and As data for groundwaters from the Upper Floridan and Aquia aquifer indicate general similarities in the geochemical behavior of these metalloids in groundwater flow systems, the subtle differences in chemical behavior suggested by the moderate to weak correlation coefficients between Sb and As species in these groundwater and the inverse relationship reported between these metalloids in the Carrizo Sand aquifer groundwaters, indicates that As and Sb do not behave identically in groundwater systems. There are a number of possible explanations for these differences.

For example, in a recent study of As and Sb in mine tailing soil samples and, in particular, laboratory soil-water batch experiments, Mitsunobu et al. (2006) found that Sb chiefly occurred in solution as Sb(V), whereas both As(V) and As(III) coexisted for Eh values ranging from 0.36 to -0.14 volts at pH 8. Based on their data they argued that Sb(V) is stable over a wide range of redox potentials (i.e., Eh), and further concluded that Sb must be reduced to Sb(III) at a lower redox potential than the reduction of As(V) to As(III). However, equilibrium thermodynamics predicts the opposite, namely that As(V) is reduced at a lower Eh than Sb. Specifically, considering the reduction of Sb(V) to Sb(III) at pH 7 via the following half-reaction

$$Sb(OH)_6^- + 3H^+ + 2e^- \leftrightarrow Sb(OH)_3^0 + 3H_2O,$$

and using thermodynamic data from Wagman et al. (1982), Brookins (1986), and Pitman et al. (1957), indicates that at equilibrium, Sb(V) is reduced to Sb(III) at an Eh of 0.26 volts. For the corresponding reduction of As(V) to As(III) at pH 7 via the equation

$$HAsO_4^{2-} + 4H^+ + 2e^- \leftrightarrow H_3AsO_3^0 + H_2O,$$

the equilbrium Eh is computed to be 0.013 volts. Therefore, at a given pH As reduction should occur at a lower Eh than Sb reduction. The results of our geochemical modeling discussed below further support the lower Eh of arsenate reduction compared to antimonate. Instead, in addition to molecular structure (i.e., coordination; Wilson et al., 2010) and pH, differences in redox kinetics, biogeochemistry, and possibly even elemental abundances (e.g., As is ~6.5-fold higher than Sb in the Earth's crust; Taylor

and McLennan, 1985; Wedepohl, 1995) probably exert substantial controls on As and Sb species concentrations in groundwater flow systems.

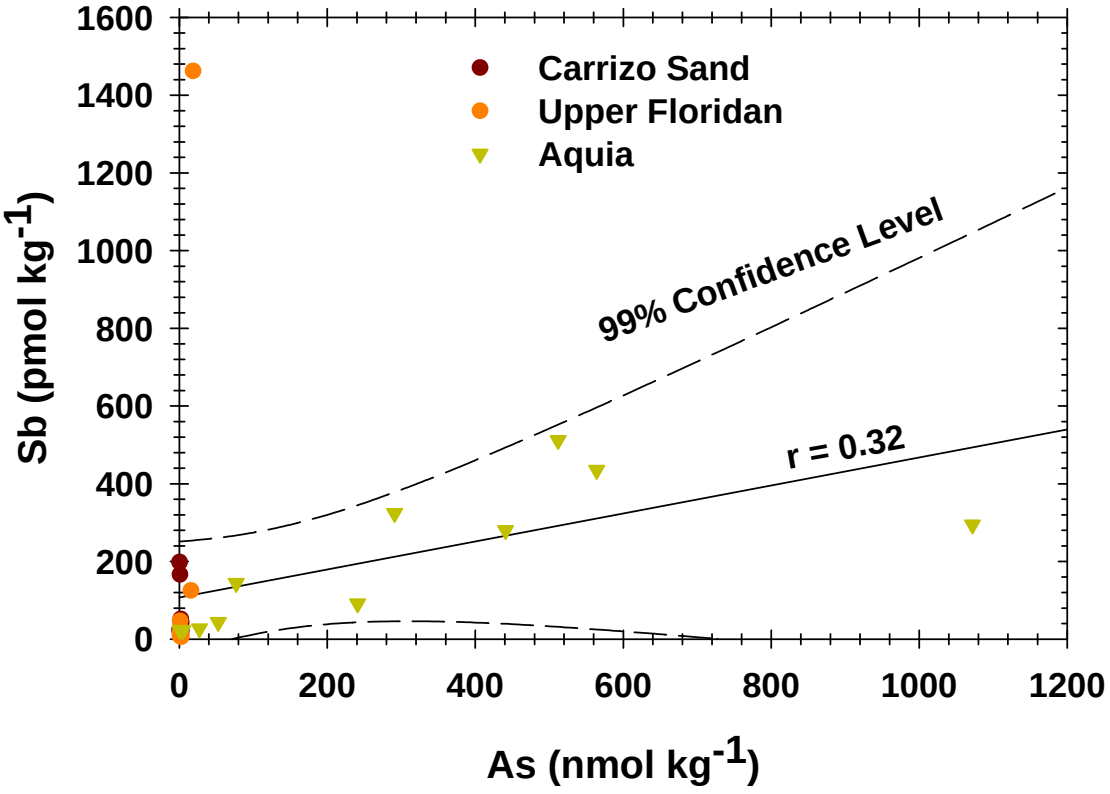

Figure 3.5 Scatter plot of total As vs. Sb in groundwaters from the Carrizo Sand, Upper Floridan, and Aquia aquifers showing the correlation coefficient along with the 99% confidence level of the correlation.

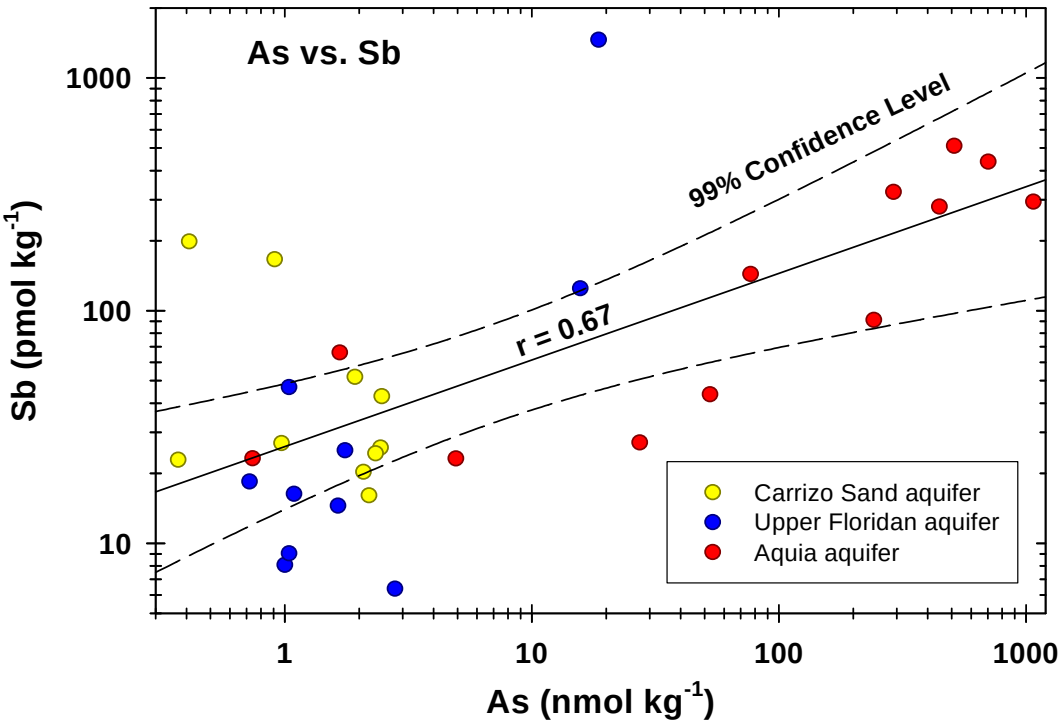

Figure 3.6 Scatter plot of total As vs. Sb in groundwaters from the Carrizo Sand, Upper Floridan, and Aquia aquifers showing the correlation coefficient for the log transformed data along with the 99% confidence level of the correlation.

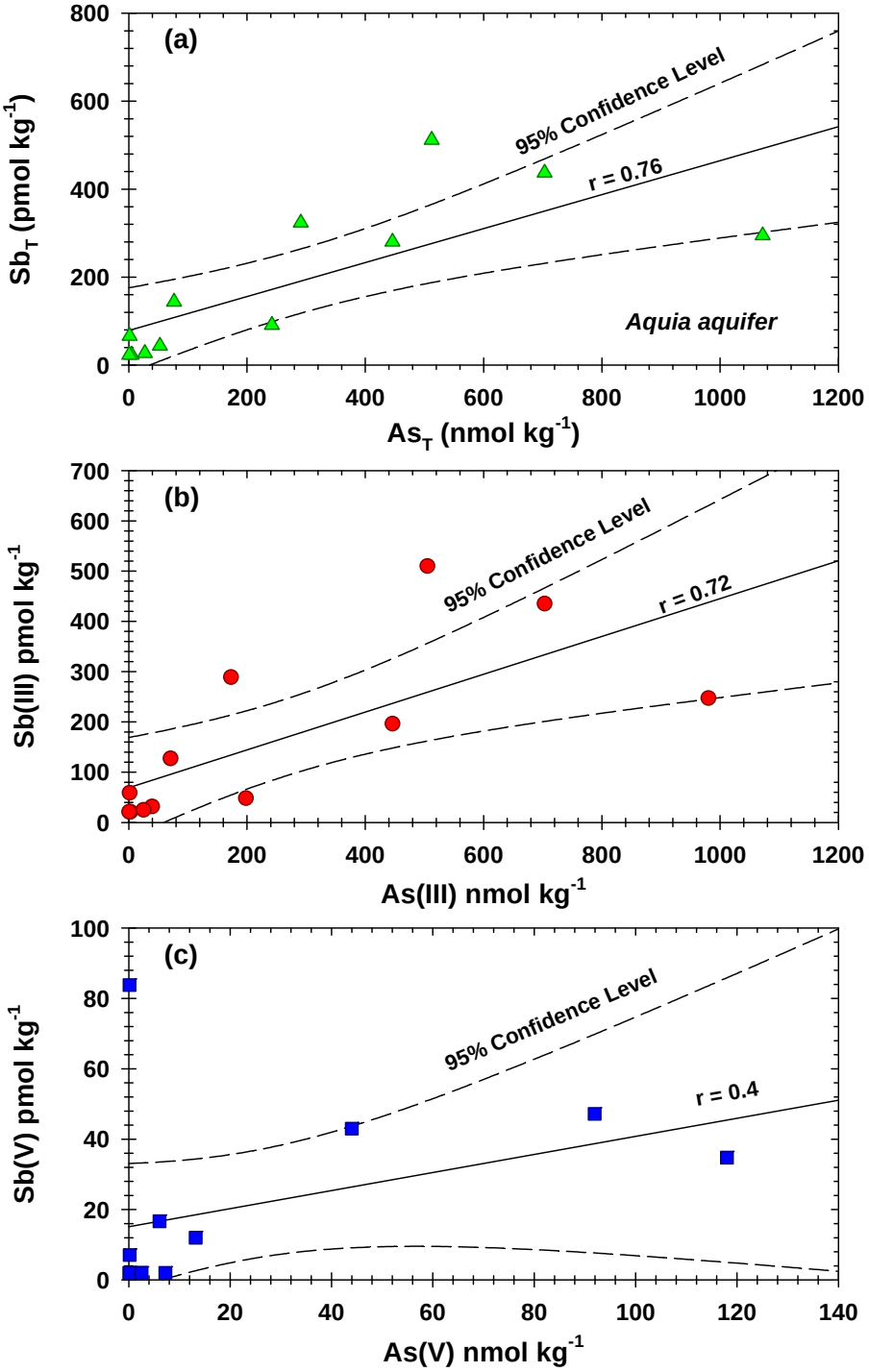

Figure 3.7 Scatter plots for (a) As_T vs. Sb_T, (b) As(III) vs. Sb(III), and (c) As(V) vs. Sb(V) for Aquia aquifer groundwaters. Correlation coefficients, r, are also plotted for linear regression curves along with the corresponding 95% confidence levels.

3.5.2 Hydrogeochemical controls on As and Sb concentrations – Carrizo Sand aquifer

Within the Carrizo Sand aquifer As and Sb concentrations exhibit systematic changes along the flow path that correspond to changes in dissolved Fe(II) and Fe(III) concentrations, dissolved S(-II) concentrations, and pH (Fig. 3.2). Previously we demonstrated that the release of both As(V) and As(III) to Carrizo Sand aquifer groundwaters at ~10 km down-gradient along the flow path corresponds to the region of the aquifer where Fe(III) reduction appears to buffer redox conditions (Haque and Johannesson, 2006a). Our observations are consistent with a number of other investigations that suggest that reductive dissolution of Fe(III) oxides/oxyhydroxides and subsequent release of sorbed/co-precipitated As to anaerobic groundwaters is an important mechanism by which As is mobilized in the environment (e.g., Nickson et al., 1998, 2000; McArthur et al., 2001; Dowling et al., 2002; Harvey et al., 2002; van Geen et al., 2004; Zheng et al., 2004; Polizzotto et al., 2005). With flow beyond ~12 km along the studied flow path, Fe(II) and As(V) concentrations in Carrizo groundwaters decrease. The decrease in Fe(II) and As(V) is consistent with readsorption of both aqueous species to the abundant Fe(III) oxides in the aquifer substrate, as well as the probable precipitation of siderite, $FeCO_{3(c)}$, in the aquifer. Equilibrium calculations using PHREEQE indicate that Carrizo Sand aquifer groundwaters are generally saturated with respect to siderite (Basu et al., 2007). Iron and As are also likely removed from the groundwater in the lower reaches of the studied flow path via precipitation of sulfide minerals as sulfate reductions becomes progressively more important with flow down gradient (Haque and Johannesson, 2006a; Basu et al., 2007).

The increase in As(V) [and As(III)] concentrations in the two groundwater samples from near the end of the studied flow path (i.e., SMA 74R-1, AC74R-2) could reflect pH related desorption of, for example, the $HAsO_4^{2-}$ species, in these high pH groundwaters (pH > 8.3), followed by slow reductive conversion of As(V) to As(III) (Haque and Johannesson, 2006a). Alternatively, owing to the sulfidic nature of these groundwaters (Fig. 3.2), it is also possible that the increase in As(V) concentrations in the down-gradient region of the studied flow path actually reflects formation of thioarsenic species (Wilkins et al., 2003; Haque and Johannesson, 2006a). More specifically, the negatively charged thioarsenite species likely to predominate in these sulfidic waters (e.g., AsS_2^- or $HAsS_3O^{2-}$; Jay et al., 2004; Helz and Tossel, 2008) would not pass through the anion-exchange column, thus leading to overestimates of the As(V) concentrations in these groundwaters, which were determined by difference (Haque et al., 2006a). However, geochemical modeling using the React program of the Geochemist's Workbench® (release 7.0; Bethke, 2008) suggests that As concentrations in Carrizo Sand aquifer groundwaters are insufficient for the formation of substantial amounts of dissolved thioarsenic species (Fig. 3.8).

Antimony concentrations in groundwaters from the Carrizo Sand aquifer increase with flow down-gradient along the flow path, with an especially dramatic increase in the region of the aquifer where sulfate reduction appears to be the predominant redox buffering reaction (Fig. 3.2; Tang and Johannesson, 2006; Haque and Johannesson, 2006a). The slight increase in Sb concentrations in Carrizo groundwaters in the region of the aquifer where Fe(III) reduction predominates suggests

that reductive dissolution of Fe(III) oxide/oxyhydroxides also releases sorbed and/or co-precipitated Sb to Carrizo groundwaters. However, the large increase in Sb concentrations in the region of the aquifer where sulfate reduction predominates is somewhat perplexing. It is possible that the large increase in Sb concentrations in groundwaters from the down-gradient regions of the Carrizo Sand aquifer may, in part, also reflect pH related desorption of Sb(V) as groundwater pH increases above 8 (e.g., Leuz et al., 2006; Martínez-Lladó et al., 2008).

Although we did not quantify Sb speciation in Carrizo Sand aquifer groundwaters, measured Eh values suggest that Sb(III) should predominate, occurring as the $Sb(OH)_3^0$ species (Fig. 3.8). However, the increase in dissolved S(-II) in these groundwaters also points towards the possibility that thioantimony species could be important in these groundwaters. A recent study suggests, for example, that for natural waters with pH $\geq$ 6, thioantimony species (e.g,. $Sb^{V}S_4^{3-}$, $Sb^{III}S_2^{-}$) will predominate when S(-II) $\geq$ 1 μmol kg^{-1} and Sb $\geq$ 1 nmol kg^{-1} (Filella and May, 2003). The highest Sb concentration measured in Carrizo groundwaters is only ~ 0.2 nmol kg^{-1}, whereas the dissolved S(-II) concentration ranges between 2.6 and 20 μmol kg^{-1} in the down-gradient, sulfidic groundwaters (Fig. 3.2). Therefore, owing to the high S(-II) concentrations of these groundwater, it is reasonable to expect that a portion of the Sb in Carrizo Sand groundwaters occurs as thioantimony species. This is supported by our geochemical modeling that predicts the predominance of the thioantimonite species $HSb_2S_4^-$ in sulfidic groundwaters from the lower reaches of the studied flow path within the Carrizo Sand aquifer (Fig. 3.8). Furthermore, whereas the presence $Sb^{V}S_4^{3-}$ in

sulfidic groundwaters may seem counterintuitive, previous studies have shown that Sb(V) species can coexist with dissolved S(-II) in natural waters (Bertine and Lee, 1983; Cutter, 1991; Filella and May, 2003).

Although the increase in Sb concentration in Carrizo Sand groundwater cannot be unequivocally ascribed to formation of thioantimony species, it is important to note that these anionic species would exhibit low affinities for surface adsorption in these high pH groundwaters, suggesting that thioantimony species would be relatively mobile in the high pH groundwaters of the Carrizo Sand aquifer. The increase in Sb concentrations in sulfidic groundwaters of the Carrizo Sand aquifer is thus consistent with greater mobility of negatively charged, thioantimony species in these waters. We note that our geochemical modeling indicates that Sb removal by precipitation of stibnite, $Sb_2S_{3(c)}$, is unlikely in Carrizo Sand aquifer groundwaters (Fig. 3.8), although Sb removal by adsorption onto precipitating sulfide minerals cannot be ruled out. Others have shown, for example, that As can be absorbed by metal sulfides (Bostick and Fendorf, 2003; Bostick et al., 2003). Hence, the decrease in Sb concentrations in groundwater from well SMA 74R-1 at the end of the studied flow path may indicate Sb removal with precipitating sulfide minerals.

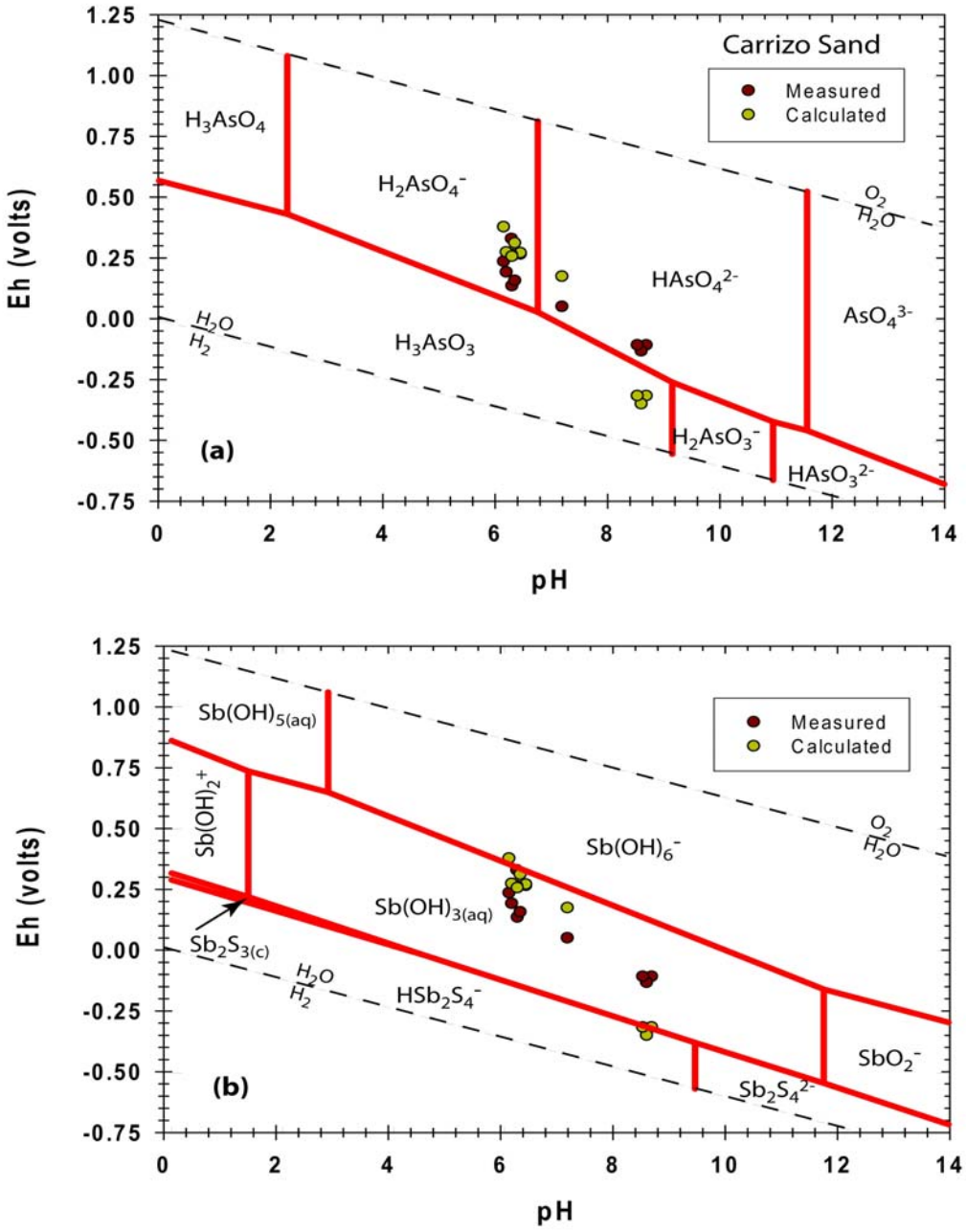

Figure 3.8 Eh vs. pH plots speciation of As and Sb in Carrizo Sand aquifer groundwaters calculated for $[As]_T = 10^{-8.79}$ moles kg^{-1}, $[Sb]_T = 10^{-10.2}$ moles kg^{-1}, $[HCO_3^-] = 10^{-2.52}$ moles kg^{-1}, $[SO_4^{2-}] = 10^{-3.31}$ moles kg^{-1}, and $[Fe]_T = 10^{-4.89}$ moles kg^{-1}. These values represent the mean values for all of the groundwaters collected along the studied flow path. Realgar, orpiment, scorodite, and arsenopyrite were suppressed in the calculations to illustrate only the aqueous speciation of As. Brown circles show where the groundwaters plot based on their field measured Eh values, whereas the gold circles reflect the Eh computed using the React program of the Geochemist's Workbench® (release 7.0; Bethke, 2008) using the geochemical data listed in Appendix A.

3.5.3 Hydrogeochemical controls on As and Sb concentrations – Upper Floridan aquifer

Within the Upper Floridan aquifer, total dissolved As and Sb concentrations show similar trends with flow down-gradient along the flow path (Fig. 3.3). Both exhibit relatively high concentrations in the recharge area (i.e., well ROMP 76A; 0 km) near Polk City, and subsequently decreases to substantially lower concentrations with flow beyond the ROMP 59 well located roughly 32 km down-gradient along the flow path. Arsenic and Sb concentrations thereafter remain low for the remainder of the flow path (Fig. 3.3). For the well at Polk City (ROMP 76A), As(V) is the predominant form of As in Upper Floridan groundwaters (Fig. 3.3). Similar to the Carrizo Sand aquifer, we did not collect samples to measure Sb speciation in Upper Floridan aquifer groundwaters. The subsequent decrease in As(V), and Sb_T, concentrations with flow beyond the ROMP 76A well corresponds to a slight decrease in pH (from 7.93 to 7.82; Appendix B), suggesting that $HAsO_4^{2-}$, and possibly $Sb(OH)_6^-$, are being adsorbed to aquifer mineral surface sites in these relatively more oxic groundwaters (Haque and Johannesson, 2006b). The pH of ROMP 76A groundwater is close to the point of zero charge (PZC) of Fe(III) oxides/oxyhydroxides (PZC ~ 8; Dzombak and Morel, 1990; Appelo et al., 2002) and $CaCO_3$ (PZC ~ 8 – 9.5; Somasundaran and Agar, 1967). Therefore, as the pH of Upper Floridan aquifer groundwater decreases with flow from ROMP 76A to ROMP 59 (32 km; pH 7.82), the surface charge or Fe(III) oxides/oxyhydroxides and $CaCO_3$ should become progressively more positive, thus facilitating adsorption of dissociated As(V) and Sb(V) species (Somasundaran and

Agar, 1967; Harmon et al., 2004; Haque and Johannesson, 2006b; Leuz et al., 2006; Martínez-Lladó et al., 2008).

In addition to the decrease in overall As concentrations (i.e, As_T; Appendix B), the speciation of As switches from As(V) to predominantly As(III) as groundwater flows from ROMP 76A towards ROMP 59 (Fig. 3.3). The chief form of iron in these groundwaters also changes from Fe(III) [i.e., presumably colloidal] to Fe(II), indicating that ferric iron reduction apparently buffers the redox conditions of the Upper Floridan aquifer along this 32 km portion of the flow path (Haque and Johannesson, 2006b). Thus, the change in As speciation between the ROMP 76A and ROMP 59 wells is consistent with As(V) release via reductive dissolution of Fe(III) oxides/oxyhydroxides, followed by reduction of As(V) to As(III) (Oremland and Stolz, 2005; Haque and Johannesson, 2006b). It is also possible that sorbed or co-precipitated As(III) is being released to Upper Floridan aquifer groundwaters during reductive dissolution of Fe(III) oxides/oxyhydroxides (Cummings et al., 1999; Dixit and Hering, 2003; Islam et al., 2004; Oremland and Stolz, 2005). However, the large decrease in Sb concentration in Upper Floridan groundwaters with flow from ROMP 76A to ROMP 59 suggests that reductive dissolution of Fe(III) oxides/oxyhydroxides in this portion of the aquifer is not releasing substantial amounts of sorbed or co-precipitated Sb to the groundwaters. Without Sb speciation data, it is impossible to evaluate whether Sb(V) is being reduced to Sb(III) along this portion of the flow path. Nevertheless, Sb_T concentrations drop by a factor of 58 with flow between the ROMP 76A and ROMP 45 wells, whereas the As_T only decrease by a factor of 10, indicating that whatever form Sb occurs as in these

groundwaters, it is strongly removed from solution between ROMP 76A and 59 (Fig. 3.3; Appendix B).

With flow down-gradient beyond ~32 km (i.e., beyond the ROMP 59 well), As concentration decrease dramatically and remain low (i.e., mean [± SD] As = 1.38 ± 0.66 nmol kg^{-1}) for the remainder of the flow path (Fig. 3.3). Antimony concentrations also drop, albeit slightly, with flow from ROMP 59 to ROMP 45 (46.3 km), and remain low for the remainder of the studied flow path (mean ± SD for Sb = 18 ± 13.2 pmol/kg). In addition, Fe(II) concentrations decrease to levels near or below the method detection limit (0.36 μmol kg^{-1}) in groundwaters collected down-gradient of the ROMP 59 well. Except for groundwater from ROMP 59, which is close to saturation with respect to siderite (log $SI_{siderite}$ = -0.5, where SI = saturation index), all of the other groundwaters sampled from the Upper Floridan aquifer are undersaturated with respect to siderite (-2.5 = log $SI_{siderite}$ = -1.0), indicating that Fe(II) removal from these groundwaters does not occur by siderite precipitation (Basu et al., 2007). The increase in dissolved S(-II) and corresponding decrease in Fe(II) concentrations with flow down-gradient beyond ROMP 59 is consistent with a change from Fe(III) reduction to sulfate reduction as the chief redox buffering reaction in the down-gradient regions of the flow path. Because siderite precipitation is not energetically favorable in Upper Floridan aquifer groundwaters, the subsequent decrease in Fe(II) likely reflects either readsorption of Fe(II) to aquifer mineral surface sites and/or precipitation of Fe(II) sulfide (e.g., pyrite) in these sulfidic waters.

Except for the groundwaters from near the recharge zone (i.e., wells ROMP 76A and ROMP 59), Eh values measured during sample collection are consistent with As chiefly occurring in Upper Floridan aquifer groundwaters as arsenite (Fig. 3.9a). However, geochemical modeling predicts that the majority of Upper Floridan aquifer groundwaters are at equilibrium with respect to an arsenic sulfide mineral such as reaglar or orpiment (Fig. 3.9a), suggesting that precipitation of As sulfides may limit the concentration of As in Upper Floridan aquifer groundwaters. These observations are broadly consistent with a recent investigation of the affects of dissolved S and Fe on aqueous As concentration in groundwaters as redox conditions change (O'Day et al., 2004). Specifically, using x-ray adsorption spectroscopy, these authors found that realgar (i.e., AsS) was the chief As-containing mineral in aquifer sediments under SO_4 reducing conditions where SO_4 concentrations ranged between 1 and 3 mmol kg^{-1} (O'Day et al., 2004). Moreover, our model calculations and the study by O'Day et al. (2004) are in agreement with a number of other investigations that indicate As removal from groundwaters undergoing SO_4 reduction by precipitating sulfide minerals (e.g., Moore et al., 1988; Rittle et al., 1995; McCreadie et al., 2000; Inskeep et al., 2002; Kirk et al., 2004).

With regards to Sb in Upper Floridan aquifer groundwaters, equilibrium thermodynamics would predict that Sb(III) in the form of the neutrally charged $Sb(OH)_3^0$ species is the dominant form of Sb in these groundwaters (Fig. 3.9b). Indeed, only groundwater from well ROMP 76A in the recharge zone has sufficiently elevated Eh for the possible predominance of the oxidized form of Sb(V) in solution, occurring

as the $Sb(OH)_6^-$ species (Fig. 3.9b). Geochemical modeling of Upper Floridan aquifer groundwater using the React program of the Geochemist's Workbench® indicates that the Sb(III) oxyanion reacts with dissolved S(-II) in these highly sulfidic groundwaters forming aqueous, thioantimonite species such $HSb_2S_4^-$ (Fig. 3.9b). As the groundwater pH decreases with flow down-gradient along the flow path (from pH 7.9 at the ROMP 76 well in Polk City to pH ~ 7 at ROMP 5-2 and 5-1 in Venice, Florida; Haque and Johannesson, 2006b), the $HSb_2S_4^-$ species would be expected to sorb to mineral surface sites owing to the increasing positive charge of mineral surfaces.

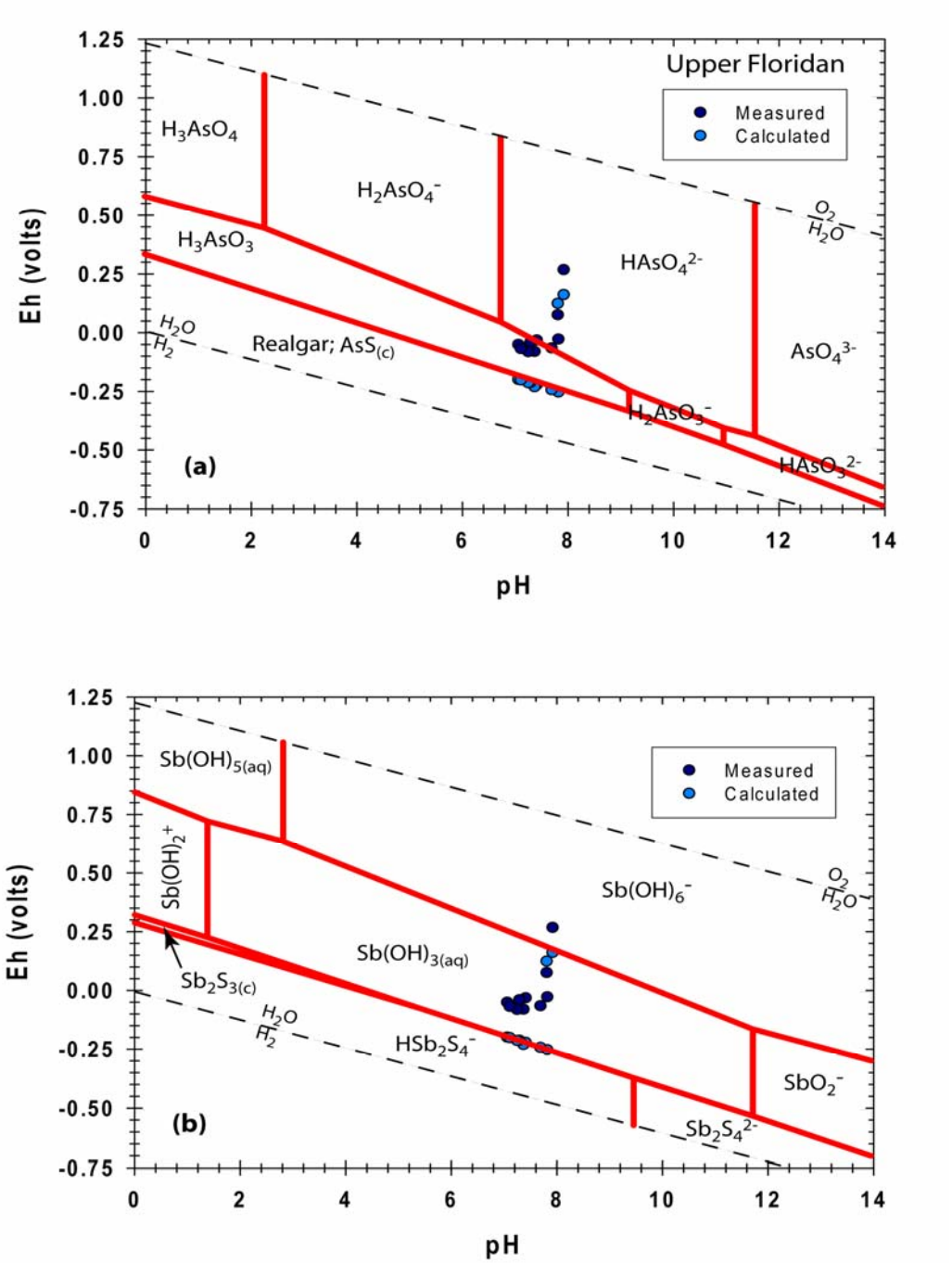

Figure 3.9 Eh vs. pH plots speciation of As and Sb in Upper Floridan aquifer groundwaters calculated for $[As]_T = 10^{-8.34}$ moles kg^{-1}, $[Sb]_T = 10^{-9.76}$ moles kg^{-1}, $[HCO_3^-] = 10^{-2.57}$ moles kg^{-1}, $[SO_4^{2-}] = 10^{-2.26}$ moles kg^{-1}, and $[Fe]_T = 10^{-5.94}$ moles kg^{-1}. Again, these values represent the mean values for all of the Upper Floridan aquifer groundwaters. Orpiment, scorodite, and arsenopyrite were suppressed in the calculations but realgar was included in the calculations because preliminary model runs indicated saturation with As sulfides. Dark blue circles represent the measured Eh values, whereas the light blue circles are the Eh value calculated with the Geochemist's Workbench® using the geochemical data listed in Appendix B.

3.5.4 Hydrogeochemical controls on As and Sb concentrations – Aquia aquifer

Groundwater from the Aquia aquifer differs from both the Carrizo Sand and Upper Floridan aquifers in that Aquia aquifer groundwaters are not sulfidic anywhere along the studied flow path (Haque et al., 2008). Specifically, dissolved S(-II) concentrations are close to or below the method detection limit (i.e., 0.16 μmol kg^{-1}) along the entire flow path (Fig. 3.4). The data are instead consistent with ferric iron reduction being the chief redox buffering reaction within the Aquia aquifer (Fig. 3.4). Consequently, following the classification scheme of Berner (1981), Aquia aquifer groundwaters are suboxic and never reach anoxic/sulfidic conditions (see also Anderson et al., 1994). Nevertheless, dissolved oxygen concentrations and Eh values generally decrease with flow down-gradient indicating that groundwaters become more reducing along the flow path, but not sulfidic (Haque et al., 2008; Appendix C).

Arsenic concentrations are relatively low near the recharge zone (i.e., first 36 km of the flow path), and increase to high concentrations along the mid-reaches (36 – 71 km) of the studied flow path, exceeding the US EPA MCL by as much as 8 times (well QA 94 0111, 52.5 km; Fig. 3.4; Haque et al., 2008). The more toxic As(III) species is the predominant species in all of the Aquia groundwater samples analyzed (Haque et al., 2008). With flow beyond ~71 km, As concentrations in Aquia groundwaters decrease and remain relatively low for the remainder of the studied flow path. Despite the substantially lower concentrations, Sb shows remarkably similar distribution along the flow path as As, with low concentrations in the recharge area, followed by elevated concentrations along the mid-reaches of the flow path, and

generally lower concentrations in groundwater from further down-gradient (Fig. 3.4). Furthermore, Sb(III) is the predominant form of Sb in Aquia aquifer groundwaters.

The observed changes in As and Sb concentrations along the Aquia flow path are generally consistent with control by pH and the changing redox conditions (Haque et al., 2008). Specifically, the elevated As and Sb concentrations along the mid-reaches of the studied flow path (e.g., ~ 52 km; Fig. 3.4) corresponds to the region in the aquifer where Fe speciation changes from presumably colloidal Fe(III) to soluble Fe(II). Thus, the data suggest that reductive dissolution of Fe(III) oxides/oxyhydroxides is the chief mechanism by which As, and Sb, are mobilized from Aquia aquifer sediments to the groundwater (Haque et al., 2008). Recent microcosm experiments further supports that As is chiefly mobilized from Aquia aquifer sediments by microbial reduction of Fe(III) oxides/oxyhydroxides in the aquifer sediments (Pearcy et al., 2010). Furthermore, sequential extraction of the Aquia aquifer sediments reveals that As is principally associated with amorphous and crystalline Fe(III) oxides/oxyhydroxides in these sediments, which requires their dissolution before As can be mobilized (Haque et al., 2008). Presumably, Sb is also associated with the same oxides/oxyhydroxides in the aquifer sediments, requiring their dissolution before Sb is mobilized to the groundwaters.

Geochemical modeling using the React program of the Geochemist's Workbench® (release 7.0) and the data in Appendix C predicts that As (III) should predominate in the majority of the Aquia aquifer groundwater samples analyzed (Fig. 3.10a). Those groundwater samples for which the model predicts substantially higher

Eh values on Fig. 3.10 actually represents the redox potential for the NO_3^-/NH_4^+ redox couple because the groundwater samples had below detection Fe(II), Fe(III), and/or S(-II) concentrations (Appendix C). Hence, estimating the redox conditions of these groundwaters by computing the Eh of the Fe^{3+}/Fe^{2+} and SO_4^{2-}/S^{2-} couples based on the activities of these species was not possible. The measured Eh values fall close to the predicted redox boundary between As(V) and As(III) on Fig. 3.10, which is not consistent with our measured As speciation in Aquia aquifer groundwaters. The fact that the measured Eh values plot within the As(V) stability field on Fig. 3.10a and not the As(III) stability field is further evidence that Eh values determined with platinum electrodes are qualitative measures, at best, of the redox state of a natural water (e.g. Whitfield, 1974; Lindberg and Runnells, 1984; Stefánsson et al., 2005).

In the case of Sb both the measured Eh values and those computed with the Geochemist's Workbench® using the activities of Fe(II), Fe(III), SO_4^{2-}, and S(-II) in Aquia aquifer groundwaters predicts that Sb(III) predominates (Fig. 3.10b). These results are consistent with our Sb speciation measurements, which indicate that Sb(III) is the chief form of Sb in solution in Aquia aquifer groundwaters (Fig. 3.4). Unlike groundwaters from the Carrizo Sand aquifer and the Upper Floridan aquifer, the geochemical modeling does not predict the formation of thioantimony species in Aquia arsenic groundwaters (Fig. 3.10b). Again, this reflects the fact that SO_4 reduction, and hence S(-II) production, is apparently not significant in the Aquia aquifer as S(-II) concentrations are at or below detection along the majority of the flow path (Haque et al., 2008).

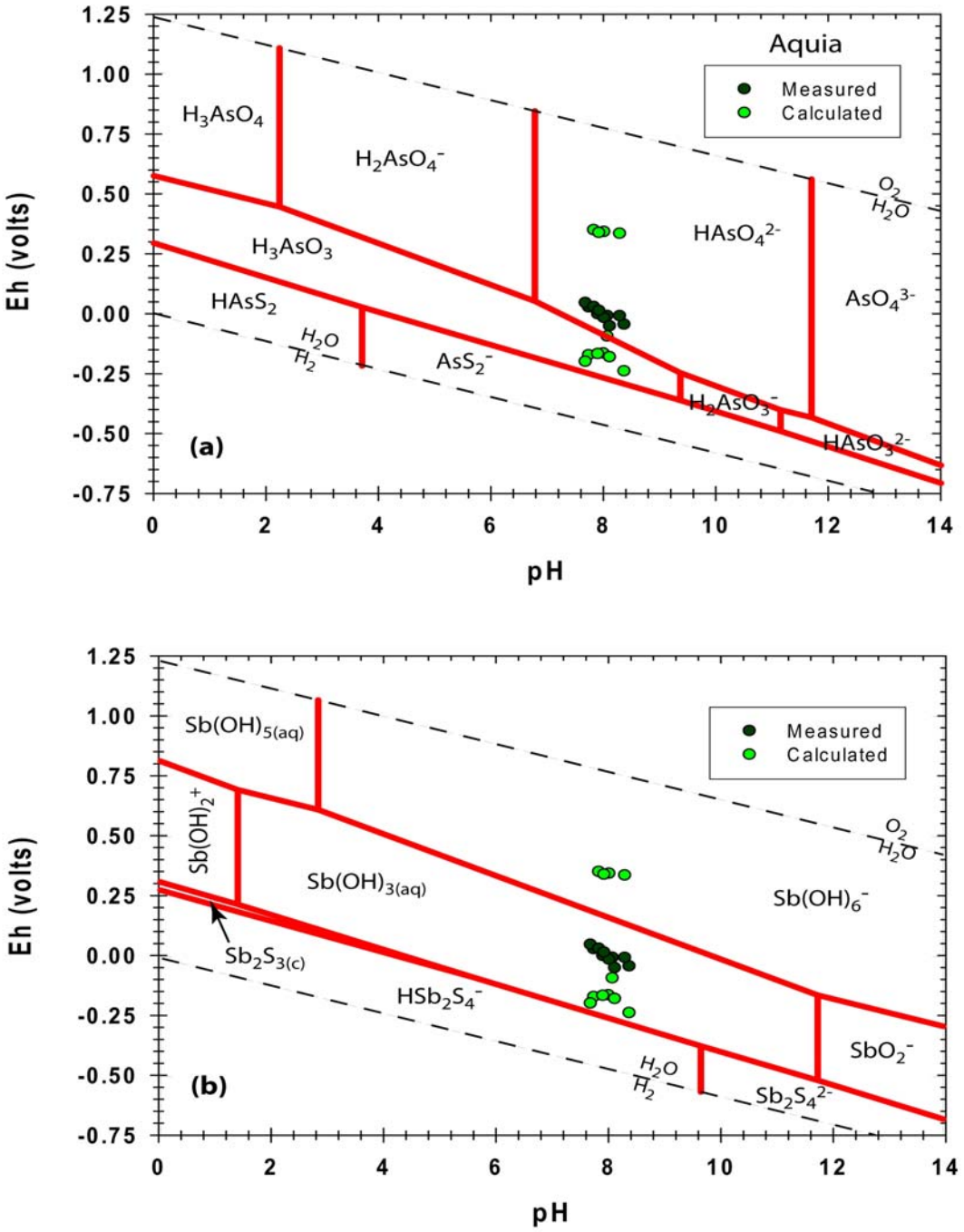

Figure 3.10 Eh vs. pH plots speciation of As and Sb in Aquia aquifer groundwaters calculated for $[As]_T = 10^{-6.52}$ moles kg^{-1}, $[Sb]_T = 10^{-9.70}$ moles kg^{-1}, $[HCO_3^-] = 10^{-2.48}$ moles kg^{-1}, $[SO_4^{2-}] = 10^{-4.22}$ moles kg^{-1}, and $[Fe]_T = 10^{-4.96}$ moles kg^{-1}, which are again the mean values for the studied Aquia aquifer groundwaters. Realgar, orpiment, scorodite, and arsenopyrite were suppressed in the calculations. Dark green circles represent the measured Eh values, whereas the light green circles are the Eh value calculated with the Geochemist's Workbench® using the geochemical data listed in Appendix C.

3.6 Conclusion

Arsenic and antimony concentrations exhibit systematic changes along all three studied flow paths in the Carrizo Sand, Upper Floridan, and Aquia aquifers corresponding to changes in dissolved Fe(II) and Fe(III) concentrations, dissolved S(-II) concentrations, and pH. For the Carrizo Sand and the Upper Floridan aquifers, our data and the geochemical model both predict the formation of thioantimonite species (i.e., $HSb_2S_4^-$) due to the sulfidic nature of the each of these groundwaters. The measured arsenic concentrations for the Carrizo Sand aquifer, which show an increase in the As(V) concentrations at the end of the studied flow path indicating a possible formation of thioarsenic species, are not supported by model calculations. On the other hand, our data and the geochemical model both predict the groundwaters of the Upper Floridan aquifer to be at equilibrium with respect to arsenic sulfide minerals such as reaglar or orpiment. The non-sulfidic groundwaters of the Aquia aquifer differ from the previous two aquifers. Our speciation data indicate the majority of As in these groundwaters should occur as As(III), whereas the geochemical model predicts As(V) to be the predominate form. On the contrary, our speciation data and the model both agree that Sb(III) should be the prevailing form of Sb in these groundwaters. The behavior of As and Sb in the groundwaters of all three aquifers indicate a statistical relationship. Our data suggests that the best correlation between As and Sb occurs in the Aquia aquifer. These results provide important insight into the relationship between As and Sb in a variety of aquifer settings.

CHAPTER 4

ADSORPTION OF ARSENIC ONTO SEDIMENTS OF THE CARRIZO SAND AQUIFER, TEXAS, USA, AND THE AQUIA AQUIFER, MARYLAND, USA

4.1 Introduction

Arsenic (As) is considered to be a priority pollutant by the Environmental Protection Agency of the United States (USEPA, 1979) and the European Union (Council of the European Communities, 1976). The US EPA maximum contaminant level (MCL) for drinking waters has been set at 10 ppb (133 nmol/kg). The World Health Organization and the European Union have also set maximum admissible concentrations for As of 10 ppb (Council of the European Union, 1998). As is one of the most toxic naturally occurring carcinogens found in the environment (Smith et al., 1992; NRC, 1999, 2001; Nriagu, 2002). In groundwater flow systems, inorganic As occurs primarily in two oxidation states, arsenate [As(V)] and arsenite [As(III)] (Mariner et al., 1996; Ferguson and Gavis 1972), and As(III) is estimated to be between ~10 to 60 times more toxic than As(V). A thorough understanding of the geochemical interactions of As within the environment is required to prevent As pollution and to predict the risk of As in groundwater flow systems. Knowledge of the sources of As, the mechanisms controlling its release and mobility, as well as its natural attenuation processes are crucial to minimize the occurrence of As in groundwater flow systems, to

access the risk of As contamination, and to design and implement remediation and treatment plans for aquifers with high As groundwaters (Cheng et al., 2009).

Speciation of As controls its mobility as well as its toxicity in the environment including groundwater flow systems (Amirbaham et al., 2006). Arsenic is mobilized through a combination of natural processes such as weathering reactions, biological activity, and volcanic emissions as well as through a range of anthropogenic activities (Smedley and Kinniburgh 2002). There are about 245 As-bearing minerals in nature, which release As when subject to weathering (NRC, 1997). Most environmental As occurs as a result of mobilization under natural conditions. Thermodynamics predicts that the As(V) species, arsenic acid (i.e. $H_2AsO_4^-$ and $HAsO_4^{2-}$), predominates in oxidizing environments at a pH between 6 and 9 and the As(III) species, arsenious acid (i.e. H_3AsO_3), is more thermodynamically stable in reducing conditions at a pH below 9 (Banerjee et al., 2008).

Adsorption is known to be an important mechanism by which As is removed from groundwaters onto oxidized sediments containing Fe (III) oxides (Pierce and Moore, 1980; Wilkie and Hering, 1996; Roberts et al., 2004). Adsorption efficiency depends on several factors, including pH, the concentration and oxidation state of As, the concentrations of other solutes competing with As for adsorption sites, and the adsorption capacity of the sediment (Stollenwerk et al., 2007). One general trend in adsorption efficiency is that as the pH of the groundwater increases, the ability for arsenate to desorb from aquifer surface sites increases (e.g., Smedley and Kinniburgh 2002).

In this study, we conduct batch reactor experiments to examine the adsorption of As(III) and As(V) by aquifer sediments from two different locations, the Carrizo Sand aquifer located in southeastern Texas and the Aquia aquifer located in coastal Maryland.

4.2 Study Areas

4.2.1 Carrizo Sand aquifer

The study site within the Carrizo Sand aquifer is located in southeastern Texas (Figure 4.1; Haque and Johannesson 2006a). The aquifer, which consists of Eocene sands, is a confined aquifer that crops out nearly parallel to the Gulf Coast. Rainfall recharges the Carrizo Sand at the outcrop and the aquifer dips southeast towards the Gulf of Mexico at a rate of 100 to 130 feet per mile (Pearson and White, 1967; Castro et al., 2000; Castro and Goblet, 2003). The composition of the aquifer is mostly fine- to medium-grained quartz sand with minor amounts of clay, lignite, calcite, and pyrite (Pearson and White, 1967). Basu et al. (2007) showed that goethite and hematite occur as coatings along with fine-grained kaolinite and illite grains on the Carrizo Sand particles. From the outcrop in Atascosa County to the south into McMullen County, the thickness of the Carrizo Sand aquifer increases along the flow path, varying from 100 to 360m (Castro et al., 2000). The porosity of the aquifer is estimated to range from ~30 to 40% (Pearson and White, 1967). Using ^{14}C measurements, Pearson and White (1967) estimated that the age of the groundwater increases from ~5,000 years near the outcrop area in northern Atascosa County to ~30,000 years in southern McMullen

County. In this study, sediment samples were collected from where the aquifer outcrops in Atascosa County (see Haque and Johannesson, 2006a; Basu et al., 2007).

4.2.2 Aquia aquifer

The Aquia aquifer, located in Maryland, is a Coastal Plain aquifer. The aquifer, a Paleocene marine deposit, is confined from above by the Paleocene-Eocene Marlboro clay, and from below by the Crataceous Severn Formation (i.e., silt and clay; Chapelle, 1983). The Aquia outcrops between Washington D.C. and Annapolis, Maryland, and dips southeast towards the ocean (Aeschbach-Hertig et al., 2002). The groundwater flow patterns within the Aquia are dominated by potentiometric highs that occur in and near the outcrop are where the aquifer is recharged (Chapelle and Knobel, 1983). The composition of the aquifer is dominated by fine- to medium-grained quartz sand (50 to 75%), glauconite (20 to 40%), and carbonate shell debris (1 to 5%), and ranges from 30.5 to 45.7 meters thick (Aeschbach-Hertig et al., 2002; Chapelle, 1983; Chapelle and Knobel, 1983). In a previous study on the Aquia by Haque et al. (2008), photomicrographs of Aquia aquifer sediments showed the abundance of quartz, glauconite, and Fe(III) oxide/oxyhydroxides in the sediments. In this study, sediment samples were collected from a freshly drilled well core.

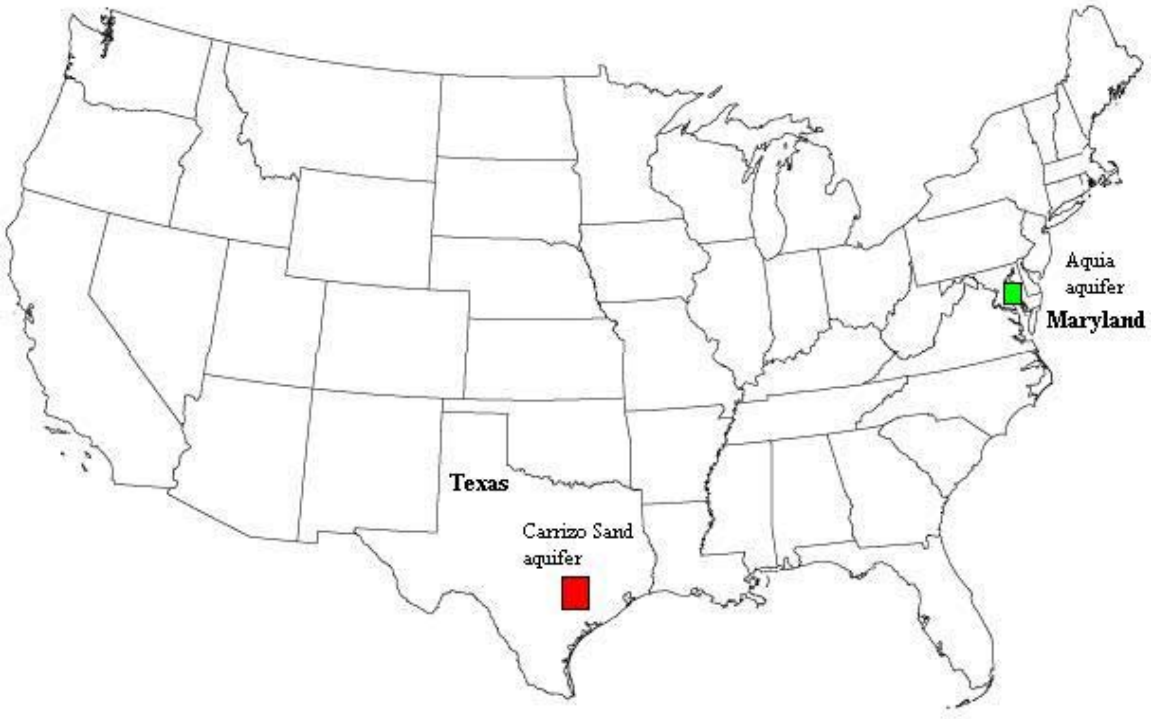

Figure 4.1 Location of the two studies areas (Carrizo Sand aquifer, Texas and Aquia aquifer, Maryland) within the United States of America.

4.3 Materials and Methods

4.3.1 Materials

All chemicals were of analytical grade. Sodium meta-arsenite ($NaAsO_2$, 98.5%) was obtained from J.T. Baker and sodium hydrogen arsenate heptahydrate ($Na_2HAsO_4*7H_2O$, 98%) was obtained from Alfa Aesar. Sodium chloride (NaCl) was obtained from Fisher Scientific and oxalic acid dehydrate ($C_2H_2O_4*2H_2O$, 99%) was obtained from Sigma-Aldrich.

A 3000 μg L^{-1} stock solution of As(V) was prepared by dissolving 12.4939 mg $Na_2HAsO_4*7H_2O$ in 0.01 M NaCl. Additionally, a 1500 μg L^{-1} stock solution of As

(III) was prepared by dissolving 2.4408 mg of $NaAsO_2$ in 0.01 M NaCl. All solutions contained 0.01 M NaCl as a background electrolyte to spproximate the ionic strengths of the groundwaters from each aquifer. The arsenic stock solutions were stored in pre-cleaned (acid-washed; Johannesson et al., 2004) high density polyethylene bottles (HDPE), with the As(III) solution being stored in an amber HDPE bottle to prevent oxidation to As(V). The pH values for all experiments were 7.5 ± 0.1, except as noted below. The pH values were adjusted using 0.1 M NaOH or HCl and monitored throughout the experiments to correct for any possible pH drift.

4.3.2 Laboratory Experiments

All batch reactor experiments described below were conducted using a solid to solution ration of 0.5 g dry sediment to 20 mL of solution in 50 mL precleaned (Johannesson et al., 2004) polypropylene centrifuge tubes. The solutions were mixed continuously on a shaker (VWR Mini Shaker) for the equilibrium reaction time, of 4 days as determined by kinetic experiments. The solutions were then separated from the sediment by centrifugation (Labofuge 400, Heraeus Instruments) at 15,000 rpm for 15 minutes followed by filtration using 0.45 μm polyethersulfone membrane filters (Whatman Puradisc).

A series of As(V) kinetics experiments were performed to determine the amount of time required for As(V) adsorption to equilibrate with the aquifer sediments. Adsorption times of As(V) were measured using an initial As(V)concentration of 800 μg/L and reaction times ranging from 0.08 to 6 days. Experiments were conducted in contact with air at room temperature (23 ± 2°C).

Following the kinetic experiments, As(III) and As(V) were studied in separate batch reactors for both the Carrizo Sand and Aquia aquifer sediments. The objective was to establish adsorption isotherms for As(III) and As(V) onto bulk Carrizo Sand and Aquia aquifer sediments. Arsenite concentrations in the experimental solutions range from 50 to 1500 μg/L and As(V) concentrations range from 50 to 3000 μg/L. The As(III) experiments were conducted in a glove box (Labconco Protector Glove Box) in dark, anaerobic conditions, under an N_2 atmosphere (dissolved $O_2 < 0.005$ mg L^{-1}). Adsorption experiments for As(V) were conducted in a laminar flow clean bench (Class 100) under laboratory air conditions. All experiments were conducted at room temperature (23 ± 2°C). The amount of As(V) adsorbed onto the sediments was determined by the difference between the initial and final aqueous concentrations. This method could not be used for As(III) because of partial oxidation to As(V). The supernantant was discarded and the sediment was reacted with 20 mL of 0.2 M oxalic acid for 30 minutes to directly measure the As(III) adsorbed (Stollenwerk et al., 2007).

Adsorption was also measured as a function of pH using an initial As(V) concentration of 500 mg/L. The pH ranges evaluated for the Carrizo sediments range from 6.16 to 8.70 and the range for the Aquia sediments are 7.57 to 9.65. These pH ranges were selected based on the range of pH directly measured for Carrizo Sand and Aquia aquifer groundwaters (Tang et al., 2005a; Haque and Johannesson, 2006a; Tang and Johannesson, 2006; Basu et al., 2007). The pH values were adjusted using 0.1 M NaOH or HCl.

4.3.3 Analytical Techniques

All dissolved As(III) and As(V) concentrations in experimental solutions were analyzed using inductively coupled plasma mass spectrometry (ICP-MS). The samples were quantified using a high resolution Finnigan MAT ELEMENT 2 (magnetic sector) ICP-MS at Tulane University. The high resolution (HR) mode of the HR-ICP-MS allows As to be distinguished from possible Cl^- interferences on ^{75}As. The ICP-MS was calibrated using aqueous standard solutions, of the same acid concentrations as in the samples, prepared from stock solutions by subsequent dilution in the range of 1 – 5000 ppb for As. The stock solutions were prepared from Perkin Elmer Pure Plus As standards. All standards and sample solutions were spiked with indium as an internal standard to correct for instrument drift. In addition, check standards were run routinely during the analysis to ensure the overall quality as well as to monitor instrument drift.

4.4 Results

4.4.1 Adsorption kinetics

The results of the kinetic experiments are presented in Figure 4.2. For the Aquia aquifer, As(V) was rapidly adsorbed in the first 24 hours and equilibrium was achieved after approximately 48 hours. The percentage of As(V) adsorbed for the Aquia aquifer ranged from 32 to 39%. Comparatively, the adsorption of As(V) to the Carrizo Sand aquifer sediments was slower with the majority of As(V) sorption occuring after approximately 100 hours. The percentage of As(V) adsorption was higher for the Carrizo Sand aquifer, ranging from 27 to 51%. From these results, 100 hours was considered the equilibrium reaction time for As(V) as well as for As(III) adsorption

onto the aquifer sediments from both the Aquia and Carrizo Sand aquifers and was used in all subsequent As(V) and As(III) adsorption experiments.

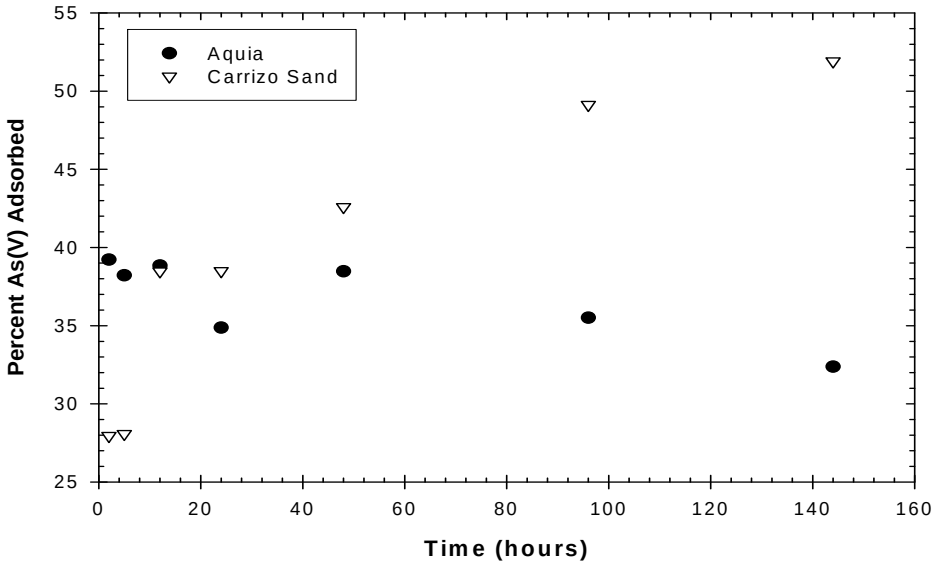

Figure 4.2 Reaction kinetics of As(V) by aquifer sediments for the Aquia and Carrizo Sand aquifers.

4.4.2 As adsorption as a function of pH

The samples from the Aquia aquifer showed that as the pH increased from 7.5 to 9.27, As(V) adsorption decreased by 5% followed by an increase of 18% at pH 9.65 (Figure 3). For the Carrizo sand aquifer, the experiment showed that as the pH increased from 6.16 to 8.70, As(V) adsorption varied slightly between 60 to 61%. In both of the studied pH ranges, our results reveal that pH will likely have a minimal effect on the transport of As(V) to aquifer sediments.

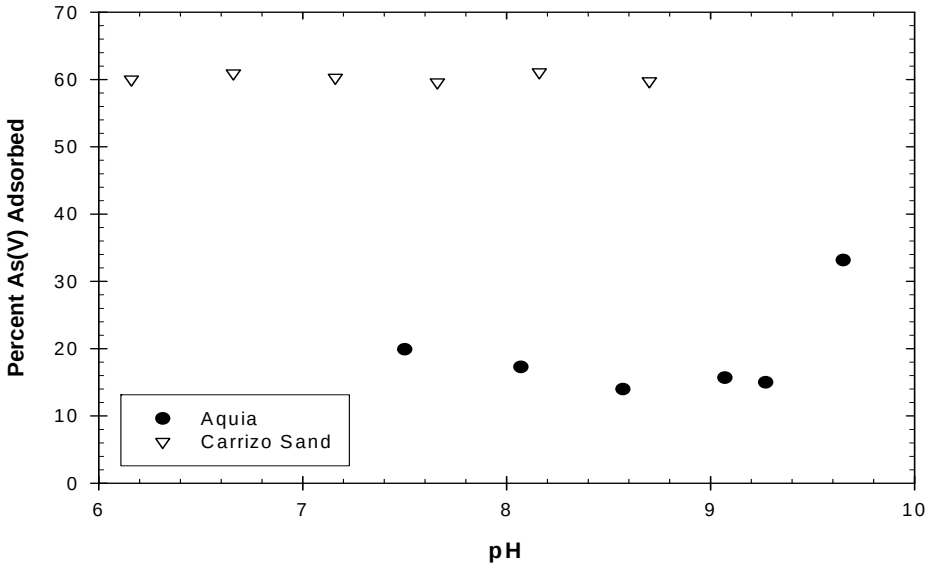

Figure 4.3 Effect of pH on adsorption of As(V) by sediments for the Aquia and Carrizo Sand aquifers.

4.4.3 Arsenic adsorption

Figure 4.4 shows the percentages of As(V) and As(III) adsorbed by aquifer sediments from the Carrizo Sand and Aquia aquifers. For the Aquia, As(V) adsorption ranged from 1 to 50% (see Figure 4.4a), and As(III) adsorption ranged from 25 to 72% (see Figure 4.4b). The Carrizo Sand displayed As(V) adsorption in the range of 20 to 90% (see Figure 4.4a) and As(III) adsorption ranging from 13 to 37% (see Figure 4.4b). Adsorption isotherms for As(V) and As(III) are presented for the Carrizo Sand and Aquia aquifers in Figure 5. The adsorption isotherms describe the retention of As species onto the aquifer sediments at various concentrations. These isotherms help predict the mobility of the As species in the groundwater flow systems (Limousin et al., 2007). As(V) adsorption onto Carrizo Sand exhibits a Langmuir-like isotherm with rapid increase in the amount of As(V) sorbed at low initial As(V) concentrations. The amount of As(V) then decreases eventually approaching an almost constant amount

adsorbed at high concentrations. Adsorption of As(III) onto Carrizo Sand may also exhibit a Langmuir-like isotherm, although it is also almost linear. As(V) sorption onto the Aquia aquifer sediments shows an S-shaped isotherm, whereas As(III) sorption to Aquia aquifer follows an almost linear distribution.

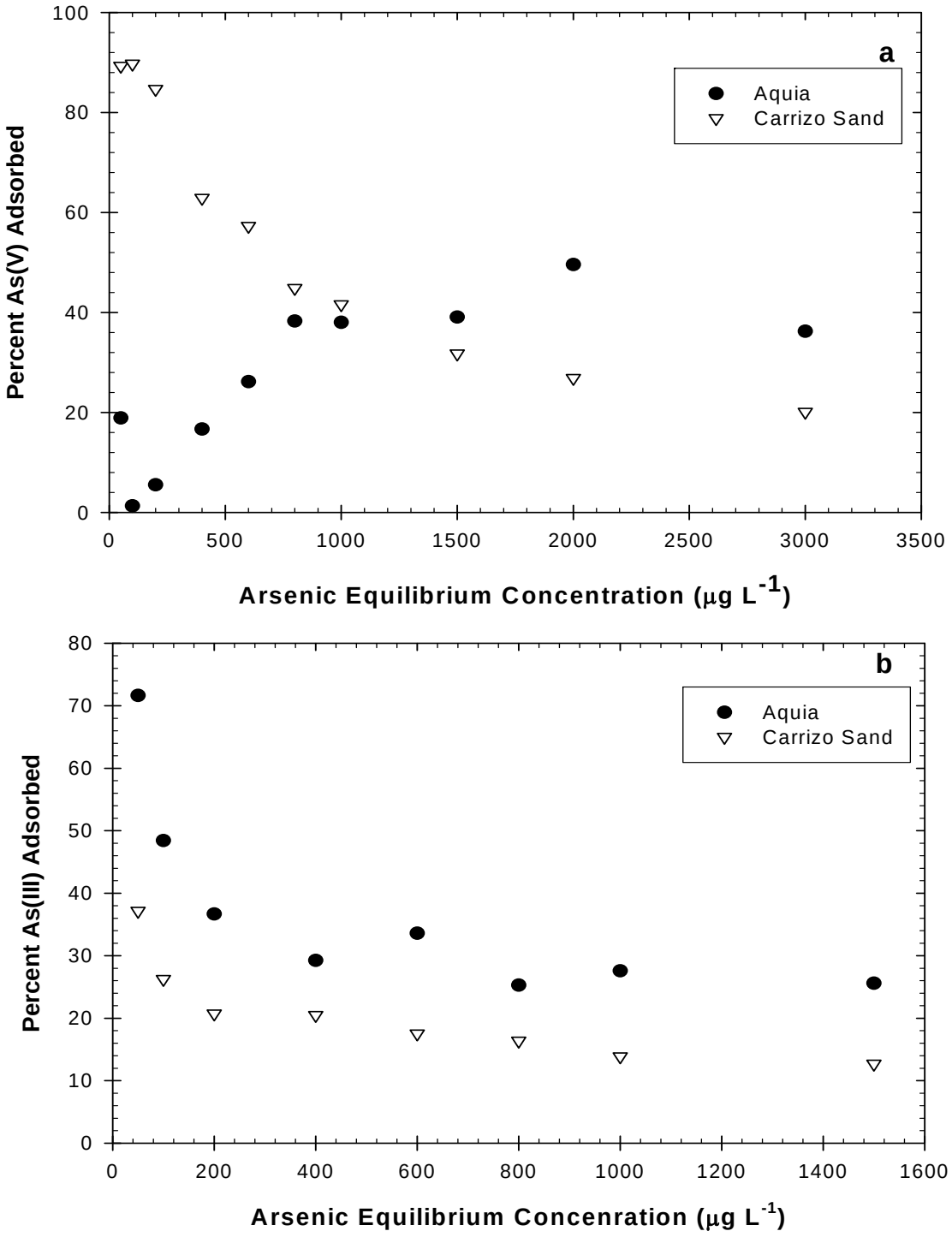

Figure 4.4 Percentages of (a) As(V) and (b) As(III) adsorbed by sediments of the Aquia and Carrizo Sand aquifers.

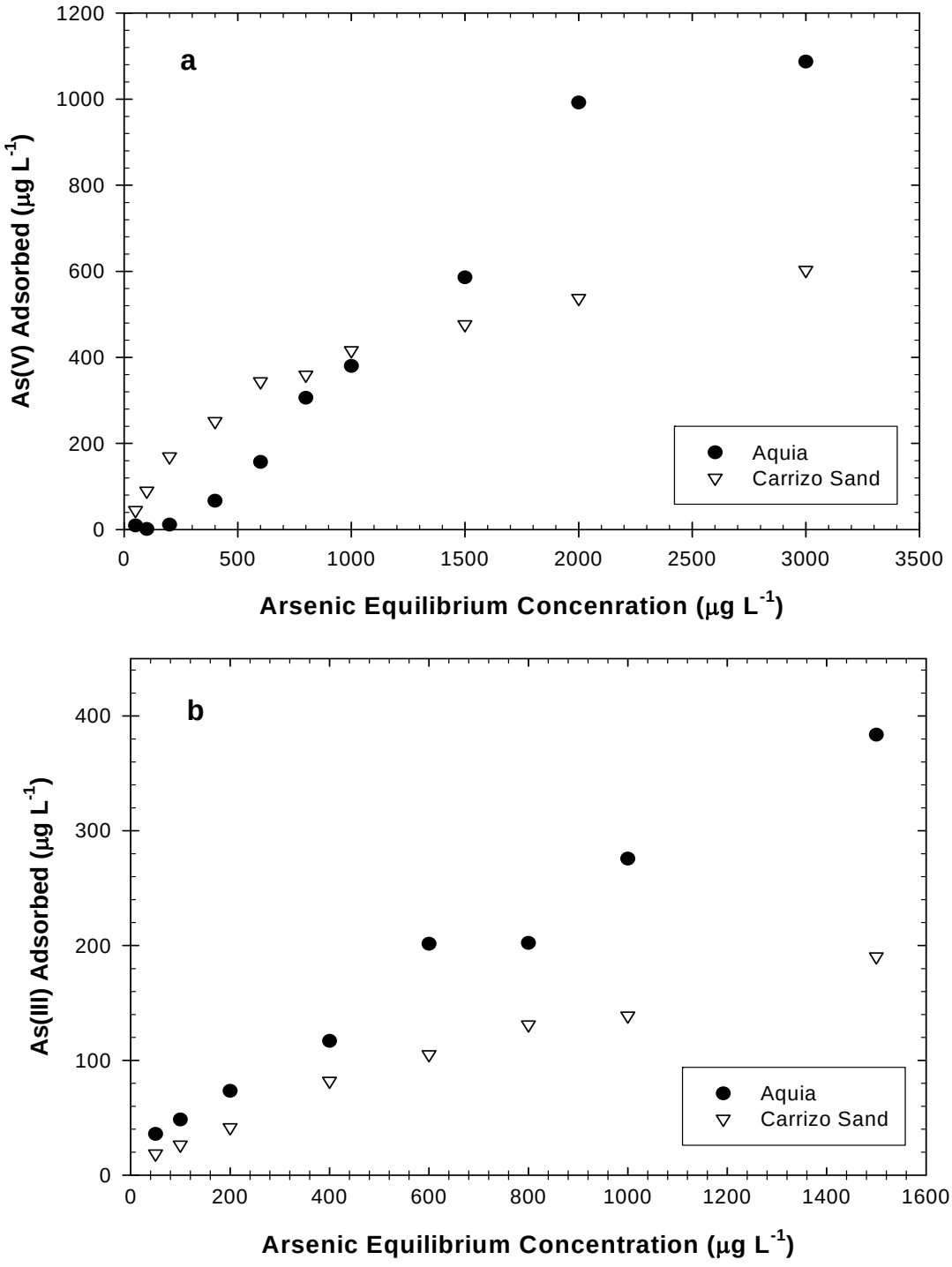

Figure 4.5 Adsorption isotherms for (a) As(V) and (b) As(III).

4.4.4 Arsenic adsorption isotherms

The Freundlich isotherm study was conducted in order to investigate the maximum adsorption capacity of the Carrizo Sand and Aquia aquifer sediments for arsenic. The relation between the amount of adsorbate (i.e. As) adsorbed by the adsorbent (aquifer sediments) and the equilibrium concentration of the adsorbate can be expressed by the linearized Freundlich adsorption isotherm as

$$\ln q_e = \ln k_f + 1/n \ln C_e \quad (4.1)$$

where q_e is the amount of adsorbate adsorbed per unit mass of the adsorbent, *Ce* is the equilibrium concentration of arsenic in solution, and n and k_f are constants depending upon the nature of the adsorbate and adsorbent, where n represents the adsorption intensity and k_f represents the adsorption capacity (Maji et al. 2008). Adsorption isotherms were constructed by plotting ln q_e versus ln C_e (See Figures 4.6 and 4.7). Regression analysis was subsequently performed on the linearized data using Sigma Plot (Version 8.0) to fit the data and determine the best-fit of equation 4.1 to each dataset (Figures 4.6, 4.7; Table 4.1).

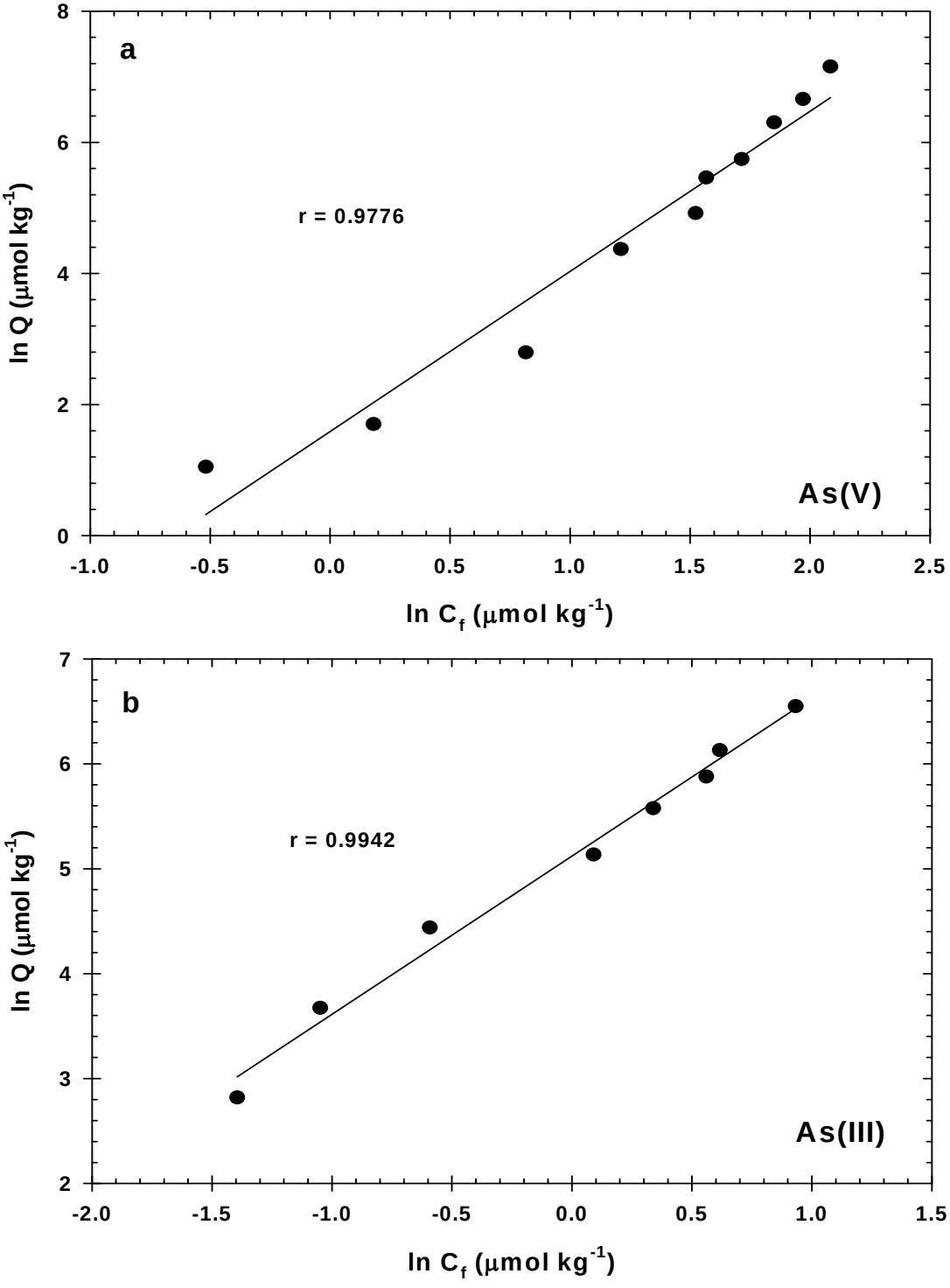

Figure 4.6 Carrizo Sand aquifer Freundlich isotherm model for As(V) adsorption (a) and As(III) adsorption (b).

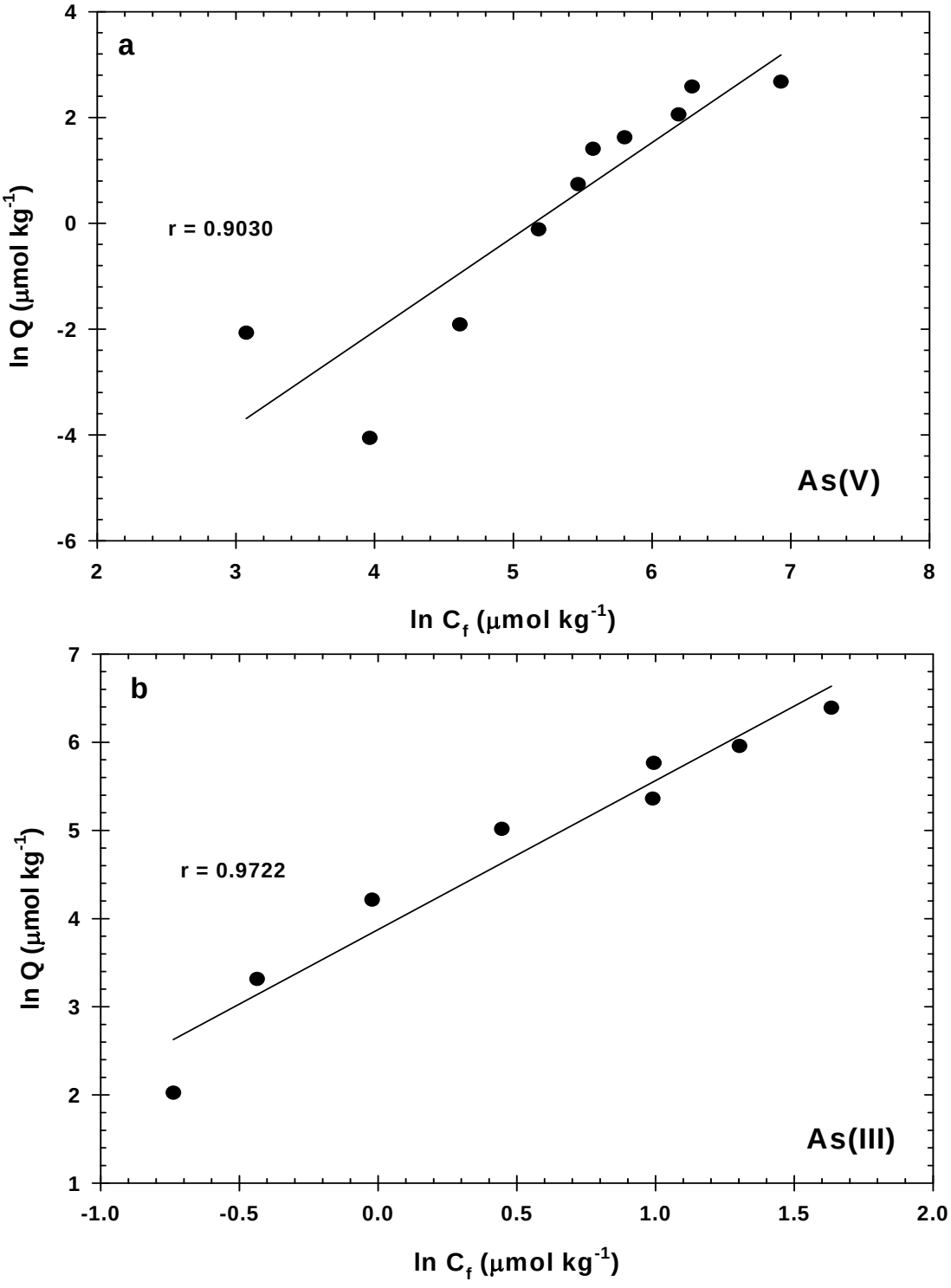

Figure 4.7 Aquia aquifer Freundlich isotherm model for As(V) adsorption (a) and As(III) adsorption (b).

Table 4.1 Freundlich isotherm linear equation components and constants.

	r	slope	y-intercept	adsorption intensity (n)	adsorption capacity (k_f)
Carrizo Sand					
As(V)	0.9776	2.4434	1.5866	0.4093	4.89
As(III)	0.9942	1.5085	5.1195	0.6629	167.25
Aquia					
As(V)	0.9030	0.4572	5.1746	2.1872	176.73
As(III)	0.9722	1.6906	3.8746	0.5915	48.16

4.5 Discussion

Reaction mechanisms and the processes occurring on the adsorbing surface can be investigated by knowing the sorption reaction rates (Skopp, 1986). The results of an As(V) adsorption-desorption kinetics study by Smith and Naidu (2009) suggests that As(V) adsorption kinetics are important in controlling the transport and bioavailability of As(V) in the soil environment. Owing to the presence of abundant Fe(III) oxide/oxyhydroxide coatings on mineral grains within both the Carrizo Sand and Aquia aquifers (Basu et al., 2007; Haque et al. 2008) and various clay mineral (kaolinite, illite, glauconite), As adsorption onto sediments of both aquifers is likely controlled by surface reactions with these minerals.

Previous studies of As adsorption kinetics onto Fe(III) hydroxides have shown that As(V) sorbs at a much faster rate than As(III) (Raven et al, 1998; Waltham and Eick, 2002). Banerjee et al. (2008) found that 80-95% of As(V) was adsorbed onto granular ferric hydroxide within the first 30 minutes and only 3-15% was adsorbed within the next 24 hours of a series of adsorption experiments. The results from the

investigation of Banerjee et al. (2008) correspond to our As(V) adsorption studies for the Aquia aquifer, which exhibit rapid adsorption within the first 24 hours. For the Carrizo Sand aquifer, maximum adsorption is achieved around 100 hours. The apparently slower adsorption rate observed for the Carrizo Sand is possibly due to the decrease in the driving concentration difference between the simulated groundwater and the aquifer sediments, leading to less transport of As(V) to the aquifer sediments (Banerjee et al., 2008).

Sorption and desorption of As species onto minerals are largely affected by pH, and hence As mobilization in aquifers is partly controlled by pH indiced adsorption/desorption (Ravenscraft et al., 2009). Decreasing pH generally leads to increased As retention onto mineral surface sites because of the shift in mineral surface charges from negative to more positive (Cheng et al., 2009). As a consequence, As species are generally less mobile in groundwater flow systems when pH < ~8. At very low pH range (less than 1) such as may occur in some acid mine drainage (e.g., Nordstrom et al., 2000), As(III) and As(V) species exist in neutral forms and As is no longer sorbed, becoming mobile again (Cheng et al., 2009). Increasing pH however commonly has the opposite affect leading to desorption of As species from mineral surface sites and hence greater As mobilization. Pierce and Moore (1980) observed that As(V) adsorption decreased continuously with increasing pH from 4 to 10, whereas Raven et al (1998) report an overall decrease in As(V) adsorption with increasing pH up to 9. More recently Stollenwerk et al. (2007) observed that as pH increased from 6.2 to

7.5, As(V) adsorption decreased by 30% for an initial As(V) concentration of 500 μg L^{-1} and by 20% for an initial concentration of 200 μg L^{-1}.

In our pH studies, little to no variance was noticed in the amount of As(V) adsorbed onto either of the aquifer sediments. In the case of the Aquia aquifer, the lack of a strong pH dependence on As(V) adsorption likely reflects the elevated pH of Aaquia aquifer groundwaters from the study site (pH > 8; Haque et al., 2008; Willis and Johannesson, in review; Willis et al., in review). For the Carrizo Sand aquifer groundwaters, however, pH ranges from ~6 to 8.5, which fall within the range overwhich As(V) adsorption should be affected (Tang et al., 2005a; Haque and Johannesson, 2006a; Tang and Johannesson, 2006; Basu et al., 2007). Consequently, pH was not considered to be an influential factor involved in As(V) adsorption within these aquifers. Therefore, more studies should be done on each of these aquifers, specifically closer to the recharge zones where the pH values are believed to be lower due to infiltration of rain water and soil zone acidification. These lower pH values might show an increase in the amount of As(V) adsorbed compared to the greater pH values shown in our study.

Adsorption is generally regarded as being one of the major controlling factors affecting the distribution of As species in the environment (Sweener et al., 1994; Qvarfort 1992). Ligand exchange reactions, such as Coulombic and Lewis acid-base interactions are known to affect the adsorption of As(V) species (i.e. $H_2AsO_4^-$ and $HAsO_4^{2-}$) onto hydrous ferric oxide (Banerjee et al., 2008). In the environment, As(III)

is sorbed more readily than As(V) on hydrous ferric oxide and goethite (Dixit and Hering, 2003).

As(III) species for both aquifers and As(V) for the Carrizo Sand aquifer display an "L"-type isotherm pattern (Figure 4.5; Limousin et al., 2007). Each of these isotherms suggest a progressive saturation of the aquifer sediment surfaces with respect to the As species. On the contrary, the adsorption isotherm pattern for As(V) sorption onto the Aquia aquifer displays an "S"-type isotherm pattern (Figure 4.5a; Limousin et al., 2007). This "S"-type isotherm is sigmoidal and has a point of inflection around 1500 μg L^{-1} of As(V). The results of the linearized Freundlich isotherms for each As species and aquifer also reiterate these findings. The correlation coefficients (r) for both As(V) and As(III) adsorption onto the Carrizo Sand aquifer and the adsorption of the As(III) species onto the Aquia aquifer all exceed 0.97 or greater indicating that the Freundlich isotherm can be used to describe these data. Although the fit of the As(V) adsorption data onto Aquia aquifer sediments to the linearized Freundlich isotherm is not as good, the relatively high concentration coefficient (r = 0.90) indicates that these data can also be decribed to a first approximation by the Freundlich isotherm. This difference in correlation coefficients might help explain why an "S"-type isotherm pattern is observed in As(V) adsorption for the Aquia aquifer (Figure 4.5a).

For the Carrizo Sand aquifer, the Freundlich isotherms (Figure 4.6) show that As(III) is strongly adsorbed (n = 0.6629, k_f = 167.25) to the aquifer sediments which suggests As(V) to be the predominate form of As on the groundwaters. In a previous study on the Carrizo Sand groundwaters by Haque and Johannesson (2006a), the

authors found As(V) to be the dominate form of dissolved As in the first ~ 15 km along the studied flow path. This high As(V) concentration in the Carrizo Sand groundwaters was attributed to reductive dissolution of Fe(III) oxyhydroxides/oxides. On the other hand, the Aquia aquifer Freundlich isotherms (Figure 4.7) illustrate As(V) to be strongly adsorbed (n = 2.1872, k_f = 176.73) which suggests a predominance of As(III) in the groundwaters. Haque et al. (2008) likewise concluded that As(III) is the most prevalent form of As along the entire studied flow path in the Aquia aquifer groundwaters. In addition, the authors suggested the high As(III) concentrations in Aquia groundwaters was due to reductive dissolution of Fe(III) oxyhydroxides/oxides as well as by Fe reducing bacteria.

4.6 Conclusion

The As adsorption data in this study demonstrate that for both the Carrizo Sand and the Aquia aquifers, the amount of As(V) adsorbed onto the aquifer sediments is not influenced by changes in pH. The results of the Freundlich isotherms are supported by previous studies showing that As(III) is strongly adsorbed to the Carrizo Sand sediments, wheras As(V) is more preferentially adsorbed onto the Aquia sediments. One possible explanation of the differences in isotherm patterns is provided by the Freundlich isotherm data. Future studies should be performed to investigate the specific reactions occurring at the aquifer mineral surface sites that influence the adsorptive capacity of the aquifer sediments. Additionally, an indepth study regarding pH dependent As adorption onto aquifer sediments should also be conducted.

CHAPTER 5

CONCLUSIONS

This chapter summarizes the main conclusions presented in each of the previous chapters. The purpose of my dissertation was to investigate the behavior of certain trace elements (specifically REEs, As, and Sb) and how redox, chemical weathering, and adsorption/desorption reactions affected the distribution and bioavalability of these trace elements along groundwater flow paths in the Carrizo Sand, the Upper Floridan, and the Aquia aquifers. Groundwater and sediment samples were collected in the field and lab studies were conducted to elucidate the geochemical properties of these groundwater flow systems and their sediments.

The results of the first study demonstrated that the Aquia aquifer groundwaters evolve along the sampled flow paths due to chemical weathering and changes in redox conditions. Groundwater REE concentrations and sequential extraction results for the Aquia aquifer sediments both indicated the REEs are associated with carbonate minerals (shell fragments). The relatively flat and consistent REE patterns in both the groundwaters and sediments of the Aquia aquifer indicated that dissolution of carbonate minerals (shell fragments) must be occurring in or near the recharge zone prior to attainment of equilibrium with respect to these carbonate phases.

The results of the As and Sb comparative study established that these two metalloids exhibit systematic changes along all three studied flow paths in the Carrizo

Sand, Upper Floridan, and Aquia aquifers. Due to the sulfidic nature of the Carrizo Sand and the Upper Floridan groundwaters, the geochemical model along with our data both predicted the formation of thioantimonite species (i.e., $HSb_2S_4^-$). The measured arsenic concentrations for the Carrizo Sand aquifer indicated a possible formation of thioarsenic species; however this prediction was not supported by our model calculations.

The groundwaters of the Upper Floridan aquifer were shown by both our data and model calculations to be at equilibrium with respect to arsenic sulfide minerals. For the non-sulfidic Aquia aquifer, the geochemical model predicted As(V) to be the predominate form, whereas our speciation data indicated the majority of As should occur as As(III). On the other hand, our speciation data and the model both concurred that Sb(III) should be the predominate form of Sb in these groundwaters. The groundwaters of all three aquifers displayed a statistical relationship between As and Sb, with the best correlation between As and Sb occuring in the Aquia aquifer.

The results of the As adsorption study revealed that the amount of As(V) adsorbed onto the both the Carrizo Sand and Aquia aquifer sediments was not influenced by changes in pH. The results of the Freundlich isotherms are supported by previous studies showing that As(III) was strongly adsorbed to the Carrizo Sand sediments while As(V) is more preferentially adsorbed onto the Aquia sediments. One possible explanation of the differences in isotherm patterns was provided by the Freundlich isotherm data.

The findings from each of the previous chapters explain how trace elements behaved and evolved in the three aquifers of study.

APPENDIX A

ADDITIONAL INFORMATION FOR THE CARRIZO SAND AQUIFER

Data for the Carizzo Sand aquifer from Tang and Johannesson (2005a). Arsenic, iron, and sulfide data are from Haque and Johannesson (2006a). Note, km indicates distance in kilometers along the flow path.

	RF-1	F-1	N-1	R-1	KS-1	N-3	G-1	Poteet	PCW-1	Peeler-1	AC74R-2	SMA74R-1
km	0.00	0.50	4.29	6.90	7.40	9.37	12.8	14.5	26.1	41.1	59.0	65.8
pH	7.32	6.56[a]	6.79	6.55	6.64	6.13	6.21[a]	6.48	7.38	8.34	8.68	8.12
Temp °C	25.5	24.6[a]	27.0	27.3	25.7	28.4	26.5[a]	27.8	32.9	28.1	35.9	47.8
Eh (mV)	--	264	233	--	327	190	133	155	48	-110	-135	-110
mmol kg^{-1}												
Ca	2.13	--	1.35	0.43	0.63	0.38	--	0.76	2.01	0.45	0.06	0.08
Mg	0.30	--	0.34	0.16	0.20	0.12	--	0.23	0.33	0.36	0.01	0.01
Na	1.98	--	1.42	1.14	1.12	0.71	--	1.16	1.15	3.96	8.74	10.24
K	0.25	--	0.19	0.14	0.13	0.13	--	0.20	0.14	0.15	0.05	0.06
Cl	1.87	--	2.11	1.12	1.43	1.06	--	1.44	0.87	0.37	1.23	1.78
Alk[¶]	2.79	1.64[a]	1.40	0.72	1.02	0.46	0.78[a]	0.94	4.10	4.63	6.56	7.84
SO_4	0.92	--	0.72	0.18	0.27	0.22	--	0.36	0.37	0.35	0.79	0.71
µmol kg^{-1}												
Fe_T	--	27.8	184	--	1.43	27.8	39.6	16.5	10.70	14.3	1.25	3.40
Fe(II)	--	27.2	134	--	BDL†	21.0	34.8	14.5	8.06	3.22	1.43	2.15
Fe(III)	--	0.54	50.1	--	1.43	6.80	4.83	1.97	2.69	11.1	ND	1.25
S(-II)	--	1.87	1.87	--	BDL*	0.62	0.94	0.31	0.94	2.81	6.24	49.9
nmol kg^{-1}												
As_T	--	2.19±0.12	2.08±0.11	--	0.97±0.05	2.44±0.13	2.47±0.13	2.33±0.13	0.37±0.02	0.91±0.05	0.41±0.02	1.92±0.10
As(III)	--	0.60±0.03	0.56±0.03	--	0.41±0.02	0.45±0.02	0.87±0.05	0.60±0.03	0.43±0.02	0.69±0.04	0.29±0.02	0.55±0.03
As(V)	--	1.59±0.09	1.52±0.08	--	0.56±0.03	1.99±0.11	1.60±0.08	1.73±0.10	ND	0.22±0.01	0.12±0.00	1.37±0.07

[a] Data from Haque and Johannesson (2006a)
[¶] Alk = alkalinity reported as HCO_3^-
*BDL for S(-II) = 0.16 µmol kg^{-1}
ND = not determined, or cannot be determined
[†] BDL for Fe_T = 0.16 µmol kg^{-1}

APPENDIX B

ADDITIONAL INFORMATION FOR THE UPPER FLORIDAN AQUIFER

Data for the Upper Floridan aquifer from Tang and Johannesson (2005a). Arsenic, iron, and sulfide data are from Haque and Johannesson (2006b). Note, km indicates distance in kilometers along the flow path.

	76A	59	45	31	25	18	19E	19W	5-2	5-1
km	0.00	32.2	46.3	78.8	90.8	112.1	122.5	132.8	137.7	144.1
pH	7.68	7.56	7.64	7.43	7.22	7.33	7.13	7.15	6.98	7.03
Temp °C	24.1	23.9	27.1	31.1	28.8	27.8	26.4	27.3	27.6	26.2
Eh (mV)	265	73	-30	-68	-34	-83	-43	-84	-53	-71
mmol kg^{-1}										
Ca	0.95	0.61	1.09	1.20	3.45	2.13	3.71	5.30	12.21	10.48
Mg	0.41	0.63	0.62	0.86	2.76	1.70	2.86	3.69	6.13	6.13
Na	0.24	0.39	0.37	0.42	0.62	0.93	1.21	1.37	1.05	2.26
K	0.03	0.02	0.04	0.06	0.09	0.07	0.08	0.14	0.11	0.12
Cl	0.28	0.29	0.27	0.34	0.48	0.95	0.99	0.82	1.28	2.54
Alk[¶]	2.38	2.32	2.96	2.06	2.62	3.59	3.17	2.80	2.53	2.49
SO_4	0.12	0.14	0.31	1.12	5.64	2.27	5.10	7.89	17.17	15.39
µmol kg^{-1}										
Fe_T	2.33	1.43	BDL†	0.54	BDL	0.54	BDL	BDL	0.90	BDL
Fe(II)	0.54	1.07	BDL‡	0.54	BDL	0.54	BDL	BDL	0.90	BDL
Fe(III)	1.79	0.36	ND	ND	ND	ND	ND	ND	0.00	ND
S(-II)	BDL*	2.00	34.0	106	100	105	86.0	82.0	63.0	70.0
nmol kg^{-1}										
As_T	18.6±0.60	15.7±0.80	1.75±0.13	0.72±0.13	1.04±0.13	1.09±0.13	1.00±0.13	1.04±0.13	2.79±0.27	1.64±0.27
As(III)	1.55±0.13	11.5±0.13	1.31±0.13	2.88±0.13	1.39±0.07	0.97±0.07	1.23±0.13	1.29±0.27	1.81±0.40	1.83±0.13
As(V)	17.0±0.47	4.16±0.67	0.44±0.00	-2.14±0.00	-0.35±0.06	0.12±0.06	-0.23±0.00	-0.25±0.14	0.98±0.13	-0.19±0.14

[¶]Alk = alkalinity reported as HCO_3^-
*BDL for S(-II) = 0.16 µmol kg^{-1}
ND = not determined, or cannot be determined
†BDL for Fe_T = 0.16 µmol kg^{-1}
‡BDL for Fe(II) = 0.36 µmol kg^{-1}

APPENDIX C

ADDITIONAL INFORMATION FOR THE AQUIA AQUIFER

Data for the Aquia aquifer. Arsenic, iron, and sulfide data are from Haque et al. (2008). Note, km indicates distance in kilometers along the flow path.

	KE 66 0125	QA 88 1277	QA 94 1322	QA 88 1268	SHA	QA 94 0111	QA 95 0611	QA 73 3626	QA 81 2298	QA 92 0451	QA EB 144
km	22.5	33.5	36.2	51.2	52	52.5	55	64.5	70.7	75.1	86.3
pH	7.57	7.69	8.01	8.08	8.38	7.91	8.02	7.84	8.3	7.93	8.12
Temp°C	16.6	15.6	18.8	16.7	19.7	16.2	16.1	16.9	17.5	17.8	15.9
Eh (mV)	25.5	44	-11	-10.5	-46	-3	-18	27.5	-11	11.5	-53
mmol kg^{-1}											
Ca	0.925	1.42	0.943	0.715	0.317	0.985	0.81	1.24	0.669	0.693	1.23
Mg	0.083	0.137	0.647	0.601	0.23	0.752	0.532	0.525	0.548	0.426	0.313
Na	0.084	0.179	0.382	0.484	2.39	0.348	0.355	0.358	0.607	0.522	0.102
K	0.056	0.072	0.313	0.362	0.152	0.393	0.323	0.239	0.363	1.27	1.08
Cl	0.205	0.062	0.026	0.022	0.043	0.053	0.039	0.057	0.038	0.042	ND
Alk[¶]	2.99	2.79	3.08	3.19	2.91	3.79	2.98	3.46	3.79	4.16	3.24
SO_4	0127	0.077	0.028	0.039	0.042	0.058	0.071	0.041	0.054	0.05	0.069
µmol kg^{-1}											
Fe_T	12.7±0.21	17.7±0.01	15.4±0.05	14.7±0.08	7.01±0.06	11.4±0.10	3.35±0.02	BDL[†]	9.94±0.03	9.01±0.01	8.29±0.01
Fe(II)	0.90±0.01	7.70±0.00	2.87±0.10	0.18±0.00	2.38±0.10	6.80±0.10	3.35±0.09	BDL[‡]	9.94±0.27	9.01±0.24	4.71±0.13
Fe(III)	11.8±2.58	10.0±0.27	12.5±0.34	14.5±0.39	4.63±0.12	4.60±0.12	ND	ND	ND	ND	3.58±0.00
S(-II)	BDL*	0.23±0.18	BDL	0.10±0.18	0.40±0.02	BDL	BDL	BDL	0.34±0.03	BDL	0.16±0.00
nmol kg^{-1}											
As_T	4.92±0.17	0.75±0.03	291±9.95	512±17.5	564±19.3	1072±36.7	411±15.1	52.7±1.8	241±8.24	76.8±2.63	27.3±0.93
As(III)	2.71±0.07	0.59±0.02	173±4.64	505±13.5	703±18.8	980±26.3	446±11.9	39.4±1.06	198±5.31	70.7±1.89	24.8±0.66
As(V)	2.21±0.07	0.15±0.00	118±3.60	7.25±0.22	ND	91.9±2.8	ND	13.2±0.40	44.0±1.34	6.05±0.08	2.51±0.08

[¶]Alk = alkalinity reported as HCO_3^-
*BDL for S(-II) = 0.16 µmol kg^{-1}
ND = not determined, or cannot be determined
[†]BDL for Fe_T = 0.16 µmol kg^{-1}
[‡]BDL for Fe(II) = 0.36 µmol kg^{-1}

REFERENCES

Aeschbach-Hertig, W., Stute, M., Clark, M., Reuter, R.F., Scholosser, P., 2002. A Paleotemperature record derived from dissolved noble gases in groundwater of the Aquia aquifer (Maryland, USA). Geochim. Cosmochim. Acta 66, 797-817.

Anawar, H. M., Akai, J., Komaki, K., Terao, H., Yoshioka, T., Ishizuka, T., et al., 2003. Geochemical occurrences of arsenic in groundwater of Bangledesh: sources and mobilization processes. J. Geochem. Explor. 77, 109-131.

Anderson, L. D., Kent, D. B., Davis, J. A., 1994. Batch experiment characterizing the reduction of Cr(VI) using suboxic material from a mildly reducing sand and gravel aquifer. Environ. Sci. Technol. 28, 178-185.

Appelo, C. A. J., 1994. Cation and proton exchange, pH variations, and carbonate reactions in a freshening aquifer. Water Resour. Res. 30, 2793-2805.

Appelo, C. A., J., Van Der Weiden, M. J., J., Tournassat, C., Charlet, L., 2002. Surface complexation of ferrous iron and carbonate on ferrihydrite and the mobilization of arsenic. Environ. Sci. Technol. 36, 3096-3103.

Arai, Y., Elzinga, E. J., Sparks, D. L., 2001. X-ray absorption spectroscopic investigation of arsenite and arsenate adsorption at the aluminum oxide-water interface. Journal of Colloid and Interface Science 235, 80-88.

Back, W., Hanshaw, B. B., 1970. Comparison of chemical hydrogeology of the carbonate peninsulas of Florida and Yucatan. J. Hydrol. 10, 330-368.

Banerjee, K., Amy, G.L., Prevost, M., Nour, S., Jekel, M., Gallagher, P.M., Blumenschein, C.D., 2008. Kinetic and thermodynamic aspects of adsorption of arsenic onto granular ferric hydroxide (GFH). Water Research 42, 3371-3378.

Banner, J.L., Wasserburg, G.J., Dobsn, P.F., Carpenter, A.B., Moore, C.H., 1989. Isotopic and trace element constraints on the origin and evolution of saline groundwaters from central Missouri. Geochim. Cosmochim. Acta 53, 383-389.

Barcelona, M.J., Holm, T.R., Schick, M.R., George, G. K., 1989. Spatial and temporal gradients in aquifer oxidation-reduction conditions. Water Resour. Res., 25, 991-1003.

Basu, R., Haque, S. E., Tang, J., Ji, J., Johannesson, K. H., 2007. Evolution of selenium concentrations and speciation in groundwater flow systems: Upper Floridan (Florida) and Carrizo Sand (Texas) aquifers. Chem. Geol. 246, 147-169.

Bau, M., Alexander, B., Chesley, J. T., Dilski, P., Brantley, S. L., 2004. Mineral dissolution in the Cape Cod aquifer, Massachusetts, USA: I. Reaction stoichiometry and impact of accessory feldspar and glauconite on strontium isotopes, solute concentrations, and REY distributions. Geochim. Cosmochim. Acta 68, 1199-1216.

Bencze, K., 1994. Antimony. In: Seiler, H.G., Sigel, A., Sigel, H. (Eds.), Handbook on Metals in Clinical and Analytical Chemistry. Marcel Dekker, New York, pp 227-236.

Berner, R. A., 1981. A new geochemical classification of sedimentary environments. J. Sediment. Petrol. 51, 359-365.

Bertine, K. K., Lee, D. S., 1983. Antimony content and speciation in the water column and interstitial waters of Saanich Inlet. In: Wong, C. S., Boyle, E. A., Bruland, K. W., Burton, J. D., Goldberg, E. D. (Eds.), Trace Metals In Seawater, Plenum (New York), pp. 21-38.

Bethke, C. M., 2008. Geochemical and Biogeochemical Modeling, 2nd ed. Cambridge University Press, Cambridge, UK, 543 p.

Bhattacharya, P., Chatterjee, D. Jacks, G., 1997. Occurrence of arsenic-contaminated groundwater in alluvial aquifers of the Delta Plain, eastern India: Options for a safe drinking water supply. Water. Res. Dev. 13, 79-92.

Bhattacharya, P., Jacks, G., Ahmed, K. M., Khan, A. A., Routh, J., 2002. Arsenic in groundwater of the Bengal Plain aquifers in Bangladesh. Bull. Envir. Contam. Toxicol. 69, 538-545.

Bhattacharya, P., Claesson, M., Bundschuh, J., Sracek, O., Fagerberg, J., Jacks, G., et al., 2006. Distribution and mobility of arsenic in the Rio Dulce alluvial aquifers in Santiago del Estero Province, Argentina. Sci. Total Environ. 358, 97-120.

Bigot, S., Treuil. M., Dumonceau, J., Fromage, F., 1984. Couplage des equations de transfert de masses et de lois d'interactions solution – solide par l'utilisation des lanthanides comme traceurs – Approche expérimentale. J. Hydrol. 70, 133-148.

Bostick, B. C., Fendorf, S., 2003. Arsenite sorption to triolite (FeS) and pyrite (FeS_2). Geochim. Cosmochim. Acta 67, 909-921.

Bostick, B. C., Fendorf, S., Manning, B. A., 2003. Arsenite adsorption on galena (PbS) and sphalerite (ZnS). Geochim. Cosmochim. Acta 67, 895-907.

Brookins, D. G., 1986. Geochemical behavior of antimony, arsenic, cadmium and thallium: Eh-pH diagrams for 25°C, 1-bar pressure. Chem. Geol. 54, 271-278.

Burdige, D. J., Gardner, K. G., 1998. Molecular weight distribution of dissolved organic carbon in marine sediment pore waters. Mar. Chem. 62, 45-64.

Bush, P. W., Johnston, R. H., 1988. Ground water hydraulics, regional flow, and ground-water development of the Floridan aquifer system in Florida and parts of Georgia, South Carolina, and Alabama. U. S. Geol. Surv. Prof. Pap. 1403-C.

Byrd, J. T., 1990. Comparative geochemistries of arsenic and antimony in rivers and estuaries. Sci. Total Environ. 97/98, 301-314.

Caceres, L., Gruttner, E., Contreras, R., 1992. Water recycling in arid regions – Chilean case. Ambio. 19, 231-243.

Carroll, S. A., 1993. Precipitation of Nd-Ca carbonate solid solution at 25°C. Geochim. Cosmochim. Acta 57, 3383-3393.

Castro, M.C., Goblet P., 2003. Calibration of regional groundwater flow models: working toward a better understanding of site-specific systems. Water Resour. Res. 39(6), 1172, doi:10.1029/2002WR001653, 2003.

Castro, M.C., Stute, M., Schlosser, P., 2000. Comparison of ^{4}He ages and ^{14}C ages in simple aquifer systems: implications for groundwater flow and chronologies. Appl. Geochem. 15, 1137-1167.

Chaillou, G., Anshultz, P., Lavaux, G., Blanc, G., 2006. Rare earth elements in the modern sediments of the Bay of Biscay (France). Mar. Chem. 100, 39-52.

Chapelle, F.H., 1983. Ground-water geochemistry and calcite cementation of the Aquia aquifer in southern Maryland. Water Resour. Res. 19, 545-558.

Chapelle, F.H., Knobel, L.L., 1983. Aqueous geochemistry and the exchangeable cation composition of glauconite in the Aquia aquifer, Maryland. Ground Water 21, 343-352.

Chapelle, F.H., Knobel, L.L., 1985. Stable carbon isotopes of bicarbonate in the Aquia aquifer, Maryland-evidence for an isotopically heavy source of carbon dioxide. Ground Water 23, 592-599.

Chapelle, F.H., Lovley, D.R., 1992. Competitive exclusion of sulfate reduction by Fe(III)-reducing bacteria: A mechanism for producing discrete zones of high-iron ground water. Ground Water 30, 29-36.

Chapelle, F. H., Zelibor, J. L., Jr., Grimes, D. J., Knobel, L. L., 1987. Bacteria in deep coastal plain sediments of Maryland: A possible source of CO_2 to groundwater. Water Resour. Res. 23, 1625-1632.

Champ, D.R., Gulens, J., Jacjson, R.E., 1979. Oxidation-reduction sequences in ground water flow systems. Can. J. Earth Sci. 16, 12-23.

Chen, Y.-W., Deng, T.-L., Filella, M., Belzile, N., 2003. Distribution and early diagenesis of antimony species in sediments and porewaters of freshwater lakes. Environ. Sci. Technol. 37, 1163-1168.

Cheng, H., Hu, Y., Luo, J., Xu, B., Zhao, J., 2009. Geochemical processes controlling fate and transport of arsenic in acid mine drainage (AMD) and natural systems. Journal of Hazardous Materials 165, 13-26.

Chowdhury, T. R., Basu, G. K., Mandal, B. K., Biswas, B. K., Samanta, G., Chowdhury, U. K., Chanda, C. R., Lodh, D., Saha, K. C., Roy, S., Kabir, S., Quamruzzaman, Q., Chakraborti, D., 2000. Arsenic poisoning in the Ganges delta. Nature 401, 545-546.

Council of the European Communities, 1976. Council Directive 76/464/EEC of 4 May 1976 on pollution caused by certain dangerous substances discharged into the aquatic environment of the Community. Official Journal L 129, 23-29.

Council of the European Union, 1998. Council Directive 98/ 83/ EC of 3 November 1998 on the quality of water intended for human comsumption. Official Journal L 330, 32-54.

Cummings, D. E., Caccavo, F., Jr., Fendorf, S., Rosenzweif, R. F., 1999. Arsenic mobilization by the dissimilatory Fe(III)-reducing bacterium *Shewanella alga* BrY. Environ. Sci. Technol. 33, 723-729.

Cutter, G. A., 1991. Dissolved arsenic and antimony in the Black Sea. Deep-Sea Res. 38, S825-S843.

Das, D., Chatterjee, A., Mandal, B. K., Samanta, G., Chakroborti, D., Chanda, B., 1995. Arsenic in ground-water in 6 districts of West Bengal, India – the biggest arsenic calmanity in the world. 2. Arsenic concentrations in drinking-water, hair, nails, urine, skin-scale and liver-tissue (biopsy) of the affected people. Analyst 120, 917-924.

De Baar, H.J.W., Bacon, M.P., Brewer, P.G., Bruland, K.W., 1983. Rare earth distributions with a positive Ce anomaly in the western North Atlantic Ocean. Nature (London). 301, 324-327.

De Baar, H.J.W., Bacon, M.P., Brewer, P.G., Bruland, K.W., 1985a. Rare earth elements in the Atlantic and Pacific Oceans. Geochim. Cosmochim. Acta 49, 1943-1959.

De Baar, H.J.W., Brewer, P.G., Bacon, M.P., 1985b. Anomalies in rare earth distributions in seawater: Gd and Tb. Geochim. Cosmochim. Acta 49, 1961-1969.

DeCarlo, E. H., Wen, X.-Y., Irving, M., 1998. The influence of redox reactions on the uptake of dissolved Ce by suspended Fe and Mn oxide particles. Aquatic Geochem. 3, 357-389.

Delany, J. M., Lundeen, S. R., 1990. The LLNL thermochemical database. Lawrence Livermore National Laboratory Report UCRL-21658. Lawrence Livermore National Laboratory

Dia, A., Gruau, G., Olivié-Lauquet, G., Riou, C., Molénat, J., Curmi, P., 2000. The distribution of rare earth elements in groundwaters: Assessing the role of source-rock compositions, redox changes and colloidal particles. Geochim. Cosmochim. Acta 64, 4131-4151.

Dixit, S., Hering, J. G., 2003. Comparison of arsenic (V) and arsenic (III) sorption to iron oxide minerals: implications for arsenic mobility. Environ. Sci. Technol. 37, 4182-4189.

Dowling, C. B., Poreda, R. J., Basu, A. R., Peters, S. L., Aggarwal, P. K., 2002 Geochemical study of arsenic release mechanisms in the Bengal Basin groundwater. Water Resour. Res. 38, 1173, doi: 10.1029/2001/WR000968.

Drever, J. I., 1997. The Geochemistry of Natural Waters: Surface and Groundwater Environments. 3rd ed. Prentic Hall, Upper Saddle River, NJ, 436 p.

Drummond, D. D., 2001. Hydrogeology of the Coastal Plain aquifer system in Queen Anne's and Talbot Counties, Maryland, with a discussion of brackish water intrusion in the Aquia aquifer. Maryland Geological Survey, Report of Investigations 72, USA.

Drummond, D. D., 2007. Water-supply potential of the Coastal Plain aquifers in Calvert, Charles, and St. Mary's Counties, Maryland, with emphasis on the upper Patapsco and lower Patapsco aquifers. Maryland Geological Survey, Report of Investigations 76.

Dzombak, D. A., Morel, F. M. M., 1990. Surface Complexation Modeling: Hydrous Ferric Oxide. John Wiley and Sons, New York, 393 p.

Eaton, A. D., Clerceri, L.S., Greenberg, A.E. (eds.), 1995. Standard Methods for the Examination of Water and Wastewater. 19th ed. American Public Health Association, Washington, DC.

Edmunds, W.M., Guendouz, A.H., Mamou, A., Moulla, A., Shand, P., Zouari, K., 2003. Groundwater evolution in the Continental Intercalaire aquifer of southern Algeria and Tunisia: trace element and isotopic indicators. Applied Geochemistry 18, 805-822.

Elderfield, H., Greaves, M.J., 1983. Determination of the rare earth elements in sea water. In: C.S. Wong, E. Boyle, K.W. Bruland, J.D. Burton, and E.D. Goldberg (eds.) Trace Metals in Sea Water. Plenum Press (New York), pp. 427-445.

Elzinga, E. J., Reeder, R. J., Withers, S. H., Peale, R. E., Mason, R. A., Beck, K. M., Hess, W. P., 2002. EXAFS study of rare-earth element coordination in calcite. Geochim. Cosmochim. Acta 66, 2875-2885.

Fee, J.A., Gaudette, Lyons, W.B., Long, D.T., 1992. Rare-earth element distibution in Lake Tyrell groundwaters, Victoria, Australia. Chem. Geol. 96, 67-93.

Ferguson, J. F., Gavis, J., 1972. A review of the arsenic cycle in natural waters. Water Res. 6, 1259-1274.

Filella, M., May, P. M., 2003. Computer simulation of the low-molecular-weight inorganic species distribution of antimony(III) and antimony(V) in natural waters. Geochim. Cosmochim. Acta 67, 4013-4031.

Filella, M., Belzile, N., Chen, Y.-W., 2002a. Antimony in the environment: a review focused on natural waters I. Occurrence. Earth-Sci. Rev. 57, 125-176.

Filella, M., Belzile, N., Chen, Y.-W., 2002b. Antimony in the environment: a review focused on natural waters II. Relevant solution chemistry. Earth-Sci. Rev. 59, 265-285.

Frost, R. R., Griffin, R. A., 1977. Effect of pH on adsorption of arsenic and selenium from landfill leachate by clay minerals. Soil Sci. Soc. Am. J. 41, 53-57.

Fryar, A.E., Macko, S.A., Mullican III, W.F., Romanak, K.D., Bennett, P.C., 2000. Nitrate reduction during ground-water recharge, Southern High Plains, Texas. Journal of Contaminant Hydrology 40, 335-363.

Gebel, T., 1997. Arsenic and antimony: comparative approach on mechanistic toxicology. Chem. Biol. Interact. 107, 131-144.

Gebel, T., 1998. Suppression of arsenic-induced chromosome mutagenicity by antimony in V79 cells. Mutat. Res. 213-218.

Gebel, T., 2000. Confounding variables in the environmental toxicity of arsenic. Toxicol. 144, 155-162.

Ghassemzadeh, F., Arab-Zavar, Mohhamad, H., McLennan, G., 2006. Arsenic and antimony in drinking water in Khohsorkh area, northeast Iran possible risks for the public health. Journal of Applied Sciences 6, 2705-2714.

Gilbert, T.W., Behymer, T.D., Castaneda, H.B., 1982. Determination of Dissolved Oxygen in Natural and Wastewaters. Am. Lab. 14, 119-134.

Goldberg, S., Glaubig, R. A., 1988. Anion sorption on a calcareous, montmorillonitic soil – Arsenic. Soil Sci. Soc. Am. J. 52, 1297-1300.

Goldsmith, S. T., Carey, A. E., Johnson, B. M., Welch, S. A., Lyons, W. B., McDowell, W. H., Pigott, J. S., 2010. Stream geochemistry, chemical weathering and CO_2 consumption potential of andesitic terrains, Dominica, Lesser Antilles. Geochim. Cosmochim. Acta 74, 85-103.

Götze, J., Plötze, M., Graupner, T., Hallbauer, D. K., Bray, C. J., 2004. Trace element incorporation into quartz: A combined study by ICP-MS, electron spin resonance,

cathodeluminescence, capillary ion analysis, and gas chromatography. Goechim. Cosmochim. Acta 68, 3741-3759.

Greaves, M.J., Elderfield, H., Klinkhammer, G.P., 1989. Determination of the rare earth elements in natural waters by isotope-dilution mass spectrometry. Anal. Chim. Acta 218, 265-280.

Guo, H., Zhang, B., Wang, G., Shen, Z. 2010. Geochemical controls on arsenic and rare earth elements approximately along a groundwater flow path in the shallow aquifer of the Hetao Basin, Inner Mongolia. Chem. Geol. 270, 117-125.

Hach, 2004. The Handbook DR/2400 Portable Spectrophotometer Procedure. USA.

Hall, G. E. M., Vaive, J. E., Beer, R., Hoashi, M., 1996. Selective leaches revisited, with emphasis on the amorphous Fe oxyhydroxide phase extraction. J. Geochem. Explor. 56, 59-78.

Hansen, H.J., 1974. Sedimentary facies of the Aquia formation in the subsurface of the Maryland Coastal Plain. Maryland Geological Survey, Report of Investigations 21.

Hanshaw, B.B., Back, W., Rubin, M., 1965a. Radiocarbon determinations for estimating groundwater flow velocities in central Florida. Science. 148, 494-495.

Hanshaw, B.B., Back, W., Rubin, M., 1965b. Carbonate equilibria and radiocarbon distribution related to groundwater flow in the Floridan Limestone aquifer, U.S.A. Hydrology of Fractured Rocks, vol. 1, Proceeding of the Dubrovnik

Symposium, International Association of Scientific Hydrology. UNESCO, pp. 601-614.

Hanson, G. N., 1980. Rare earth elements in petrogenetic studies of igneous systems. Ann. Rev. Earth Planet. Sci. 8, 371-406.

Haque, S., Johannesson, K. H., 2006a. Arsenic concentrations and speciation along a groundwater flow path: the Carrizo Sand aquifer, Texas, USA. Chem. Geol. 228, 57-71.

Haque, S.E., Johannesson, K.H., 2006b. Concentrations and speciation of arsenic along a groundwater flow-path in the Upper Floridan aquifer, Florida, USA. Environ. Geol. 50, 219-228.

Haque. S. E., Johannesson, K. H., 2007. Arsenic and antimony in groundwater flow systems. Geol. Soc. Am. Abstr. Progr., 39, 517.

Haque, S., Ji, J., Johannesson, K.H., 2008. Evaluating mobilization and transport of arsenic in sediments and groundwaters of Aquia aquifer, Maryland, USA. Journal of Contaminant Hydrology 99, 68-84.

Harmon, R. E., Lombi, E., Fortunati P., Nolan, A. L., McLaughlin, M. J., 2004. Coupling speciation and isotope dilution techniques to study arsenic mobilization in the environment. Environ. Sci. Technol. 38, 1794-1798.

Harvey, C. F., Swartz, C. H., Badruzzaman, A. B. M., Keon-Blute, N., Yu, W., Ali, M. A., Jay, J., Beckie, R., Niedan, V., Brabander, D., Oates, P. M., Ashfaque, K. N., Islam, S., Hemond, H. F., Ahmed, M. F., 2002. Arsenic mobility and groundwater extraction in Bangladesh. Science 298, 1602-1606.

Haskin, L. A., Haskin, M. A., Frey, F. A., Wildeman, T. R., 1968. Relative and absolute terrestrial abundances of the rare earths. In: L. H. Ahrens (ed.) Origin and Distribution of the Elements. Pergamon (Oxford), pp.889-912.

Helz, G. R., Tossell, J. A., 2008. Thermodynamic model for arsenic speciation in sulfidic waters: A novel use of *ab initio* computations. Geochim. Cosmochim. Acta 72, 4457-4468.

Hughes, M. F., 2002. Arsenic toxicity and potential mechanisms of action. Toxicol. Lett. 133, 1-16.

Hughes, M. F., Thomas, D. J., Kenyon, E. M., 2009. Toxicology and epidemiology of arsenic and its compounds. In: Henke, K. R. (Ed.), Arsenic: Environmental Chemistry, Health Threats and Waste Treatment. John Wiley and Sons, Chichester, UK, pp. 237-275.

Inskeep, W. P., McDermott, T. R., Fendorf, S., 2002. Arsenic (V)/(III) cycling in soils and natural waters: chemical and microbiological processes. In: Frankenberger, W. T., Jr. (Ed.), Environmental Chemistry of Arsenic, Marcel Dekker (New York), pp.183-215.

Islam, F., Gault, A., Boothman, C., Polya, D., Charnock, J., Chatterjee, D., Lyond, J., 2004. Role of metal-reducing bacteria in arsenic release from Bengal delta sediments. Nature 430, 68-71.

Jay, J. A., Blute, N. K., Hemond, H. F., Durant, J. L., 2004. Arsenic-sulfides confound anion exchange resin speciation of aqueous arsenic. Water. Res. 38, 1155-1158.

Johannesson, K.H., Stetzenbach, K.J., Hodge, V.F., Kreamer, D.K., Zhou, X., 1997a. Delineation of ground-water flow systems in the southern Great Basin using aqueous rare earth element distributions. Ground Water 35, 807-819.

Johannesson, K.H., Stetzenbch, K.J., Hodge, V.F., 1997b. Rare earth elemens as geochemical tracers of regional groundwater mixing. Geochim. Cosmochim. Acta 61, 3605-3618.

Johannesson, K.H., Farnman, I.M., Guo, C., Stetzenbach, K.J., 1999 Rare earth element fractionation and concentration variations along a groundwater flow path within a shallow, basin-fill aquifer, southern Nevada, USA. Geochim. Cosmochim. Acta 63, 2697-2708.

Johannesson, K.H., Tang, J., Daniels, J.M., Bounds, W.J., and Burdige, D.J., 2004. Rare earth element concentrations and speciation in organic-rich blackwaters of the Great Dismal Swamp, Virginia, USA. Chem. Geol. 209, 271-294.

Johannesson, K.H., Cortés, A., Ramos Leal, J.A., Ramírez, A.G., Durazo, J., 2005. Geochemistry of rare earth elements in groundwaters from a rhyolite aquifer, central México. In: K. H. Johannesson (ed.) Rare Earth Elements in Groundwater Flow Systems. Springer (Dordrecht), pp. 187-222.

Johannesson, K. H., Burdige, D. J., 2007. Balancing the global oceanic neodymium budget: Evaluating the role of groundwater. Earth Planet. Sci. Lett. 253, 129-142.

Johnston, R. G., Krause, R. E., Meyer, F. W., Ryder, P. W., Tibbals, C. H., and Hunn, J. D., 1980. Estimated potentiometric surcae for the Tertiary limestone aquifer

system, southeastern United States, prior to development. U. S., Geol. Surv. Open-File Rept. 80-406.

Kirk, M. F., Holm, T. R., Park, J., Jin, Q., Sanford, R. A., Fouke, B. W., Bethke, C. M., 2004. Bacterial sulfate reduction limits natural arsenic contamination in groundwater. Geology 32, 953-956.

Klinkhammer, G. P., German, C. R., Elderfield, H., Greaves, M. J., Mitra, A., 1994. Rare earth elements in hydrothermal fluids and plume particulates by inductively coupled plasma mass spectrometry. Mar. Chem. 45, 170-186.

Klungness, G. D., Byrne, R. H., 2000. Comparative hydrolysis behavior of the rare earths and yttrium: the influence of temperature and ionic strength. Polyhedron 19, 99-107.

Koeppenkastrop, D., DeCarlo, E. H., 1992. Sorption of rare-earth elements from seawater onto synthetic mineral particles: an experimental approach. Chem. Geol. 95, 251-263.

Koeppenkastrop, D., DeCarlo, E. H., 1993. Uptake of rare earth elements from solution by metal oxides. Environ. Sci. Technol. 27, 1796-1802.

Krom, M.D., 1980. Spectrophotometric Determination of Ammonia: A Study of a Modified Berthelot Reduction Using Salicylate and Dichloroisocyanurate, The Analyst 105, 305-316.

Lead, J. R., Hamilton-Taylor, J., Peters, A., Reiner, S., Tipping, E., 1998. Europium binding by fulvic acids. Anal. Chim. Acta 369, 171-180.

Lee, J. H., Byrne, R. H., 1992. Examination of comparative rare earth element complexation behavior using linear free-energy relationships. Geochim. Cosmochim. Acta 56, 1127-1137.

Lee, M.-K., Griffin, J., Saunders, J., Wang, Y., Jean, J.-S., 2007. Reactive transport of trace elements and isotopes in the Eutaw coastal plain aquifer, Alabama. J. Geophys. Res. 112, G02026, doi:10.1029/2006JG000238.

Leuz, A.-K., Mönch, H., Johnson, C. A., 2006. Sorption of Sb(III) and Sb(V) to goethite: Influence on Sb(III) oxidation and mobilization. Environ. Sci. Technol. 40, 7277-7282.

Leybourne, M. I., Goodfellow, W. D., Boyle, D. R., Hall, G. M., 2000. Rapid development of negative Ce anomalies in surface waters and contrasting REE patterns in groundwaters associated with Zn-Pb massive sulfide deposits. Applied Geochem. 15, 695-723.

Limousin, G., Gaudet, J.-P., Charlet, L., Szenknect, S., Barthès, V., Krimissa, M., 2007. Sorption isotherms: A review on physical bases, modeling and measurement. Applied Geochemistry 22: 249-275.

Lindberg, R.D., Runnells, D.D., 1984. Ground-water redox reactions: an analysis of equilibrium state applied to Eh measurements and geochemical modeling. Science 225, 925-927.

Luo, Y.-R, Byrne, R. H., 2000. The ionic strength dependence of rare earth and yttrium fluoride complexation at 25°C. J. Sol. Chem. 29, 1089-1099.

Luo, Y.-R, Byrne, R. H., 2001. Yttrium and rare earth element complexation by chloride ions at 25°C. J. Sol. Chem. 30, 837-845.

Luo, Y.-R, Byrne, R. H., 2004. Carbonate complexation of yttrium and the rare earth elements in natural waters. Geochim. Cosmochim Acta 68, 691-699.

Lyons, W. B., Lent, R. M., Djukic, N., Maletin, S., Pujin, V., Carey, A. E., 1992. Geochemistry of surface waters of Vojvodina, Yugoslavia. J. Hydrol. 137, 33-55.

MacRae, N. D., Nesbitt, H. W., Kronberg, B. I., 1992. Development of a positive Eu anomaly during diagenesis. Earth Planet. Sci. Lett. 109, 585-591.

Mailloux, B. J., Alexandrova, E., Keimowitz, A. R., Wovkulich, K., Freyer, G. A., Herron, M., Stolz, J. F., Kenna, T. C., Pichler, T., Polizzotto, M. L., Dong, H., Bishop, M., Knappett, P. S. K., 2009. Microbial mineral weathering for nutrient acquisition releases arsenic. Appl. Environ. Microbiol. 75, 2558-2565.

Maji, S. K., Pal, A., Pal, T. 2008. Arsenic removal from real-life groundwater by adsorption on laterite soil. Journal of Hazardous Materials 151, 811-820.

Manful, G.A., Verloo, M., de Spiegeleer, R., 1989. Arsenate sorption by soils in relation to pH and selected anions. Pedologie 39, 55-68.

Manning, B.A. and Goldberg, S., 1997. Arsenic(III) and arsenic(V) adsorption on three California soils. Soil Science 162, 886-895.

Manzoori, J.L., Sorouradin, M.H., Haji Shabani, A.M., 1999. Atomic adsorption determination of cobalt after preconcentration by 1-(2-pyridylazo)-2-naphtol immobilized on surfactant-coated alumina. Microchem. J. 63, 295-301.

Mariner, P. E., Holzmer, F. J., Jackson, R. E., Meinardus, H. W., Wolf, F. G., 1996. Effects of high pH on arsenic mobility in a shallow sandy aquifer and on aquifer permeability along the adjacent shoreline, Commencement Bay Superfun Site, Tacoma, Washington. Environ. Sci. Technol. 30, 1645-1651.

Martell, A. E., Smith, R. M., 1977. Critical Stability Constants. Other Organic Lignads, vol. 3, Plenum Press, New York.

Martínez-Lladó, X., de Pablo, J., Giménez, J., Ayora, C., Martí, V., Rovira, M., 2008. Sorption of antimony(V) onto synthetic goethite in carbonate medium. Solv. Extract. Ion Exchange 26, 289-300.

Masson, M., Schäfer, J., Blanc, G., Dabrin, A., Castelle, S., Lavaux, G., 2009. Behavior of arsenic and antimony in the surface freshwater reaches of a highly turbid estuary, the Gironde Estuary, France. Applied Geochemistry 24, 1747-1756.

McArthur, J. M., Ravenscroft, P., Safiulla, S., Thirlwall, M. F., 2001. Arsenic in groundwater: Testing pollution mechanisms for sedimentary aquifers in Bangladesh. Water Resour. Res. 37, 109-117.

McArthur, J. M., Banerjee, D. M., Hudson-Edwards, K. A., Mishra, R., Purohit, R., Ravenscroft, P., Cronin, A., Howarth, R. J., Chatterjee, A., Talukder, T., Lowry, D., Houghton, S., Chadha, D. K., 2004. Natural organic matter in sedimentary basins and its relation to arsenic in anoxic ground water: the example of West Bengal and its worldwide implications. Appl. Geochem. 19, 1255-1293.

McArthur, J. M., Ravenscroft, P., Banerjee, D. M., Milsom, J., Hudson-Edwards, K. A., Sengupta, S., Bristow, C., Sarkar, A., Tonkin, S., Purohit, R., 2008. How

paleosols influence groundwater flow and arsenic pollution: A model from the Bengal Basin and its worldwide implications. Water Resour. Res. 44, W11411, doi:10.1029/2007/WR006552.

McArthur, J. M., Banerjee, D. M., Sengupta, S., Ravencroft, P., Klump, S., Sarkar, A., Disch, B., Kipfer, R., 2010. Mirgration of As and 3H/3He ages, in groundwater from West Bengal: Implications for monitoring. Water Res. 44, 4171-4185.

McCarthy, J. F., Sanford, W. E., Stafford, P. L., 1998. Lanthanide field tracers demonstrate enhanced transport of transuranic radionuclides by natural organic matter. Environ. Sci. Technol. 32, 3901-3906.

McCleskey, R.B., Nordstrom, D.K., Maest, A.S., 2004. Preservation of water samples for arsenic (III/V) determinations: an evaluation of the literature and new analytical results. Appl. Geochem. 19, 995-1009.

McCreadie, H., Blowes, D. W., Ptacek, C. J., Jambor, J. L., 2000. Influence of reduction reactions and solid-phase composition on porewater concentrations of arsenic. Environ. Sci. Technol. 34, 3159-3166.

Meinrath, G., Takeishi, H., 1993. Solid – liquid equilibria of Nd^{3+} in carbonate solutions. J. Alloys Comp. 194, 93-00.

Meliker, J. R., Nriagu, J. O., 2007. Arsenic in drinking water and bladder cancer: review of epidemiological evidence. In: Bhattacharya, P., Mukherjee, A. B., Bundschuh, J., Zevenhoven, R., Loeppert, R. H. (Eds.), Arsenic in Soil and Groundwater Environment: Biogeochemical Interactions, Health Effects and

Remediation. Trace Metals and other Contaminants in the Environment, Vol. 9, Elsevier, Amsterdam, pp. 551-584.

Michard, A., Albarède, F., 1986. The REE content of some hydrothermal fluids. Chem. Geol. 55, 51-69.

Michard, A., 1989. Rare earth element systematics in hydrothermal fluids. Geochim. Cosmochim. Acta 53, 745-750.

Miller, J.A., 1986. Hydrogeological framework of the Floridan Aquifer system in Florida and in parts of Georgia, Alabama, and South Carolina. U.S. Geological Survey Prof. Paper 1403-B.

Mitsunobu, S., Harada, T., Takahashi, Y., 2006. Comparison of antimony behavior with that of arsenic under various soil redox conditions. Environ. Sci. Technol. 40, 7270-7276.

Moffett, J. W., 1990. Microbially mediated cerium oxidation in sea water. Nature 345, 421-423.

Moore, J. N., Ficklin, W. H., Johns, C., 1988. Partitioning of arsenic and metals in reducing sulfidic sediments. Environ. Sci. Technol. 22, 432-437.

Naidu, R., Smith, E., Huq, S.M.I., Owens, G., 2009. Sorption and bioavailability of arsenic in selected Bangladesh soils. Eviron. Geochem. Health 31, 61-68.

Navas-Acien, A., Silbergeld, E. K., Pastor-Barriuso, R., Guallar, E., 2008. Arsenic exposure and prevalence of type 2 diabetes in US adults. JAMA 300, 814-822.

Naveau, A., Monteil-Rivera, F., Dumonceau, J., Catalette, H., Simoni, E., 2006. Sorption of Sr(II) and Eu(III) onto pyrite under different redox potential conditions. J. Colloid Interface Sci. 293, 27-35.

Nickson, R., McArthur, J., Burgess, W., Ahmed, K. M., Ravenscroft, P., Rahman, M., 1998. Arsenic poisoning of Bangladesh groundwater. Nature 395, 338.

Nickson, R. T., McArthur, J. M., Ravenscroft, P., Burgess, W. G., Ahmed, K. M., 2000. Mechanism of arsenic release to groundwater, Bangladesh and West Bengal. Applied Geochem. 15, 403-413.

Nordstrom, D. K., Alpers, C. N., Ptacek, C. J., Blowers, D. W., 2000. Negative pH and extremely acidic mine waters from Iron Mountain, California. Environ. Sci. Technol. 34, 254-258.

NRC, 1997. Arsenic: Medical and Biological Effects of Environmental Pollutants. National Academy of Sciences, Washington, DC.

NRC, 1999. Arsenic in Drinking Water. National Academy Press, Washington, DC.

NRC, 2001. Arsenic in Drinking Water (2001 Update). National Academy Press, Washington, DC.

Nriagu, J.O., 2002. Arsenic poisoning through the ages. In: Environmental Chemistry of Arsenic (W.T. Frankenberger, Editor), New York, Marcel Dekker, pp. 1-26.

O'Day, P. A., Vlassopoulos, D., Root, R., Rivera, N., 2004. The influence of sulfur and iron on dissolved arsenic concentrations in the shallow subsurface under changing redox conditions. Proc. Nat. Acad. Sci. 101, 13703-13708.

Olías, M., Cerón, J. C., Fernández, I., De la Rosa, J., 2005. Distribution of rare earth elements in an alluvial aquifer affected by acid mine drainage: the Guadiamar aquifer (SW Spain). Environ. Pollut. 135, 53-64.

Oremland, R. S., Stolz, J.F., 2005. Arsenic, microbes and contaminated aquifers. Trend Microbiol. 13, 45-49.

Page, R. A., 1957. The questionable age of the Aquia Formation. J. Paleontol. 33, 347-350.

Park, J., Sanford, R.A., Bethke, C.M., 2006. Geochemical and microbiological zonation of the Middendorf aquifer, South Carolina. Chem. Geol. 230, 88-104.

Parkhurst, D. L., Appelo, C. A. J., 1999. User's guide to PHREEQC – a computer program for speciation, batch-reaction, one-dimensional transport, and inverse geochemical calculations. U. S. Geol. Surv. Water Resour. Invest., 99-4259.

Pauling, L. (1988) General Chemistry. Dover Publications (New York), 959 p.

Pearcy, C. A., Chevis, D. A., Haug, J. T., Jeffires, H. A., Yang, N., Tang, J., Grimm, D. A., Johannesson, K. H., 2010. Evidence of microbially mediated arsenic mobilization from sediments of the Aquia aquifer, Maryland, USA. Applied Geochem. (in press).

Pearson, Jr., F. J., White, D. E., 1967. Carbon 14 ages and flow rates of water in Carrizo sand, Atascosa County, Texas. Water Resour. Res. 3, 251-261.

Penny, E., Lee, M. L., Morton, C., 2003. Groundwater and microbial processes of Alabama coastal plain aquifers. Water Resour. Res. 39, No. 11. 1320, doi:10.1029/2003WR001963.

Peters, S. C., 2008. Arsenic in groundwater in the Northern Appalachian Mountain belt: a review of patterns and processes. Journal of Contaminant Hydrology 99, 8-21.

Pierce, M. L. and Moore, C. B., 1980. Adsorption of Arsenite on Amorphous Iron Hydroxide from Dilute Aqueous Solution. Environ. Sci. Technol. 14, 214-216.

Pitman, A. L., Pourbaix, M., de Zoubov, N., 1957. Potential-pH diagram of the antimony water system: Its applications to properties of the metal, its compounds, its corrosion, and antimony electordes. J. Electrochem. Soc. 104, 594-600.

Plummer, L. N., Parkhurst, D. L., Thorstenson, D.C., 1983. Development of reaction models for ground-water systems. Geochim. Cosmochim. Acta. 47, 665-686.

Plummer, L. N., Sprinkle, C. L., 2001. Radiocarbon dating of dissolved inorganic carbon in groundwater from confined parts of the Upper Floridan aquifer, Floridan, USA. Hydrogeol J. 9, 127-150.

Polizzotto, M. L., Harvey, C. F., Sutton, S. R, Fendorf, S., 2005. Processes conducive to release and transport of arsenic into aquifers of Bangladesh. Proc. Nat. Acad. Sci. 102, 18819-18823.

Pourret, O., Devranche, M., Gruau, G., Dia, A., 2007. Organic complexation of rare earth elements in natural waters: Evaluating model calculations from ultrafiltration data. Geochim. Cosmochim. Acta 71, 2718-1735.

Purdy, C. B., Burr, Helz, G. R., Mignerey, A. C., 1996. Aquia Aquifer Dissolved Cl-and $^{36}Cl/Cl$: Implications for Flow Velocities. Water Resour. Res. 32, 1163-1171.

Quinn, K. A., Byrne, R. H., Schijf, J., 2004. Comparative scavenging of yttrium and the rare earth elements in seawater: Competitive influences of solution and surface complexation. Aquatic Geochem. 10, 59-80.

Quinn, K. A., Byrne, R. H., Schijf, J., 2006. Sorption of yttrium and rare earth elements by amorphous ferric hydroxide: Influence of solution complexation with carbonate. Geochim. Cosmochim. Acta 70, 4151-4165.

Qvarfort, V. 1992. The high occurance of arsenic in Macadam products from an iron mine in central Sweden: significance for environmental contamination. Environ. Geochem. Health 14, 87-90.

Ravenscroft, P., Brammer, H., Richards, K., 2009. Arsenic Pollution: A Global Synthesis. Wiley-Blackwell (Oxford, UK) 588 p.

Ratnaike, R. N., 2003. Acute and chronic arsenic toxicity. Postgrad. Med. J. 79, 391-396.

Raven, K. P., Jain, A., Loeppert, R. H., 1998. Arsenite and arsenate adsorption on ferrihydrite: kinetics, equilibrium, and adsorption envelopes. Environ. Sci. Technol. 32, 344-349.

Rittle, K. A., Drever, J. I., Colberg, P. J. S., 1995. Precipitation of arsenic during bacterial sulfate reduction. Geomicrobiol. J. 13, 1-11.

Romero, F., M., Armienta, M., A., Carrillo-Chavez, A., 2004. Arsenic sorption by carbonate-rich aquifer material, a control on arsenic mobility at Zimapan, Mexico. Environ. Contam. Toxicol. 14, 1-13.

Rye, R.O., Back, W., Hanshaw, B.B., Rightmire, C.T., Pearson, F.J., 1981. The origin and isotopic composition of dissolved sulfide in groundwater from carbonate aquifers in Florida and Texas. Geochim. Cosmochim. Acta. 45, 1941-1950.

Sacks, L.A., Herman, J.S., Kauffman, S.J., 1995. Controls on high sulfate concentrations in the Upper Floridan aquifer in southwest Florida. Water Resour. Res. 31, 2541-2551.

Saunders, A. D., 1984. The rare earth element characteristics of igneous rocks from the ocean basins. In: P. Henderson (ed.) Rare Earth Element Geochemistry. Elsevier (Amsterdam), pp. 205-236.

Schelske, C.L., Eadie, B.J., Krausse, G.L., 1984. Measured and predicted fluxes of biogenic silica in Lake Michigan. Limnol. Oceanogr. 29, 99-110.

Schijf, J., de Baar, H. J. W., Millero, F. J., 1995. Vertical distributions and speciation of dissolved rare earth elements in the anoxic brines of Bannock Basin, eastern Mediterranean Sea. Geochim. Cosmochim. Acta, 59, 3285-3299.

Schijf, J., Byrne, R. H., 1999. Determination of stability constants for the mono- and difluoro-complexes of Y and the REE, using a cation-exchange resin and ICP-MS. Polyhedron 18, 2839-2844.

Schijf, J., Byrne, R. H., 2004. Determination of $_{SO4}\beta_1$ for yttrium and the rare earth elements at I = 0.66 m and t = 25°C – Implications for YREE solution speciation in sulfate-rich waters. Geochim. Cosmochim. Acta 68, 2825-2837.

Shamsudduhu, M., Uddin, A., Saunders, J. A., Lee, M.-K., 2008. Quaternary stratigraphy, sediment characteristics and geochmistry of arsenic-contaminated

alluvial aquifers in the Ganges-Brahmaputra floodplain in central Bangladesh. Journal of Conaminant Hydrology 99, 112-136.

Shannon, R. D., 1976. Revised effective ionic radii and systematic studies of interatomic distances in halides and chalcogenides. Acta Cryst. A 32, 751-767.

Shannon, W.M., Wood, S.A. (2005) The analysis of pictogram quantities of rare earth elements in natural waters. In: K.H. Johannesson (ed.) Rare Earth Elements in Groundwater Flow Systems. Springer (Dordrecht), pp. 1-37.

Sholkovitz, E.R., 1989. Artifacts associated with the chemical leaching of sediments for rare-earth elements. Chem. Geol. 77, 47-51.

Sholkovitz, E. R., Landing, W. M., Lewis, B. L., 1994. Ocean particle chemistry: The fractionation of rare earth elements between suspended particles and seawater. Geochim. Cosmochim. Acta 58, 1567-1579.

Sholkovitz, E. R., Shen, G. Y., 1995. The incorporation of rare earth elements in modern coral. Geochim. Cosmochim. Acta 59, 2749-2756.

Skopp, J. 1986. Analysis of time-dependent chemical processes in soils. Journal of Environmental Quality 15, 205-213.

Smedley, P.L., 1991. The geochemistry of rare earth elements in groundwater from the Carnmenellis area, southwest England. Geochem. Cosmochim. Acta 55, 2767-2779.

Smedley, P. L., Kinniburgh, D. G., 2002. A review of the source, behavior and distribution of arsenic in natural waters. Appl. Geochem. 17, 517-568.

Smith, A., Hopenhayn-Rich, C., Bates, M., Goeden, H., Hertz-Picciotto, I., Duggan, H., Wood, R., Kosnett, Smith, M., 1992. Cancer risks from arsenic in drinking water. Environ. Health Perspect. 97, 259-267.

Smith, E. H., Lu, W., Vengris, T., Binkiene, R., 1996. Sorption of heavy metals by Lithuanian glauconite. Wat. Res. 30, 2883-2892.

Smith, E., Naidu, R., Alston, A.M., 1999. Chemistry of arsenic in soils: I. Sorption of arsenate and arsenite by four Australian soils. Journal of Environmental Quality 28, 1719-1726.

Smith, E., Naidu, R., 2009. Chemistry of inorganic arsenic in soils: kinetics of arsenic adsorption-desorption. Environ, Chechem. Health 31, 49-59.

Somasundaran, P., Aqar, G. E., 1967. The zero point of charge of calcite. J. Colloids Interface Sci. 24, 433-440.

Sonke, J. E., Salters, V. J. M., 2006. Lanthanide – humic substances complexation. I. Experimental evidence for a lanthanide contraction effect. Geochim. Cosmochim. Acta 70, 1495-1506.

Stefánsson, A., Arnórsson, S., Sveinbjörnsdóttir, Á., 2005. Redox reactions and potentials in natural waters at disequilibrium. Chem. Geol. 221, 289-311.

Stetzenbach, K. J., Amano, M., Kreamer, D. K., Hodge, V. F., 1994. Testing the limits of ICP-MS: Determination of trace elements in ground water at the parts-per-trillion level. Ground Water 32, 976-985.

Stollenwerk, K. G., Breit, G. N., Welch, A. H., Yount, J. C., Whitney, J. W., Foster, A. L., Uddin, M. N., Majumder, R. K., Ahmed, N., 2007. Arsenic attenuation by

oxidized aquifer sediments in Bangladesh. Science of the Total Environment 379, 133-150.

Stookey, L., 1970. Ferrozone – a new spectrophotometric reagent for iron. Anal. Chem. 42, 779-781.

Stringfield, V.T., 1966. Artesian water in Tertiary limestone in the southeasterns States. U.S. Geological Survey Prof Paper. 517.

Stute, M., Schlosser, P., Clark, J. F., Broecker, W. S., 1992. Paleotemperatures in the southwestern United States derived from noble gases in ground water. Science 256, 1000-1003.

Sverjensky, D. A., 1984. Europium redox equilibria in aqueous solution. Earth Planet. Sci. Lett. 67, 70-78.

Sweener, R., Vankeer, I., DeVos, W., 1994. Heavy metal contamination in overbank sediments of the Geul River (east Belgium): its implications to former Pb-Zn mining activities. Environ. Geol. 24, 12-21.

Tang, J., Johannesson, K.H., 2003. Speciation of rare earth elements in natural terrestrial waters: assessing the role of dissolved organic matter from the modeling approach. Geochim. Cosmochim. Acta 67, 2321-2339.

Tang, J., Whittecar, G.R., Johannesson, K.H., Daniels, A.L., 2004. Potential contaminants at a dredged spoil placement site, Charles City County, Virginia, as revealed by sequential extraction. Geochemical Transactions 5, 49-60.

Tang, J., Johannesson, K. H., 2005a. Rare earth element concentrations, speciation, and fractionation along groundwater flow paths: The Carrizo Sand (Texas) and Upper

Floridan aquifers. In: K. H. Johannesson (ed.) Rare Earth Elements in Groundwater Flow Systems, Springer (Dordrecht), pp. 223-251.

Tang, J., Johannesson, K. H., 2005b. Adsorption or rare earth elements onto Carrizo sand: Experimental investigations and modeling with surface complexation. Geochim. Cosmochim. Acta 69, 5247-5261.

Tang, J., Johannesson, K.H., 2006. Controls on the geochemistry of rare earth elements along a groundwater flow path in the Carrizo Sand aquifer, Texas, USA. Chem. Geol. 225, 156-171.

Tang, J., Johannesson, K. H., in review. Ligand extraction of rare earth elements from aquifer sediments: Implications for rare earth element complexation with organic matter in natural waters. Geochim. Cosmochim. Acta.

Taylor, S. R., McLennan, S. R., 1985. The Continental Crust: Its Composition and Evolution. Blackwell Scientific Publications, Oxford, 312 p.

Taylor, S. R., McLennan, S. M., 1988. The significance of the rare earths in geochemistry and cosmochemistry. In Handbook on the Physics and Chemistry of Rare Earths. Vol. 11 (ed. K.A. Gschneidner, Jr. and L Erying), pp 485-479.

Telford, K., Maher, W., Krikowa, F., Foster, S., Ellwood, M. J., Ashley, P. M., Lockwood, P. V., Wilson, S. C., 2009. Bioaccumulation of antimony and arsenic in a highly contaminated stream adjacent to the Hillgrove Mone, NSW, Australia. Environmental Chemistry 6, 133-143.

Tessier, A., Champbell, P. G. C., Bisson, M., 1979. Sequential extraction procedure for the speciation of particulate trace metals. Anal. Chem. 51, 844-851.

Tighe, M., Shley, P., Lockwood, P., Wilson, S., 2005. Soil, water, and pasture enrichment of antimony and arsenic within a coastal floodplain system. Science of the Total Environment 347, 175-186.

Tipping, E., Hetherington, N. B., Hilton, J., Thompson, D. W., Bowles, E., Hamilton-Taylor, J., 1985. Artifacts in the use of selective chemical extractions to determine distributions of metals between oxides of manganese and iron. Anal. Chem. 57, 1944-1946.

Tipping, E., 1993. Modelling the binding of europium and actinides by humic substances. Radiochim. Acta 62, 141-152.

Tipping, E., 1994. WHAM – A computer equilibrium model and computer code for waters, sediments, and soils incorporating a discrete site/electrostatic model of ion-binding by humic substances. Comput. Geosci. 20, 973-1023.

Tipping, E., 1998. Humic ion-binding model VI: an improved description of the interaction of protons and metal ions with humic substances. Aquatic Geochem. 4, 3-48.

Tipping, E., 2002. Cation Binding by Humic Substances. Cambridge Environmental Chemistry Series. Cambridge Univ. Press. 434 pp.

Tipping, E., Hurley, M. A., 1992. A unifying model of cation binding by humic substances. Geochim. Cosmochim. Acta 56, 3627-3641.

Tweed, S. O., Weaver, T. R., Cartwright, I., Schaefer, B., 2006. Behavior of rare earth elements in groundwater during flow and mixing in fractured rock aquifers: An

example from the Dandenong Ranges, southeast Australia. Chem. Geol. 234, 291-307.

United States Environmental Protection Agency, 1979. Water Related Fate of the 129 Priority Pollutants, vol. 1. USEPA, Washington, DC, USA, Doc. 745-R-00-007.

van Geen, A., Rose, J., Thoral, S., Garnier, J. M., Zheng, Y., Bottero, J. Y., 2004. Decoupling of As and Fe release to Bangladesh groundwater under reducing conditions. Part II: Evidence from sediment incubations. Geochim. Cosmochim. Acta 68, 3475-3486.

van Middlesworth, P. E., Wood, S. A., 1998. The aqueous geochemistry of the rare earth elements and yttrium. Part 7. REE, Th and U contents in thermal springs associated with the Idaho Batholith. Aquatic Geochem. 7, 861-884.

Wagman, D. D., Evans, W. H., Parker, V. B., Schumm, R. H., Halow, I., Bailey, S. M., Churney, K. L., Nuttall, R. L., 1982. The NBS tables of chemical thermodynamic properties: Selected values for inorganic and C_1 and C_2 organic substances in SI units. J. Phys. Chem. Ref. Data 11, Suppl No. 2, p. 1-392.

Waltham, C.A. and Eick, M.J., 2002. Kinetics of Arsenic Adsorption on Goethite in the Presence of Sorbed Silicic Acid. Soil Sci. Soc. Am. J. 66, 818-825.

Wedepohl, K. H., 1995. The composition of the continental crust. Geochim. Cosmochim. Acta 59, 1217-1232.

Welch, A. H., Westjohn, D. B., Helsel, D. R., Wanty, R. B., 2000. Arsenic in groundwater of the United State – occurrence and geochemistry. Ground Water 38, 589-604.

Welch, K. A., Lyons, W. B., Graham, E., Neumann, K., Thomas, J. M., Mikeselml, D., 1996. Determination of major element chemistry in terrestrial waters from Antarctica by ion chromatography. J. Chromatog. A739, 257-263.

Whitfield, M. S., 1974. Thermodynamic limitations on the use of the platinum electrode in Eh measurements. Limnol. Oceanogr. 19, 857-865.

Wicks, C. M., Herman, J. S., 1994. The effect of confining unit on the geochemical evolution of ground water in the Upper Floridan aquifer system. J. Hydrol. 153, 139-155.

Wilkie, J. A., Hering, J. G., 1998. Rapid oxidation of geothermal As(III) in streamwaters of the eastern Sierra Neveda. Environ. Sci. Technol. 32, 657-662.

Wilkin, R. T., Wallschläger, D., Ford, R. G., 2003. Speciation of arsenic in sulfidic waters. Geochem. Trans. 4, 1-7.

Willis, S. S., Haque, S. E., Johannesson, K. H., in review. Arsenic and antimony in groundwater flow systems: A comparative study. Aquatic Geochemistry.

Willis, S. S., Johannesson, K. H., in review. Controls on the geochemistry of rare earth elements in sediments and groundwaters of the Aquia aquifer, Maryland, USA. Chemical Geology.

Wilson, S. C., Lockwood, P. V., Ashley, P. M., Tighe, M., 2010. The chemistry and behavior of antimony in the soil environment with comparisons to arsenic: A critical review. Environ. Poll. 158, 1169-1181.

Wolff, R. G. 1967. X-ray and chemical study of weathering of glauconite. Am. Mineral. 52, 1129-1138.

Wood, S. A., 1990. The aqueous geochemistry of the rare-earth elements and yttrium. 1. Review of available low-temperature data for inorganic complexes and the inorganic REE speciation of natural waters. Chem. Geol. 82, 159-186.

Yamamoto, Y., Takahashi, Y., Shimizu, H., 2005. Systematics of stability constants of fluvate complexes with rare earth ions. Chem. Lett. 34, 880-881.

Yoshida, T., Yamauchi, H., Sun, G. F., 2004. Chronic health effects in people exposed to arsenic via drinking water: dose-response relationships in review. Toxicol. Appl. Pharmacol. 198, 243-252.

Zheng, Y., van Geen, A., Stute, M., Dhar, R., Mo, Z., Cheng, Z., Horneman, A., Gavrieli, I., Simpson, H. J., Versteeg, R., Steckler, M., Gravzioli-Venie,r A., Goodbred, S., Shahnewaz, M., Shamsudduha, M., Hoque, M. A., Ahmed, K. M., 2005. Geochemical and hydrogeological contrasts between shallow and deeper aquifers in two villages of Araihazar, Bangladesh: Implications for deeper aquifers as drinking water sources. Geochim. Cosmochim. Acta 69, 5203-5218.

Zhong, S., Mucci, A., 1995. Partitioning of rare earth elements (REEs) between calcite and seawater solutions at 25°C and 1 atm, and high dissolved REE concentrations. Geochim. Cosmochim. Acta 59, 443-453.

BIOGRAPHICAL INFORMATION

Stephanie Scholten Willis, born in Dallas, Texas, earned a Bachelor of Science in Chemistry from The University of Texas at Austin in May 2002 and a Master of Science in Chemistry from The University of Texas at Arlington in December 2005. While earning her Doctorate in Earth and Environmental Science at The University of Texas at Arlington, she worked as an Air Quality Specialist at The Benham Companies, LLC, an SAIC Company. Upon completion of her PhD in 2010, Stephanie plans to continue working for Benham.